

**STRENGTHENING SUPPORT CONDITIONS OF DOUBLY
CORRUGATED THIN-WALLED STEEL ARCH STRUCTURES**

**RENFORCEMENT DES APPUIS DE STRUCTURES EN
ARC EN ACIER À PAROIS MINCES DOUBLEMENT ONDULÉES**

A Thesis Submitted to the Division of Graduate Studies
of the Royal Military College of Canada
by

Yung Ku Kang, rmc
Major

In Partial Fulfillment of the Requirements for the Degree of
Master of Applied Science

August 2022

© This thesis may be used within the Department of National Defence but
copyright for open publication remains the property of the author.

*To Winston and Eleanor –
let this parachute remind you
to never say “I can’t”.*

ACKNOWLEDGEMENT

I would like to thank my supervisors Dr. Gordon Wight and Dr. Marc-André Dagenais for their guidance, support, and encouragement that I received throughout the last two years. The research project and its experimental program lacked guidance from relevant literature; it made the supervisors' imagination and competence all the more crucial to success.

In-house technical support from Mr. Dexter Gaskin and Mr. Steve Vanvolkingburgh were absolutely central to the successful setup and conduct of the experiments. Their extensive knowledge, resourcefulness, and problem-solving skills guided me through the minefield that is laboratory work, with all twenty fingers and toes intact.

I am grateful to have had the passionate support from Mr. Louis Saulnier with photography, videography, instrumentation setup and data analysis. I appreciated having Officer Cadets Robison and Ramos Rodriguez help with construction and contribute fresh perspectives. Expertise from 14 Construction Engineering Squadron members, Sgt Collins and MCpl Schulek in particular, was absolutely essential to preparing test specimens on RMC grounds.

This project was made possible with the funding and general interest from Director, Architecture and Engineering Services staff and A4 CE - 1 Canadian Air Division staff.

I was fortunate to have Capt Seguin as a partner in course work and in associated research. Countless mutually beneficial successes were direct results of his thoughtful approach and dedication.

My most sincere thanks are owed to my wife, Melissa. The generally hectic life through COVID-19 difficulties with our first child Winston was intensified with the arrival of our second child Eleanor. Through it all, Melissa always encouraged me and made many sacrifices to support my studies.

ABSTRACT

Lightweight, cold-formed steel arch systems known as K-Span structures are ideal for creating large open spaces suitable for both civilian and military purposes. However, collapses reported in several countries raise concern regarding their capacity to support heavy snow loads, especially for base support condition-deficient structures. Given that there is a general lack of research, understanding, and applicable code, the use of existing and future K-Span structures carries an uncertain degree of risk. Accordingly, no practical method has yet been developed for strengthening existing K-Span structures to reduce this risk. This thesis document proposes an innovative strengthening technique for base support condition-deficient K-Span structures managed by the Department of National Defence (DND).

A theoretically possible two-dimensional redistribution of internal forces in a loaded K-Span structure was developed into a practical retrofit, implemented on full-scale specimens and analyzed for its effect on structural behaviour. The retrofit involved strengthening the existing hinges base supports with a series of small steel struts welded to stiffen the hinged mechanism. Two specimens with retrofitted support conditions were loaded past failure with symmetric and asymmetric snow loading patterns as prescribed by the National Building Code of Canada (NBCC). Retrofitted specimens under symmetric and asymmetric loading exhibited ultimate capacity improvements of 31.7% and 19.4% respectively, with an intermediate structural stiffness when compared to the performance of specimens with pinned low stiffness and fixed high stiffness support conditions.

Numerical models represented the structural effect of the retrofit by the introduction of rotational springs with an approximate stiffness of 2.4 kN·m/deg on deficient support conditions. This strengthening technique is a scalable retrofit design, and it may be adapted for support condition-deficient K-Span structures of varying dimensions.

RÉSUMÉ

Les structures en arc en acier formé à froid connues sous le nom de structures « K-Span » sont idéales pour créer de grands espaces ouverts adaptés à des fins civiles et militaires. Cependant, l'effondrement de certaines de ces structures dans différents pays soulève des inquiétudes quant à leur capacité à supporter de lourdes charges de neige, particulièrement dans le cas des structures ayant des connexions d'appuis déficientes. Étant donné qu'il existe un manque général de recherche, de compréhension et de code applicable à de telles structures, l'utilisation des structures « K-Span » existantes et futures comporte un certain degré de risque. Par conséquent, aucune méthode pratique n'a encore été développée pour renforcer ces structures existantes afin de réduire ce risque. Ce document propose une technique de renforcement innovante pour les structures « K-Span » gérées par le ministère de la Défense nationale (MDN) ayant des connexions d'appuis déficientes.

Une redistribution bidimensionnelle théoriquement possible des forces internes dans une structure « K-Span » chargée grâce à une méthode de renforcement pratique a été développée, appliquée sur des spécimens à grande échelle et analysée pour son effet structurel. La méthode de renforcement consiste à souder une série d'entretoises au niveau des appuis afin d'en augmenter la rigidité. Deux spécimens ont été renforcés aux appuis et chargés au-delà de la rupture selon une distribution de neige symétriques et asymétriques tel que prescrit par le Code national du bâtiment du Canada (CNBC). Les spécimens renforcés sous chargement symétrique et asymétrique ont présenté une augmentation de la résistance ultime de 31,7 % et 19,4 % respectivement, avec une rigidité structurelle intermédiaire, comparativement aux spécimens avec des conditions d'appuis pure ayant des appuis rotulés à faible rigidité et aux spécimens ayant des appuis fixes à rigidité élevée.

Des modèles numériques développés dans cette recherche ont démontré que l'effet structurel du renforcement était l'introduction aux appuis de ressorts d'une rigidité de rotation approximative à 2,4 kN·m/deg aux conditions d'appuis déficientes. Cette technique de renforcement peut être adaptée aux structures « K-Span » de différentes dimensions à travers le monde.

CO-AUTHORSHIP STATEMENT

This thesis was written in the manuscript-based format as described in the Royal Military College of Canada Thesis Preparation Guidelines. The author of this thesis, Major Yung Ku Kang, was the main author for the manuscript contained in this document as Chapter 3, while co-authors provided guidance, assistance and feedback. As the author intends to submit the manuscript for publication in a peer-reviewed journal, the manuscript will include both academic supervisors as co-authors.

TABLE OF CONTENTS

ACKNOWLEDGEMENT	iii
ABSTRACT.....	iv
RÉSUMÉ	v
CO-AUTHORSHIP STATEMENT.....	vi
TABLE OF CONTENTS.....	vii
LIST OF FIGURES	xi
LIST OF TABLES.....	xv
LIST OF ACRONYMS	xvi
LIST OF SYMBOLS	xvii
Chapter 1 INTRODUCTION	1
1.1 Background.....	1
1.2 Aim	3
1.3 Scope.....	3
1.4 Thesis Organization	3
1.5 Description of Appendices.....	4
Chapter 2 LITERATURE REVIEW	5
2.1 General.....	5
2.2 K-Span Structures	5
2.2.1 MIC-120 Arch Fabrication.....	6
2.2.2 Construction Method	8
2.2.3 Collapses	9
2.3 Cold-Formed Steel.....	10

2.3.1	Characteristics.....	10
2.3.2	Double Corrugation	12
2.3.3	Column-Like Interaction Behaviours.....	13
2.3.4	Codes and Specifications	14
2.4	Structural Capacity.....	16
2.4.1	Bending Capacity.....	17
2.4.2	Support Conditions	18
2.4.3	Strengthening Methods	20
2.5	Experimental Testing	24
2.5.1	Full-Scale Testing	25
2.5.2	Full-Scale Instrumentation.....	26
2.5.3	Full-Scale Experimental and Numerical Results	27
2.6	Summary	27
Chapter 3 MANUSCRIPT: “STRENGTHENING SUPPORT CONDITIONS IN DOUBLE CORRUGATED ARCH STRUCTURES”		28
3.1	Abstract.....	28
3.2	Introduction.....	28
3.2.1	K-Span Structure.....	28
3.2.2	Bending Capacities	30
3.2.3	Strengthening Methods	30
3.3	Research Objectives and Scope	31
3.4	Experimental Program	31
3.4.1	Specimens	31
3.4.2	Loading Scheme.....	32

3.4.3	Instrumentation	33
3.4.4	Retrofit Design.....	34
3.4.5	Test Procedures.....	36
3.5	Experimental Results	36
3.5.1	Symmetric Loading.....	37
3.5.2	Asymmetric Loading	40
3.5.3	Retrofitted Support Condition.....	42
3.6	Numerical Work.....	45
3.6.1	Shell Model.....	45
3.6.2	Solid Model.....	49
3.6.3	Frame Element Model.....	51
3.6.4	Numerical Work Summary	51
3.7	Conclusions.....	52
3.8	Acknowledgements.....	52
3.9	References.....	52
Chapter 4	CONCLUSIONS AND RECOMMENDATIONS	55
4.1	General.....	55
4.2	Conclusions.....	55
4.3	Recommendations.....	56
	REFERENCES	57
	APPENDICES	60
Appendix A	SELECT AS BUILT DRAWINGS FROM THE COLLAPSED K-SPAN STRUCTURE	61

Appendix B NBCC SNOW AND RAIN LOAD CONVERSION TO POINT LOADS AND ACTUATOR LOADS.....	64
Appendix C PROPOSED STRENGTHENING TECHNIQUE	69
Curriculum Vitae	70

LIST OF FIGURES

Figure 1.1 - K-Span structure in CFB Petawawa [2]	1
Figure 1.2 - Collapsed K-Span structure in CFB Petawawa [3]	2
Figure 2.1 - Various civilian usage of K-Span structures [8]	5
Figure 2.2 - M.I.C. Industries (a) MIC-120 and (b) MIC-240 cross-sections (mm) [8]	6
Figure 2.3 - Common arch cross-sections in China (a) MMR-118, (b) MMR-178 and (c) MMR-238 (mm) [6]	6
Figure 2.4 - MIC-120 ABM in CAF inventory	7
Figure 2.5 - (a) longitudinally corrugated profile and (b) doubly-corrugated profile [8] ...	7
Figure 2.6 - MIC-120 ABM main components [15]	7
Figure 2.7 - Seaming machine (a) stationary and (b) in action [15]	8
Figure 2.8 - Four MIC-120 panels seamed together [16]	8
Figure 2.9 - A set of six seamed MIC-120 panels erected by crane [8] [15]	8
Figure 2.10 - (a) M.I.C. Industries drawing, (b) sample hinge drawing and (c) hinge picture [15] [16]	9
Figure 2.11 - K-Span collapses in (a) Gdansk and (b) Tuszyn, Poland [1] [5]	10
Figure 2.12 - (a) Lab test specimen cut-out locations and (b) material properties [8]	11
Figure 2.13 - Stages of stress distribution in thin-walled cold-formed steel [18]	11
Figure 2.14 - (a) MIC-120 gross cross-section and (b) MIC-120 effective cross-section (mm) [8]	12
Figure 2.15 - Accordion-behaviour of MIC-240 specimen under compression and negative moment [1]	13
Figure 2.16 - Numerical and experimental axial load-moment interaction diagram for single- and double-panel MIC-120 components [3]	13
Figure 2.17 - Eurocode 3 cold-formed steel cross-section classes [25]	15
Figure 2.18 - Hinge-like connection method between K-Span arches and base [23]	15

Figure 2.19 - Equivalent cross-sectional characteristics of a profile similar to MIC-120 [23]	16
Figure 2.20 - (a) Stress profile of MIC-120 cross-section under positive bending moment and (b) Seamed lips buckling [3] [8]	17
Figure 2.21 - Bending moments of a 1.00 mm thick, four-arch model with 16 m span on (a) fixed supports (b) pinned supports [16]	19
Figure 2.22 - Various Quonset Hut structure support conditions with (a) construction clip, (b) base plate and (c) ends embedded in concrete [33].....	19
Figure 2.23 - Theoretical and experimental load-deflection curves for various support conditions [33]	20
Figure 2.24 - Primary and secondary buckling path and bifurcation [29]	21
Figure 2.25 - Tension cable layouts used to control deflection [6] [29]	21
Figure 2.26 - Primary and secondary buckling path, with and without cables [29].....	22
Figure 2.27 - Reducing self-supporting span with cantilever beams protruding from supports [34]	22
Figure 2.28 - Fixing the arches in concrete (option not taken) [34]	23
Figure 2.29 - Collapsed K-Span structure in Russia [13]	23
Figure 2.30 - Effect of stiffeners on Quonset Hut deflections (ft) [33]	24
Figure 2.31 - Testing K-Span arches in load-controlled manner [6] [12].....	26
Figure 2.32 - Testing K-Span arches in displacement-controlled manner [1]	26
Figure 3.1 - Example of MIC-120 K-Span structure at CFB Petawawa [4]	29
Figure 3.2 - Connection methods defining support conditions	30
Figure 3.3 - Loading system specifically designed for experiment	32
Figure 3.4 - Point load locations for symmetric and asymmetric loading (m).....	32
Figure 3.5 - Each loading point equipped with a 20 kN load cell.....	33
Figure 3.6 - String potentiometer and LVDT locations (m)	34

Figure 3.7 - Bending moment diagrams with various support conditions (kN·m)	34
Figure 3.8 - Isometric view of hinge assembly with proposed retrofits.....	35
Figure 3.9 - Hinged support stiffened via SMAW welding	36
Figure 3.10 - Front view prior to (a) loading and (b) unloading stages	37
Figure 3.11 - Buckling under (a) positive and (b) negative bending moment	38
Figure 3.12 - Maximum load-deflection curve comparisons in (a) vertical and (b) horizontal directions.....	39
Figure 3.13 - Maximum load-deflection curve comparisons in (a) vertical and (b) horizontal directions.....	39
Figure 3.14 - Front view prior to (a) loading and (b) unloading stages	40
Figure 3.15 - Buckling under (a) positive and (b) negative bending moment	41
Figure 3.16 - Maximum load-deflection comparisons in (a) vertical and (b) horizontal directions.....	41
Figure 3.17 - Maximum load-deflection comparisons in (a) vertical and (b) horizontal directions.....	42
Figure 3.18 - Post-peak specimens on various support conditions	44
Figure 3.19 - Post-peak retrofitted support condition	44
Figure 3.20 - Full range LVDT deflection comparisons under symmetric loading.....	45
Figure 3.21 - Hinge Load-angle curves under (a) symmetric and (b) asymmetric loading patterns.....	45
Figure 3.22 - (a) Shell with loading points highlighted green and (b) mesh with mostly 50 mm size elements.....	46
Figure 3.23 - Boundary conditions representing (a) fixed and (b) pinned support conditions	46
Figure 3.24 - Total deflections of a retrofitted model under 15 kN of symmetric loading (mm).....	47
Figure 3.25 - Comparisons of experimental and FEA load-deflection curves with labels corresponding to 1-in-50-year snow loads in select Canadian locations	48

Figure 3.26 - Hinge assembly solid model	50
Figure 3.27 - X-axis deflection in upper half of hinge assembly	50
Figure A.1 - Side and front elevation views (mm) [2]	61
Figure A.2 - Hinge support condition details (mm) [2]	62
Figure A.3 - Excerpt from K-Span arch installation detail (mm) [2]	63
Figure B.1 - Specified snow and rain load equation from NBCC section 4.1.6.2.	64
Figure B.2 - Distributed load calculations with average S_s and S_r that applies for CAF installations across Canada	65
Figure B.3 - Half-arch for symmetric loading points (m)	66
Figure B.4 - Half-arch for asymmetric loading points (m)	67
Figure B.5 - Calculations for forces representing 1-in-50-year snow and rain events in CFB Goose Bay, under symmetric asymmetric loading patterns	68

LIST OF TABLES

Table 2.1 - ABM-120 K-Span arches bending capacity results from [11] and [32].....	18
Table 3.1 - Loads representing 1-in-50-year snow (S_s) and rain (S_r) loads in select Canadian locations	33
Table 3.2 - Ultimate capacity and serviceability comparisons under symmetric loading.	40
Table 3.3 - Ultimate capacity and serviceability comparisons under asymmetric loading	42
Table 3.4 - Shell model mesh convergence check using maximum y-axis deflections at 10 kN total load.....	49
Table 3.5 - Solid model mesh convergence check using x-axis deflections at LVDT location.....	50
Table 3.6 - Iterative process for determining hinge stiffness by observing moment-hinge angle relationship	51

LIST OF ACRONYMS

ABM	Automatic Building Machine
ADM(IE)	Assistant Deputy Minister (Infrastructure & Environment)
ASCE	American Society of Civil Engineers
A4 CE	Air Logistics Construction Engineering
CAF	Canadian Armed Forces
CECS	China Engineering Construction Standardization
CER	Combat Engineer Regiment
CES	Construction Engineering Squadron
CFB	Canadian Forces Base
DAES	Director, Architecture & Engineering Services
DIC	Digital Image Correlation
DND	Department of National Defence
DOF	Degree of Freedom
EC3	Eurocode 3 - Design of Steel Structures
FEA	Finite Element Analysis
LVDT	Linear Variable Displacement Transducer
NBCC	National Building Code of Canada
RMC	Royal Military College
SMAW	Shielded Metal Arc Welding
S136	S136-16 North American Specification for the Design of Cold-Formed Steel Structural Members
USA	United States of America

LIST OF SYMBOLS

C_a	Accumulation factor
C_b	Basic roof snow load factor
C_s	Slope factor
C_w	Wind exposure factor
deg	Degree
DL	Distributed load
ft	Foot
f_u	Ultimate strength
f_y	Yield strength
GPa	Gigapascal
hrs	Hours
Hz	Hertz
in	Inch
I_s	Building importance factor
K	Stiffness
kN	Kilonewton
kPa	Kilopascal
L	Length
m	Metre
m^2	Metre squared
mm	Millimetre
MPa	Megapascal
sqft	Square Foot
S_r	1-in-50-year associated rain load (kPa)
S_s	1-in-50-year ground snow load (kPa)
x	Horizontal distance from roof peak

Chapter 1 INTRODUCTION

1.1 Background

During the 1940s, there was a worldwide demand for prefabricated, rapidly-erectable and easy-to-build temporary military structures. As a response, thin steel panel arch systems known as Quonset Huts were introduced. Combining advantages in adaptable, simple and inexpensive construction, these Quonset Huts served the military well and eventually gained popularity in civilian settings. They soon became a common structure around the world. By the 1980s, M.I.C. Industries based in the United States of America (USA) had developed portable machines, known as Automatic Building Machines (ABM). These machines built steel arches on-site, to be assembled into a structure known as a K-Span. The ABM eliminated the logistical difficulty of shipping prefabricated parts to construction sites. Furthermore, the K-Span structure was a purely self-supporting, weatherproof and maintenance-free structure; it required no columns, beams, trusses, bolts, nuts, rivets, sealants, etc. The ABM were initially intended for sale to American military engineering units, but it also quickly became common in civilian settings worldwide, especially in Eastern Europe, the Middle East and China. Over time, unlicensed versions of the ABM were built and sold, with or without proper training, and application and construction methods of K-Span structures started to diverge across the world. [1]



Figure 1.1 - K-Span structure in CFB Petawawa [2]

The ABM was introduced to the Canadian Armed Forces (CAF) and the Department of National Defence (DND) in the 1990s. CAF personnel from the 14 Construction Engineering Squadron (14 CES) and Combat Engineer Regiments (CER) built dozens of K-Span structures in various Canadian Forces Bases (CFB) across Canada. The ABM showcased its adaptability in building large structures in austere environments like Canadian Forces Station Alert: the northernmost inhabited location in the world. Figure 1.1 shows an example of a structure in CFB Petawawa built using painted cold-formed galvanized steel [2]. Post construction and commissioning, the responsibility of operation and maintenance of the structures was transferred to the Assistant Deputy Minister -

Infrastructure and Environment (ADM(IE)) staff. To this day, 14 CES continues to maintain its capability to build K-Span structures on short notice [3]. Although the K-Span structures were intended to satisfy semi-permanent infrastructure requirements, in reality, DND expects virtually the same level of reliability as normal buildings designed to the National Building Code of Canada (NBCC) standards. Overall, the structures fulfilled their purpose for nearly three decades after their introduction in Canada, and ADM(IE) staff continues to request more be built.

On 14 March 2019, a K-Span structure was reported to have collapsed at CFB Petawawa, as shown in Figure 1.2 [3]. Since CFB Petawawa is not subject to the most extreme climatic conditions possible in Canada according to the NBCC, this collapse put the structural integrity of the rest of the K-Span structures in DND inventory into question. The initial reviews of the collapsed K-Span drawings showed that it was not built to M.I.C. Industries' instructions, but that it was built using a deliberate and unique construction method. As many other K-Span structures in other CFBs were constructed in the same fashion, a DND-wide bulletin was put into effect, containing inspection instructions and a moratorium on further construction [4].



Figure 1.2 - Collapsed K-Span structure in CFB Petawawa [3]

A thorough literature review revealed that many collapses have also occurred in China, Poland, Slovakia and Russia [1] [5] [6]. There are many hypotheses concerning the main factors causing K-Span structures to collapse. During recent years, the majority of research was directed to understanding local failure and behaviours of K-Span parts and presenting findings that may lead to code development [1]. To date, there is no published code in any country that covers the unique properties of the K-Span geometry and material [1] [3] [7] [8] [9]. There is a dearth of research on strengthening existing K-Span structures, especially in a practical and non-intrusive manner. Without an organized approach to structural assessment, certification and/or necessary retrofits, collapses of K-Span structures may continue to occur around the world.

1.2 Aim

The aim of this research project was to develop a strengthening technique that may address the apparent deficiency in DND K-Span structures. With the unique base support conditions hypothesized to be the main cause of the deficiency as they amplify the bending moments under load, the project aimed to:

- Design a non-intrusive retrofit capable of reducing the magnitude of bending moments throughout the arches under symmetric and asymmetric loading;
- Conduct full-scale experiments with specimens on retrofitted supports to observe its modified load-deflection behaviours, ultimate capacity and serviceability; and
- Conduct non-linear finite element analysis (FEA) to model the experiments and quantify the effect of the retrofit.

1.3 Scope

The scope of this research project was limited to focus on testing the possibility of modifying the structural behaviours of existing DND K-Span structures. An experimental program was organized to load full-scale, ABM-produced K-Span arches past ultimate failure, with the goal of observing two-dimensional post-retrofit behaviours through their elastic and plastic range. Given the constraints of the laboratory dimensions and significant cost and labour involved in specimen construction, the experimental program was limited to testing two, 7 m span, four-panel, sets of arches. The specimens were tested without out-of-plane bracing, representing the most vulnerable arches of a K-Span structure that lack any stiffening effects from end walls.

The specimens were loaded by a hydraulic actuator through a system of pulleys and cables, simulating symmetrically and asymmetrically distributed snow and rain loads. A total combination of 40 load cells, string potentiometers and Linear Variable Displacement Transducers (LVDT) were installed to measure loads and deflections in the two in-plane axes, at discrete points on regular intervals.

With a focus for snow and rain load ranges possible on CAF installations, comparisons between its experimental load-deflection data and its accompanying control data from Seguin et al. (2022) collected with the identical laboratory setup established quantifiable differences in structural capacities [9]. Geometrically non-linear FEA involving shell elements, solid elements and frame elements quantified the effect of the retrofit.

1.4 Thesis Organization

This document is organized in the article-based format as described in the RMC Thesis Preparation Guidelines [10] and contains four chapters. Chapter 1 introduces the research project, covering its background history and development, aim and scope. Chapter 2 offers a review of relevant concepts, past experiments and analysis available in literature. Chapter 3 is an individual article to be submitted to an appropriate engineering journal for publication. It consists of a manuscript that offers its own concise literature review concentrating on the most applicable information from the general literature review contained in Chapter 2, to provide its readers sufficient background knowledge. Because it

is an independent manuscript, an independent reference list is included and reference numbering restarts at 1. It presents the experimental setup and program, results, and supporting numerical work. Chapter 4 provides a summary of research conclusions and recommendations for future researchers.

1.5 Description of Appendices

Important information was inserted sufficiently and appropriately through the four chapters of the main document. The appendices include additional material that guided the project through its innovative retrofit design and experimental program. Appendix A presents portions of the as-built drawings and plans from the collapsed K-Span structure in CFB Petawawa that were relevant to developing the strengthening technique. Appendix B contains the procedure that determined the loading scheme to facilitate NBCC roof snow and rain loads, as well as a sample conversion of 1-in-50-year snow and rain load pressure into a single load to be induced through a hydraulic actuator. Appendix C shows details of the retrofit implemented on full-scale replicas of the support condition-deficient K-Span structures in DND.

Chapter 2 LITERATURE REVIEW

2.1 General

This chapter offers a review of available literature on the topics relevant to the scope of this research project. It provides readers background in subject matters regarding MIC-120 type K-Span arch characteristics and adaptation worldwide, and its current predicament with a lack of codes and guidelines. It explores past analyses and experiments that established structural capacities for select K-Span arch dimensions, and attempted strengthening measures.

2.2 K-Span Structures

K-Span structures were originally designed for use by the American military engineering community, often tasked to construct semi-permanent, multi-purpose structures in far-flung locations with little logistical support upon arrival. As a result, M.I.C. Industries created a self-sufficient trailer-mounted mobile factory that fits in common military cargo aircraft. The ABM along with steel coil stock, diesel fuel, and a small crew could rapidly form a superstructure. The USA Army engineering community had approved of the structural soundness and remarked that a “12-person crew can construct 5000 sqft of bare structure (no utilities) in 12 hrs” [11]. As K-Span structures served the American uniformed services well, they also gained popularity in civilian construction. They have been adopted in over 70 countries for building schools, sports halls, storage buildings, markets, factories, etc., as seen in Figure 2.1 [8].



Figure 2.1 - Various civilian usage of K-Span structures [8]

K-Span structures are an assembly of individual curved arch and straight cold-formed steel panels. Figure 2.2 and Figure 2.3 show common individual K-Span profiles in use. Unlike common cold-formed steel construction designs consisting of columns, beams, trusses, corrugated sheet metal cladding, etc., K-span arches are entirely self-supporting materials serving as roof and walls. Single or multiple K-Span structures are connected to bases, which vary greatly in design across the world; they range from reinforced concrete to retired and adapted sea containers [1].

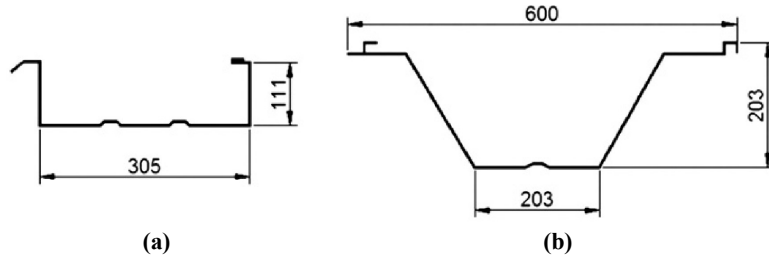


Figure 2.2 - M.I.C. Industries (a) MIC-120 and (b) MIC-240 cross-sections (mm) [8]

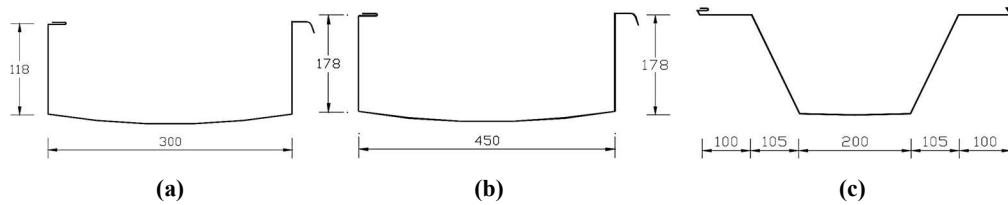


Figure 2.3 - Common arch cross-sections in China (a) MMR-118, (b) MMR-178 and (c) MMR-238 (mm) [6]

There are an inestimable number of K-Span structures across the world, as they are identified with diverse names. From limited sources, it is estimated that Canada and Poland each possess dozens of K-Span structures [5]. Russia is estimated to have hundreds [12] [13]. China built thousands since the system's introduction in the early 1990s; "as of 2001, it [China] was constructing over 2 million m² per year" of K-Span-type structures, which is comparable to approximately 3,000 structures, similar to that which collapsed in CFB Petawawa and is referred to in Chapter 1 [14]. The proliferation of K-Span structures is expected to intensify worldwide; research into safe usage is essential. This research project analyzed only the MIC-120 model, as all CAF K-Span structures are built with MIC-120 profiles.

2.2.1 MIC-120 Arch Fabrication

MIC-120 arches are produced using an ABM, shown in Figure 2.4. A steel coil stock with thickness ranging from 0.5 mm to 1.5 mm is first cold-rolled through the ABM to create a profile with longitudinal corrugations, as shown in Figure 2.5(a) [1]. It is cut at a pre-determined interval, calculated to be the arc length of the final arch panel. It is then cold-rolled through the ABM in a second process to form transverse corrugations and curve the panel, as shown in Figure 2.5(b). The two-step process is depicted in Figure 2.6 [15]. The fabricated arches are formed to create spans any distance between 3.7 m and 24 m [15].



Figure 2.4 - MIC-120 ABM in CAF inventory

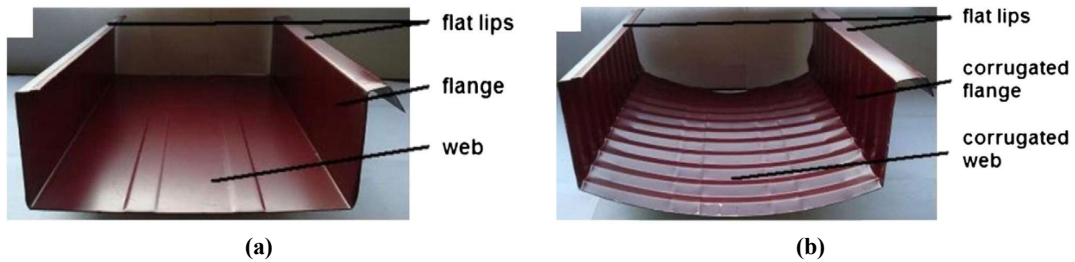


Figure 2.5 - (a) longitudinally corrugated profile and (b) doubly-corrugated profile [8]

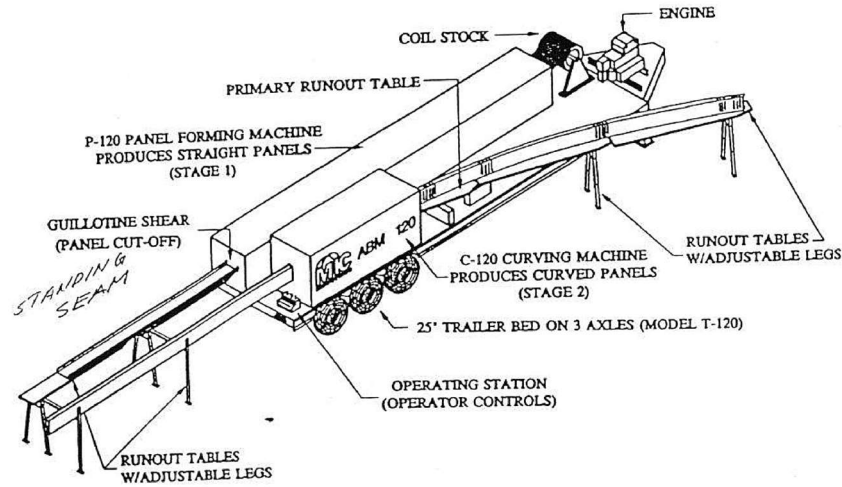


Figure 2.6 - MIC-120 ABM main components [15]

A standalone seaming machine seen in Figure 2.7 connects panels together by traveling along the arches and crimping flat lips over the receiving flat lip of the adjacent arch. Without any fasteners or sealants, a weatherproof and maintenance-free structure is created [15]. Figure 2.8 [16] shows the profile of a typical four-panel set of arches seamed together and ready to be erected by crane.



Figure 2.7 - Seaming machine (a) stationary and (b) in action [15]

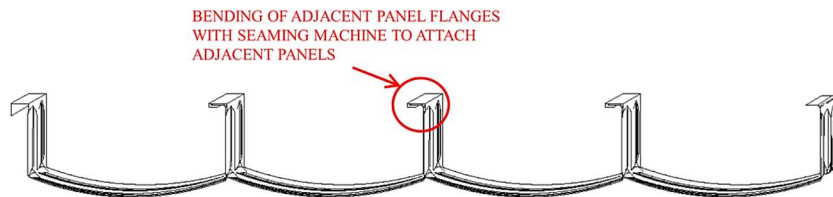


Figure 2.8 - Four MIC-120 panels seamed together [16]

2.2.2 Construction Method

The first set of four- to six-panels is lifted by crane, as seen in Figure 2.9, to form one end of a K-Span structure. It is plumbed, squared and secured onto prepared base supports. Additional sets are also lifted into place by crane, with the seaming procedure in between sets. This is continued until the intended longitudinal length of the structure is attained [15].



Figure 2.9 - A set of six seamed MIC-120 panels erected by crane [8] [15]

The connection method between K-Span arches and the base is a very important element that has diverged widely since its beginnings. The original instructions from M.I.C. Industries involved a reinforced concrete base, poured with the K-Span arches embedded approximately 180 mm (7 in) in the reinforced concrete footing, as seen in Figure 2.10(a) [15]. Modified connection methods worldwide caused intentional or unintentional changes

to structural capacities. A review of post-collapse photographs and its drawings [2] [17] clearly show that several Canadian K-Span arches are not embedded in reinforced concrete bases as per M.I.C. Industries instructions. The bottom ends of the K-Span arches are bolted onto hinges that span the length of the building. The common method in Eastern Europe and China also omits a concrete pour after K-Span arches are erected; the arch ends are bolted onto steel angles attached to a concrete or steel base [1]. Additionally, there are many undocumented site-specific connection methods devised and used around the world.

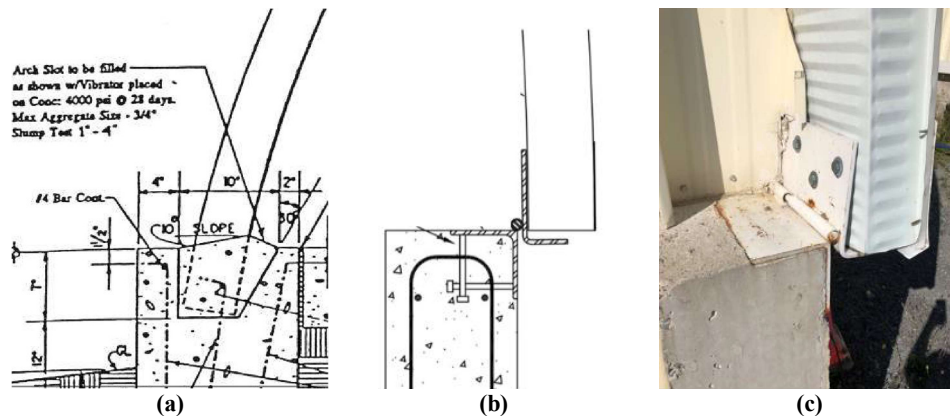


Figure 2.10 - (a) M.I.C. Industries drawing, (b) sample hinge drawing and (c) hinge picture [15] [16]

Besides the K-Span arches, the next most structurally essential component of the structures are the end walls, usually at both longitudinal limits of the structure. End wall construction has also varied extensively as seen in Figure 2.1, involving a combination of materials such as steel, masonry, timber and glass, as well as featuring large openings for garage doors, personnel doors and windows. The default end wall components as per M.I.C. Industries' instructions consisted of straight K-Span panels, intended to reduce dependence on another material [15]. Figure 1.1 shows an example, where straight panels as seen in Figure 2.5(a) were cut to exact length, erected vertically and seamed together. Unlike the connection method at the base of the arches that could affect the structural capacity significantly, the exact properties of the end walls are regarded to be less important to the overall assessment of a K-Span structure.

2.2.3 Collapses

A K-Span structure located in CFB Petawawa, approximately 160 km northwest of Ottawa, Ontario, collapsed suddenly in 2019 [3] [16]. Limited analytical work and FEA of the collapsed structure suggested that its ultimate factored capacity did not meet factored 1-in-50-year snow and rain loads as per NBCC [16].

Figure 2.11 shows two K-Span structures in Poland that collapsed in 2010, halting two unrelated K-Span construction projects underway. The collapse drew attention as the structures were reported to have failed under 30% of allowable snow loads calculated with European standards [5]. Similar collapses have been reported in Slovakia and Russia [1].

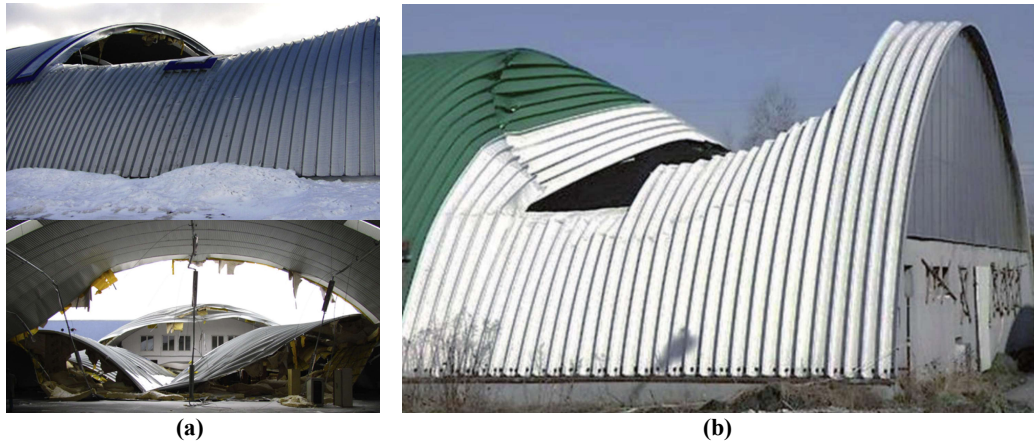


Figure 2.11 - K-Span collapses in (a) Gdansk and (b) Tuszyn, Poland [1] [5]

Following the introduction of K-Span structures in China, a single heavy snow fall in 1996 caused more than 30,000 m² of K-Span structures to collapse in northeastern China [6]. For perspective, it was roughly equivalent in floor area to 40 K-Span structures, likes of which collapsed in CFB Petawawa. Subsequently, as of 2001, it was documented that “many have been collapsed in recent years, nearly every area in China [when subjected to] heavy snow or typhoon” while new construction continues at a pace of over 2,000,000 m² per year [14].

Evidently, K-Span structural integrity is not an exclusively Canadian problem. The documented collapses suggest that snow loads usually contribute to a failure. More than 70 countries are building K-Span structures under diverse environmental conditions with various construction methods, at an immeasurable pace. Further collapses could be expected around the world.

2.3 Cold-Formed Steel

K-Span arches are entirely made of cold-formed steel. While diverse construction methods, end wall design and climatic conditions affect overall structural integrity, the underlying strength of K-Span structures depends on the properties and behaviours of cold-formed steel arches. The ABM employs a cold-forming technique called cold-rolling, at the construction site to produce profiles as seen in Figure 2.5. As a result, the arches exhibit different material properties from the originally isotropic steel coil stock, and behave in a unique way that is not fully understood, nor governed by a code in any country.

2.3.1 Characteristics

Compared to regular hot-rolled steel widely used as principal structural members, cold-formed steel is usually thin gauge material often used in light-duty structural applications [3]. K-Span arches encompass a large width to thickness ratio, which is associated with topics such as orthotropy, post-buckling strength and effective width method.

The process of cold-rolling longitudinally and transversely through the ABM generates strain hardening on the corner areas of the MIC-120 profile. Through laboratory testing of strips cut from straight and curved panels as seen in Figure 2.12, it was found that

transverse corrugations cause negligible change to yield and ultimate strength from the virgin material. However, the longitudinal corrugations cause the corner areas to feature increased yield and ultimate strength. Thus, K-Span arches could be considered orthotropic plates or shells [14].

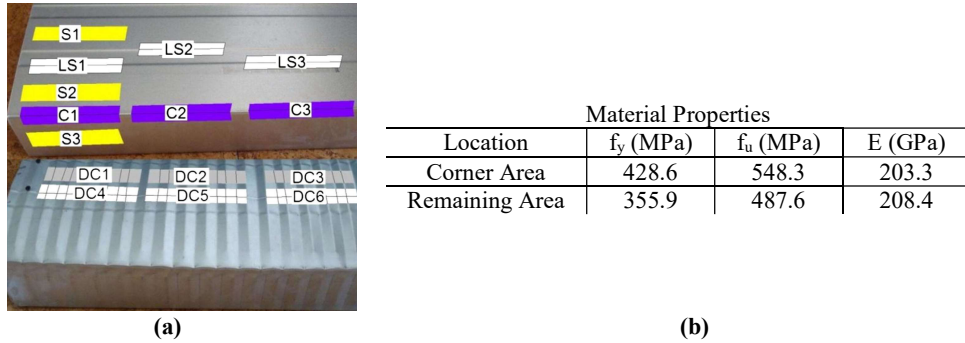


Figure 2.12 - (a) Lab test specimen cut-out locations and (b) material properties [8]

Cold-formed steel is prone to buckling at a stress below yield strength when subject to compression and/or bending moment, as is the case for most thin-walled members of any material. However, cold-formed steel is not categorically considered to have failed at the first instance of buckling. Figure 2.13 shows the stages of stress distribution in a typical cold-formed profile under compression, in pre-buckling and post-buckling stages. Similar to the profile in Figure 2.13, a K-Span profile would theoretically redistribute its stress towards bent corner areas in its profile post-buckling and sustain further loading through a blend of its elastic and plastic ranges.

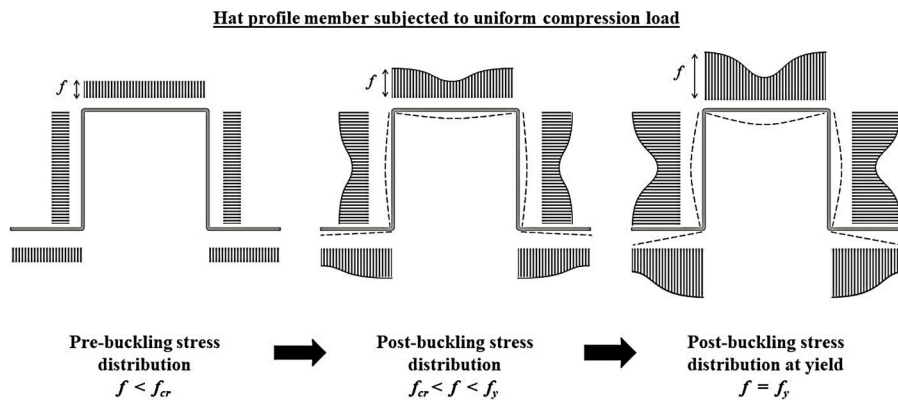


Figure 2.13 - Stages of stress distribution in thin-walled cold-formed steel [18]

Given the difficulties in accounting for buckling, non-uniform stress distribution and redistribution in cold-formed steel profiles, a simplified method using an “effective width” is used for practical design. It involves the reduction of a given gross cross-section under a non-uniform stress to an effective cross-section under a uniform stress [19] [20]. Subsequent resistance calculations are based on the computed effective widths and effective areas, with significantly different properties such as moment of inertia and centre of gravity. Figure 2.14(a) shows a MIC-120 K-Span gross cross-section and its area,

compared to its significantly reduced and disjointed effective widths and effective area in Figure 2.14(b).

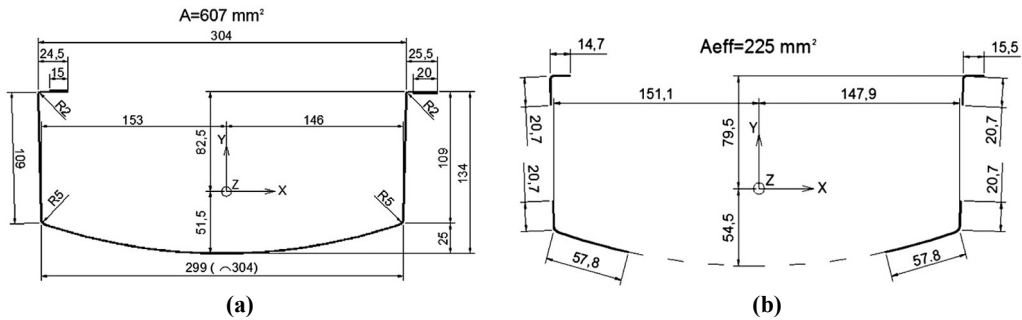


Figure 2.14 - (a) MIC-120 gross cross-section and (b) MIC-120 effective cross-section (mm) [8]

2.3.2 Double Corrugation

While many K-Span cross-sectional panels as seen in Figure 2.2 and Figure 2.3 exist, they are all self-supporting steel arches cold-rolled to cause corrugations in the longitudinal and transverse directions. The distinctive bi-directional corrugations make K-Spans doubly-corrugated; it inhibits the use of existing cold-formed steel codes for design [1] [5] [8]. Single-corrugation is universally known as corrugation, a stiffening process at the core of cold-formed steel, and widely used and explored in currently available codes. However, there is a lack of codes, or annexes of codes that govern the design criteria for doubly-corrugated cold-formed steel.

Recent research that compared smooth wall singly-corrugated specimens with curved doubly-corrugated specimens have shown that a loss in bending capacity could be upwards of 45% [1] [7] [8] [21], and is thought to be a main contributor to various K-Span structure collapses. The transverse corrugations have been described by Cybulski et al. (2014) to exhibit “accordion behaviour” as seen in Figure 2.15, where they deform elastically and plastically under axial compression approximately twice as much when compared to smooth wall specimens, in addition to having less positive or negative bending capacity [1] [8]. K-Span arches are able to sustain loads past their critical buckling point, with their transverse corrugations experiencing accordion-like compression and local snap-through buckling events, with elastic and plastic deformations.

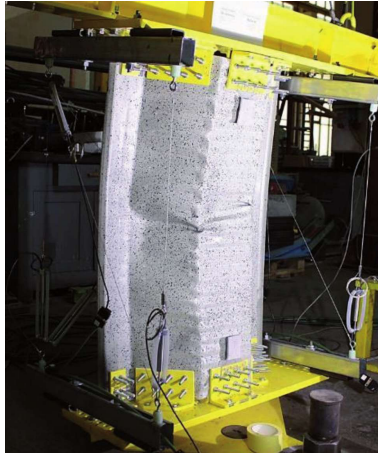


Figure 2.15 - Accordion-behaviour of MIC-240 specimen under compression and negative moment [1]

2.3.3 Column-Like Interaction Behaviours

The failure-envelope of K-Span arch components have been established with results from experiments as seen in Figure 2.15, recording positive or negative bending capacities in conjunction with compression capacities [1] [3] [22]. The resulting graph seen in Figure 2.16 by Lepine et al. (2022) resembles an axial load-bending moment interaction diagram used to characterize acceptable combinations of axial load and bending moment capacities of a column [3]. The load combinations within the triangles are deemed safe, which may be turned into factored snow load pressures that the particular component could theoretically support as part of a K-Span structure. Additionally, it could be used to guide overall design, for example, the axial load resistance would be increased if the bending moment is reduced throughout the arches via manipulation of structural support conditions.

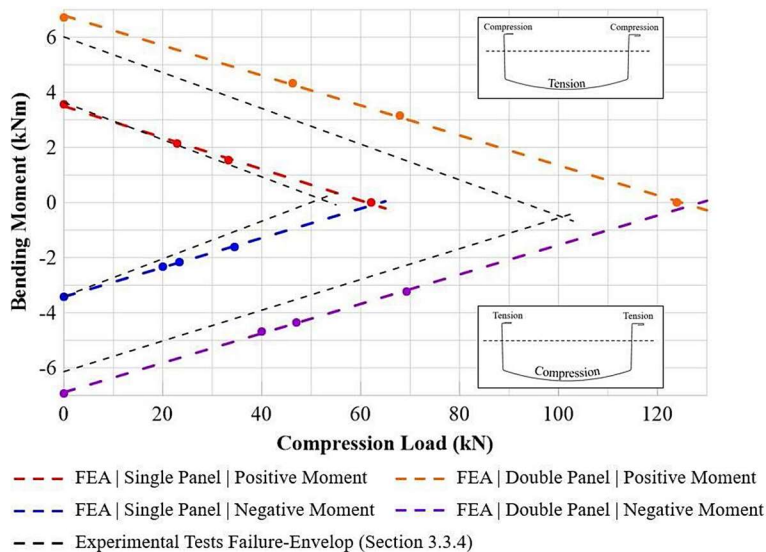


Figure 2.16 - Numerical and experimental axial load-moment interaction diagram for single- and double-panel MIC-120 components [3]

2.3.4 Codes and Specifications

Current cold-formed steel codes in North America and Europe only cover the effects of longitudinal corrugations, expecting thin-walled members to behave according to the plate buckling mechanism [3]. There are no codes covering cold-formed steel with transverse corrugations and its accordion-like behaviour. There exists a specification under trial in China since 2005, the Technical Specification for Arched Corrugated Steel Roof (Trial) CECS 167:2004 (CECS167) [23].

2.3.4.1 North America

The K-Span structure was developed in the USA to withstand design load combinations found in the standard, American Society of Civil Engineers 7 (ASCE-7) Minimum Design Loads for Buildings and Other Structures [24]. A design report produced by M.I.C. Industries in 2019 suggests that the K-Span arches were developed in a two-dimensional manner, for each individual arch to resist shear, bending and/or compression as prescribed by the specification, American Iron and Steel Institute S136 North American Specification for the Design of Cold-Formed Steel Structural Members (S136) [24]. Consequently, the K-Span structure is theoretically not limited to any longitudinal length and any additional strength from the end walls is considered a bonus.

S136 does not cover the design criteria for doubly-corrugated cold-formed steel. As it stands, the assumption is that a K-Span profile will follow the typical plate buckling mechanism expected of singly-corrugated members. It is assumed that the K-Span development process found the analysis in S136 to be adequately conservative. Various studies into K-Span profiles agree that overall structural capacity depends the most on bending resistance [11] [16] [22]. Experiments by Walentysnki et al. (2011) and Sweeney et al. (1991) determined a range of positive and negative bending capacities for the MIC-120 profile. Notably, MacDonald (2022) was able to determine comparable bending capacities analytically using S136, based on distortional buckling capacity; it accounted for transverse corrugations by calculating a larger equivalent thickness and used an artificially increased moment of inertia [16]. However, this approach disagrees with the experimental findings by Cybulski et al. (2014) that suggest a smaller equivalent thickness [1] [8].

2.3.4.2 Europe

Eurocode 3 Design of Steel Structures Part 1-3 General Rules - Supplementary Rules for Cold-Formed Members and Sheeting (EC3) is the standard for cold-formed steel design in Europe. As shown in Figure 2.17, a K-Span profile would be identified as a Class 4 member expected to buckle before reaching yield stress, given its ratio between width and thickness [8] [25]. Similar to S136, EC3 does not cover the effects of transverse corrugations and expects plate buckling mechanism [1] [3] [7] [8] [21]. In recent years, experimental and numerical work in Europe has shown that depending on the radius of K-Span arches, the loss in load-carrying capacity compared to EC3 calculations could be approximately 45%, leading to dangerous overestimation of structural capacity. With the majority of recent research effort concentrated in Europe, a standard for doubly-corrugated self-supporting arches could be expected from Europe.

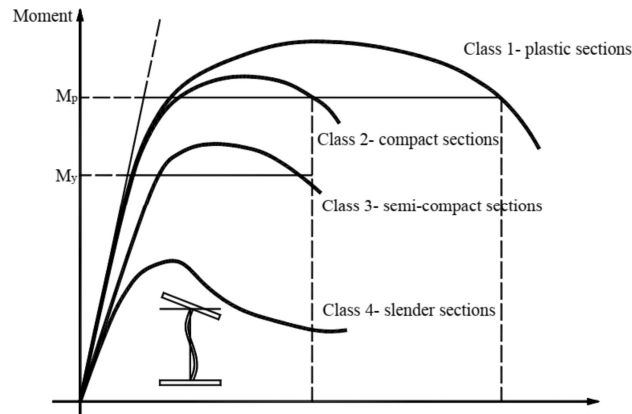


Figure 2.17 - Eurocode 3 cold-formed steel cross-section classes [25]

2.3.4.3 China

China is the largest user of K-Span or K-Span-like structures around the world. From limited suggestions in references, it could be gathered that hundreds of K-Span structures have collapsed. Many investigations, and results from small- and full-scale research projects were compiled to produce a bank of empirical data, leading to China publishing the world's first specification in 2005, the trial version of CECS167 [23]. It incorporates recommendations for calculations and design, and several provisions in construction and inspections that must be respected by domestic projects. However, it seems largely unknown and/or overlooked by researchers outside of China. Whether CECS167 is to evolve into an official code or remain a trial specification is unclear.

CECS167 provides simple calculations under linear elastic and small strain assumptions, using a planar arch model. Notably, it only considers hinge-like connections of K-Span arches to bases as seen in Figure 2.18, diverging entirely from the initial K-Span doctrine requiring fixed connections. It offers equivalent section and geometrical properties and coefficients for applications that cover various steel thicknesses and strengths, arch radii, rise-to-span ratio for the two common K-Span profiles as seen in Figure 2.2. An example table of cross-sectional properties for YJ3011, a close match to MIC-120 profile, is shown in Figure 2.19. Most importantly, it offers two conservative methods to check the two-dimensional, in-plane resistance of individual arches under the intended loads [23] [26].

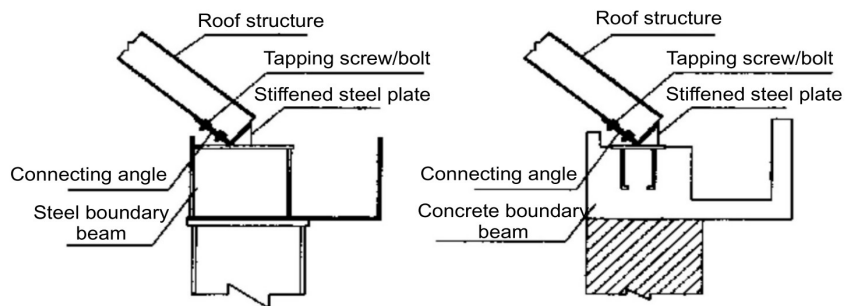


Figure 2.18 - Hinge-like connection method between K-Span arches and base [23]

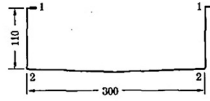


Figure D.0.1 Rectangular groove structural unit

Table D.0.1 Equivalent section characteristics per unit width of arched corrugated steel roof in Type YJ3011

Plate thickness (mm)	A_{eq} (cm ²)	I_{eq} (cm ⁴)	$W_{eq}^{(1)}$ (cm ³)	$W_{eq}^{(2)}$ (cm ³)
0.8	2.4764+0.14734r -0.00179r ²	60.68807+2.64452r -0.03807r ²	8.19225+0.37417r -0.00749r ²	10.00449+0.40023r -0.00145r ²
0.9	2.85387+0.19519r -0.00249r ²	70.79445+3.21631r -0.03679r ²	9.82775+0.40017r -0.00672r ²	11.33902+0.56181r -0.00163r ²
1.0	3.48511+0.21613r -0.00218r ²	83.43775+3.61434r -0.03024r ²	11.92385+0.38327r -0.00481r ²	12.97903+0.69044r -0.00163r ²
1.1	3.80873+0.29297r -0.00374r ²	88.45267+5.34056r -0.06855r ²	13.22833+0.49589r -0.00731r ²	12.3685+1.21533r -0.0109r ²
1.2	4.20758+0.37243r -0.00552r ²	95.22149+7.09513r -0.11142r ²	14.86424+0.5822r -0.00923r ²	11.17039+1.89924r -0.02771r ²
1.3	5.55946+0.35368r -0.00479r ²	124.87838+6.42439r -0.09176r ²	17.9959+0.51334r -0.00725r ²	16.6607+1.87232r -0.02585r ²

Figure 2.19 - Equivalent cross-sectional characteristics of a profile similar to MIC-120 [23]

Numerous Chinese references with experiments and FEA validate the utility of CECS167 in providing a simplified and conservative design process [27]. Due to the general lack of references with full English translations, some references only provided anecdotal information through translated abstracts.

2.4 Structural Capacity

K-Span structures were developed using a two-dimensional frame element approach, with each individual arch designed to resist in-plane shear, bending and/or compression. It imposed no lower or upper limits to the longitudinal length; it is apparent that three-dimensional considerations such as the ratio between arch span and longitudinal length, end wall strength and out-of-plane behaviours are lacking [24] [28]. Satisfactory service with the American military engineering community demonstrated over time that its two-dimensional design was adequately conservative. However, collapses for non-American users triggered in-depth analyses beyond two-dimensional frame elements. Two parallel streams of research emerged largely from China and Europe.

Starting in the 1990s, numerous collapses in China signaled an urgent requirement for a governing document. In order to publish design guidelines, Chinese researchers emphasized large-scale testing and planar arch modelling [6] [29], rather than in-depth studies of non-linear materials, geometry and post-buckling behaviours. The main hypothesis supported by testing, was that behaviour in global stability and buckling controlled the structural capacity more than the material strength [27] [29]. In some cases, large-scale tests were conducted on intact arches, in-situ beside collapsed structures, [6]. As well, the anisotropic properties of a doubly-corrugated surface were approximated with orthotropic plate analyses using FEA. Empirical data gathered from research were turned into formulas using equivalent characteristics and elastic constants to provide simple safety

calculations. Ultimately, it converged to the standardization of design, construction and inspection methods under the trial specification CECS167. Further research continued to validate the formulas and tables of constants in CECS167 [26]. No translated literature was available to report on CECS167-compliant structures. Regardless, thousands of K-Span structures built pre-CECS167 may remain susceptible to sudden collapse.

In the recent years, European researchers emphasized precise small-scale testing and three-dimensional modelling of doubly-corrugated profiles. Their behaviours with non-linear material and imperfect geometry, large deflections and all in-plane and out-of-plane buckling modes were tested and represented in FEA [1] [7] [8] [30]. The current focus is improving FEA to accurately model K-Span structures through elastic buckling, non-linear buckling and post-buckling behaviour. Walentynski from the Silesian University of Technology is the most published author on K-Span structures working towards a European specification. Interestingly, however, Walentynski et al. (2011) in their comprehensive review [1] of research into K-Span structures with over a hundred references do not note the existence of CECS167.

2.4.1 Bending Capacity

It is widely accepted that buckling and hinge formation under bending moments control the ultimate capacity of K-span structures [1] [8] [11] [16]. In Canada, MacDonald (2022) concluded that the ultimate capacity of a K-Span structure is controlled by positive bending capacity under asymmetrical snow and rain loads, regardless of construction method [16]. The concept was that the compression under positive bending as seen in Figure 2.20(a) would always cause the seamed flat lips to locally buckle first, as seen in Figure 2.20(b), in agreement with European researchers [22]. The wind loads were excluded for the asymmetrical loading cases, as the windward side of the structure would be nearly free of snow according to the NBCC, and any wind would counteract the critical positive bending on the windward side [31]. The frame element FEA indicated that some of the K-Span structures in DND are at risk of failure under 1-in-50-year snow events and require retrofit [16]. Lepine et al. (2022) conducted small-scale capacity tests using single and double MIC-120 panels produced by CAF members, but its findings did not definitively support the theory that positive bending capacity governs collapses [3].

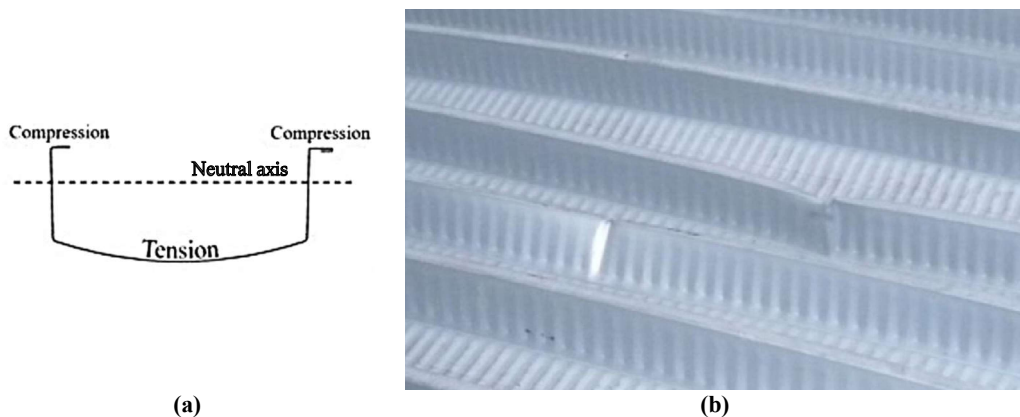


Figure 2.20 - (a) Stress profile of MIC-120 cross-section under positive bending moment and (b) Seamed lips buckling [3] [8]

Positive and negative bending capacities of four-panel sets of arches obtained experimentally in [11] and [32] are found in Table 2.1. Of note, Sweeney et al. (1991) built specimens as per M.I.C. Industries instructions, and obtained bending capacities at the fixed support and on the arches away from the support. Walentynski et al. (2011) built European-style specimens on articulated supports, obtaining bending capacities only away from the support. Due to different steel yield strengths and thicknesses, and arch spans, it is difficult to ascertain trends. However, it suggests that positive bending capacity, away from base, is likely the critical property that limits overall structural capacity. Although S136 does not specifically cover doubly-corrugated members, MacDonald (2022) was able to calculate similar unfactored positive bending capacities comparable to those found experimentally in Table 2.1 [16].

Table 2.1 - ABM-120 K-Span arches bending capacity results from [11] and [32]

Reference	Steel Yield (MPa)	Thickness (mm)	Capacity Type	4 Panel Positive Bending Capacity (kN·m)	4 Panel Negative Bending Capacity (kN·m)
Sweeney et al. (1991)	345	0.85	Away from support	6.4 to 9.1	9.1 to 10.7
			At fixed support	16.1 to 18.2	12.8 to 13.9
Walentynski et al. (2011)	280	1.00	Away from support	10.4	11.6

2.4.2 Support Conditions

The most important divergence in K-Span construction technique worldwide is the connection method between K-Span arches and their base supports. Despite M.I.C. Industries' instructions calling for K-Span arches to be embedded in reinforced concrete, most documented construction plans such as those from the collapsed K-Span in CFB Petawawa used articulated methods for connection [2]. European and Chinese K-Span arches are bolted to concrete or steel bases using thin pieces of steel angles, considered to be elastically articulated connections [1] [23]; however, estimated properties of the elastic articulation were not available in literature. In most cases, the structures were commonly described as hinge supported. In essence, most K-span structures worldwide were built on pinned supports rather than fixed supports, with substantially altered bending moment diagrams under loading.

The difference in distribution and magnitude of the bending moments with identical geometry, material and loading schemes could be seen in Figure 2.21, with (a) on fixed supports (a) and on pinned supports (b). Assuming that buckling and hinge formation under positive bending governs overall capacity, it is clear that support conditions influence behaviours and capacities.

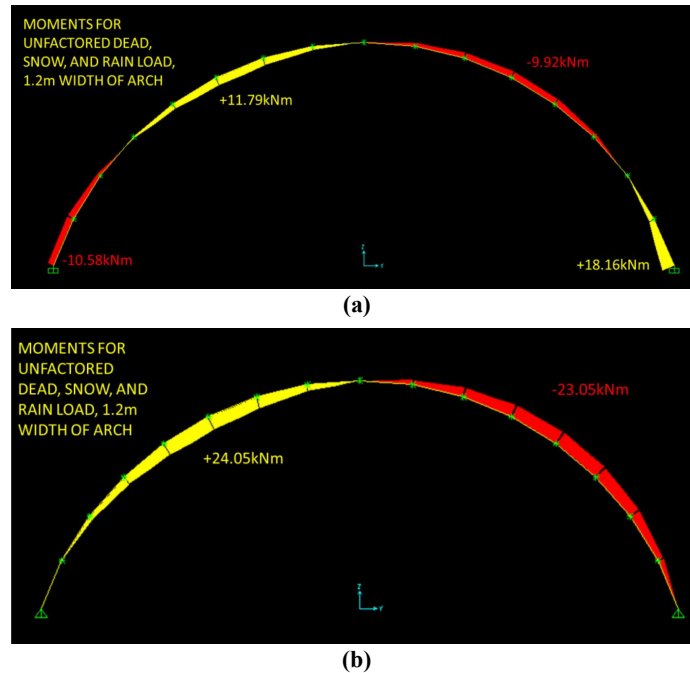


Figure 2.21 - Bending moments of a 1.00 mm thick, four-arch model with 16 m span on (a) fixed supports (b) pinned supports [16]

Quonset Hut structures (precursor to K-Span structures) are bolted rather than seamed together but possess similar doubly-corrugated profile characteristics. Support conditions seen in Figure 2.22 [33] were tested to observe differences imparted in structural behaviours. Experiments with symmetric loading showed that a Quonset Hut on fixed supports experienced positive moment reduced by 60% at the arch apex, negative moments reduced by 48% on either side, and its buckling load almost doubled when compared to hinged supports. As visualized in Figure 2.23, the experimental load-deflection curves for the three support conditions did not match those of the theoretically 100% fixed and 100% pinned [33]. Nevertheless, it is evident a retrofit could change the degree of fixity and control deflections.

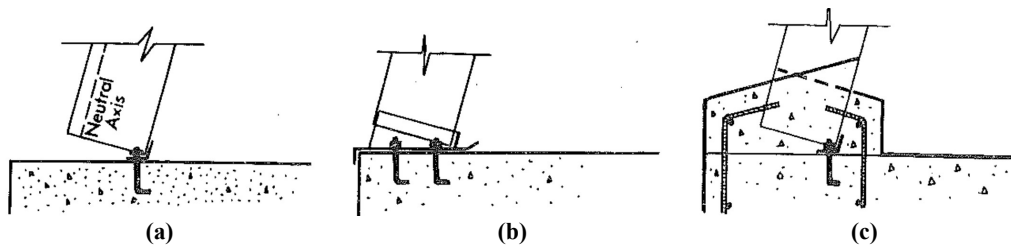


Figure 2.22 - Various Quonset Hut structure support conditions with (a) construction clip, (b) base plate and (c) ends embedded in concrete [33]

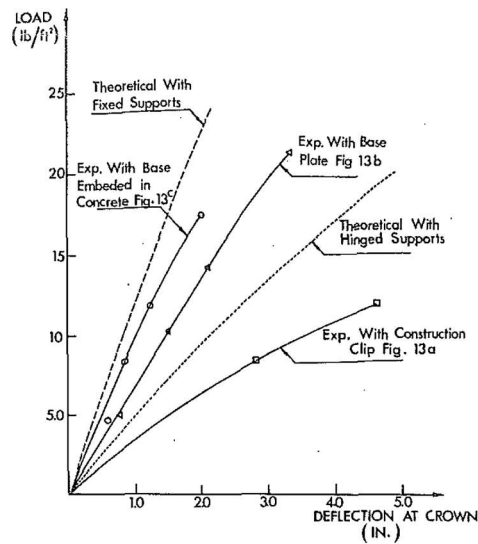


Figure 2.23 - Theoretical and experimental load-deflection curves for various support conditions [33]

European and Chinese literature do not mention any K-Span structures ever being built on fixed supports. It is stated in Walentynski et al. (2021) that elastic supports that fall between a restraint and articular support is the most appropriate support for K-Span structures [1], but the rationale remains unexplained. Literature regarding general-profile arch capacities with different support conditions reiterate the better distribution of moments, higher capacities, and higher buckling load of fixed supports, particularly for slender arches [30]. Additionally, the stiffness of the supports was found to affect the bifurcation loads and delay the onset of secondary path behaviour, where due to construction imperfection, even uniformly loaded arches eventually deflect further to one side. However, research regarding support conditions specific to the unique K-Span profiles are currently lacking; any research would be an essential contribution to more accurate FEA [1].

The rationale for building K-Span structures on articulated connections could be its unrivaled simplicity and speed. The unintended consequences are most apparent in the observable load-deflection behaviour, which may provide warning for potential collapses and prompt the need for inspection and strengthening [5]. Recent testing at RMC confirmed that support conditions greatly affect serviceability and ultimate capacities of K-Span arches [9].

2.4.3 Strengthening Methods

Deficient K-Span structures have been strengthened experimentally or modelled using FEA in sporadic instances in uncoordinated research over different periods of time [6] [13] [29] [34]. Quonset Hut structures have been strengthened as well, and the findings contribute to potential K-Span strengthening methods [33]. The objective of strengthening was to achieve one or more of the following actions: enhance distribution of bending moment, improve serviceability by reducing load-deflection, delay primary and secondary global buckling, and improve three-dimensional load-sharing using purlins.

The methods could be divided into two-dimensional (in-plane) and three-dimensional (out-of-plane) approaches. They vary widely in terms of cost, practicality and results, however, are possible to adopt for deficient K-Span structures in DND.

2.4.3.1 In-Plane Methods

K-Span arches are slender, very flexible and deflect visibly under loading. This leads to global buckling and hinge formation. Under symmetric loading, the concept is that the arches deflect and behave along a primary buckling path as seen in Figure 2.24(a). However, due to geometric imperfections, bifurcation eventually occurs, and the arch adopts a secondary buckling path, as seen in Figure 2.24(b), deflecting further to one side. Since the bending moments are greater in magnitude in the secondary buckling path, the K-Span structure is at greater risk of collapsing. Prior to the publication of CECS167, Liu et al. (1999) experimentally, and Ju and Guo (2002) numerically, used tension cables to control deflections and delay global buckling, as seen in Figure 2.25 .

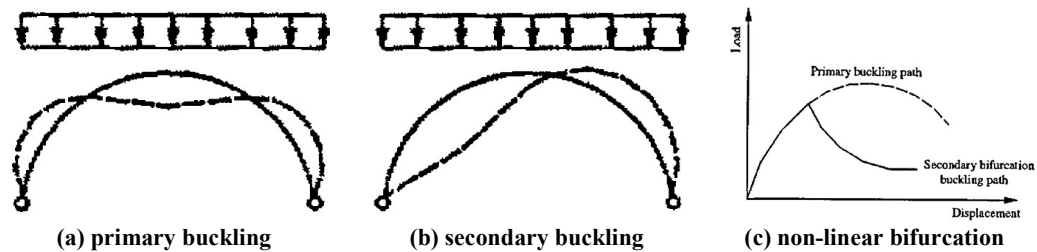


Figure 2.24 - Primary and secondary buckling path and bifurcation [29]

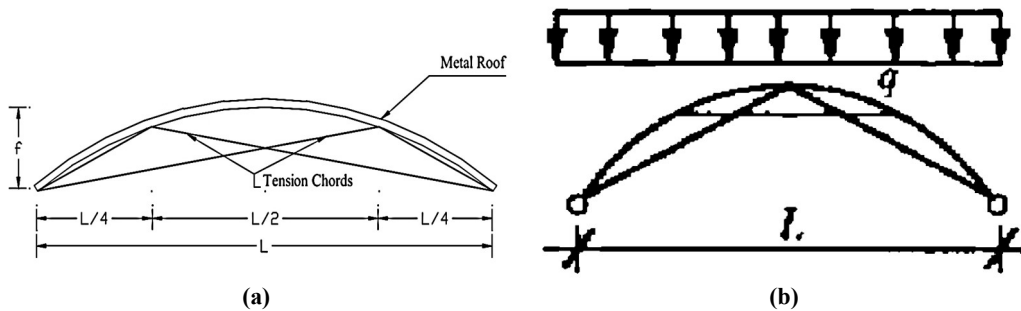


Figure 2.25 - Tension cable layouts used to control deflection [6] [29]

In [6], installation of tension chords resulted in two very different observations. Under symmetric loading, the tension cables increased the ultimate load bearing capacity by approximately 6%. Under asymmetric loading, the ultimate load bearing capacity had approximately doubled. With asymmetric loads causing positive bending expected to govern ultimate loads, the tension cables could modify the K-Span such that another feature of the structure governs ultimate loads. Although not validated experimentally, the cable layout by Ju and Guo (2002) as seen in Figure 2.25(b) is more practical for preserving operational space under the K-Span arches. As well, it is likely to raise load bearing capacities under symmetrical loading as well as asymmetrical loading, and prevent secondary bifurcation as seen in Figure 2.26.

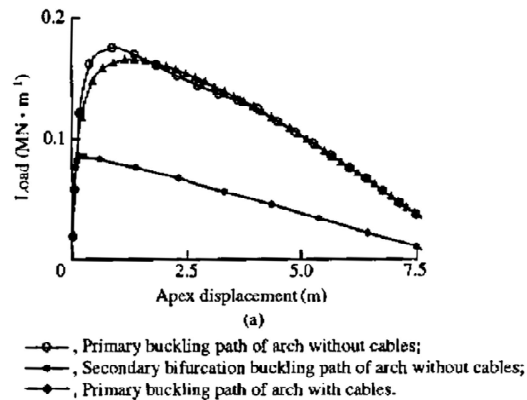


Figure 2.26 - Primary and secondary buckling path, with and without cables [29]

Tension cables would maintain the original shape of the arch, reducing second order effects such as P-delta. Accordingly, as explored in Chapter 2.3.3, the reduced bending moments would enable the arch to support more compression under load, within the safe side of the axial load-moment interaction diagram seen in Figure 2.16 [3].

Another in-plane method of manipulating K-Span arches is to reduce the effective self-supporting span. On a new construction project, Wang et al. (2012) was able to meet the dimensional requirements of the client and the CECS167 requirements by building cantilever beams that reduced the span from 35.6 m to 30.2 m, as shown in Figure 2.27. This method is attractive as it raises load bearing capacities without intruding into the operational space, however, it is not very practical to employ on existing K-Span structures.



Figure 2.27 - Reducing self-supporting span with cantilever beams protruding from supports [34]

The other option considered in [34] was fixing the arch ends in reinforced concrete, as shown in Figure 2.28. Although it was the prescribed construction method in the 1980s, the divergence of methods over decades and proliferation of pinned supports (described as “traditional” by Wang et al. (2012)) made this an unusual approach. It was afforded an FEA calculation and it predicted a more rigid structure when compared to the selected option with cantilever beams. However, this option was considered impractical and

discarded. Notably, this was the only instance in any literature specific to K-Span structures where raising the degree of fixity was considered as a strengthening technique.

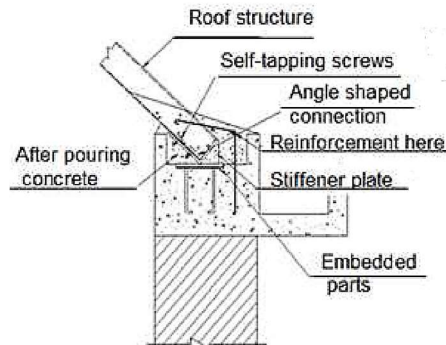


Figure 2.28 - Fixing the arches in concrete (option not taken) [34]

2.4.3.2 Out-of-Plane Methods

K-Span structures are essentially three-dimensional projections of arches designed to withstand two-dimensional loads. Therefore, load and resistance calculations are conducted in two-dimensions as if each arch stands alone in free space. Intuitively, the arches seamed together are capable of some degree of three-dimensional action, as they share loads with adjacent arches. End walls provide local stiffness to arches, but its effect diminishes as the distance from the end wall increases. Figure 2.29 is an example of a collapse, where, unlike the front end wall, the rear end wall stiffness presumably did not sufficiently restrain collapse at the rear end of the structure. Depending on the ratio between span and longitudinal length, K-Span structures could be considered a shell instead of individual arches. Greater engagement of end wall strength and load-sharing between arches were studied as a viable strengthening method.



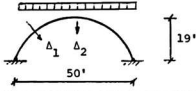
Figure 2.29 - Collapsed K-Span structure in Russia [13]

Quonset Huts were strengthened by Pierce et al. (1980) with steel purlins introducing rigidity in the longitudinal direction. The main premise of the experiment was to turn the original structure consisting of individual arches into an integrated shell by connecting the arches further and transferring end-wall strength throughout, and supporting loads in unison. For both fixed and hinged support conditions, Figure 2.30 shows the effect of the stiffeners on load-deflections at mid-arch and quarter-arch locations. It is evident that adding more rows of purlins reduce deflections and increase buckling load, with

remarkable effect on hinged support conditions. The differences in effectiveness in the 50 ft and 76 ft specimens suggest that as the ratio of longitudinal length to arch span increases, the stiffening effect diminishes. With the increase in out-of-plane engagement of end wall strength and load-sharing between arches, buckling may not be the critical weakness of the overall structural integrity [33]. Retrofit using purlins would be feasible for DND K-Span structures, given its relatively simple application and absence of intrusion into operational workspace.

Table 4a – Deflection and Buckling Loads of a Cylindrical Building

$t = 0.03$ in,
Radius, $R = 310$ in,
 $\phi_e = 75.1^\circ$



	D_x	Length of Shell						
		50 ft			76 ft			
		Δ_1	Δ_2	P_{cr}	Δ_1	Δ_2	P_{cr}	
Hinged Longitudinal Edges	Arch Analysis	0.0	0.151	0.306	40	0.151	0.306	40
	Construction stiffeners	6400	0.083	0.139	197	0.101	0.291	142
	2 stiffeners	23200	0.042	0.066	229			
	3 stiffeners	39011	0.031	0.049	269	0.082	0.134	197
	5 stiffeners	46000	0.028	0.044	275	0.076	0.123	204
	9 stiffeners	78020	0.020	0.033	292	0.061	0.095	223
Fixed Longitudinal Edges	Arch Analysis	0.0	0.063	0.113	90	0.063	0.113	90
	Construction stiffeners	6400	0.051	0.109				
	2 stiffeners	23200	0.035	0.060		0.054	0.130	
	3 stiffeners	39011	0.027	0.047		0.052	0.104	
	5 stiffeners	46000	0.025	0.043		0.050	0.097	
	9 stiffeners	78020	0.019	0.034		0.045	0.079	

Figure 2.30 - Effect of stiffeners on Quonset Hut deflections (ft) [33]

The development of K-Span structure strengthening measures are urgently required in Russia given its climatic conditions and collapses. The proposed method was bracing existing K-Span structures underneath with a traditional frame consisting of solid section frame arches and purlins. Therefore, the K-Span arches would act as outer cladding that transfers the majority of the loads to the new frame. Certainly, the bending moment in the K-Span profile is nearly removed, by up to 85%, and its buckling behaviours no longer affect the ultimate capacities. Even with the addition of a new frame on an existing K-Span structure, it is estimated that the total amount of steel saved compared to normal frame structures, is up to 20% [13]. This strengthening method is virtually building new unique structures tailored to support existing structures. It is an effective but less practical and less efficient retrofit that defeats the purpose of using K-Span structures.

2.5 Experimental Testing

The varied experiences with K-Span structures around the world compelled different experimental programs in research. In countries such as China and Russia, the sheer number of collapses necessitated urgent studies to establish guidelines, improve safety and develop strengthening methods. Understandably, the science behind K-Span behaviour was not the focus, and it may never be explored in-depth. In other countries, the relatively low numbers of K-Span structures and collapses afforded researchers the time for methodical and thorough studies. Unfortunately, research remains sporadic and

uncoordinated, as evidenced by the lack of acknowledgement of CECS167 by most researchers.

Physical experimentation with K-Span structures were generally split into two scales. Small-scale tests of K-Span arch components were conducted with the purpose of understanding and accurately modelling local behaviours of the unique doubly-corrugated profiles [1] [3] [7] [8] [11] [22]. Large-scale testing of K-span arches involved loading full-scale virgin sets of arches in a laboratory or outside, or loading existing sets of arches to observe global failure behaviours [6] [9] [11] [12] [27] [35]. Since large-scale tests always required a significant amount funds, heavy equipment, materials and instrumentation, most of the research worldwide consisted of small-scale testing with a heavy FEA component. With recent MIC-120 small-scale experiments completed by Lepine et al. (2021), the scope of this project was aimed at full-scale testing.

2.5.1 Full-Scale Testing

Testing an entire K-Span structure to failure is cost-prohibitive, given the funds and effort necessary for a single specimen of a particular geometric property to produce one result set. The practical setup for a full-scale test normally includes sets of arches, upwards of six panels seamed together and loaded to failure [6] [9] [11] [12]. The assumption is that a K-Span structure is relatively long compared to its arch span, therefore, a set of K-Span arches without any additional strength represents the two-dimensional performance of the majority of the structure, largely unaffected by the stiffening effects provided by end walls to their neighboring arches [6] [28].

Although the purpose of the two-dimensional experiments with sets of arches was to observe in-plane serviceability and ultimate capacity, it inadvertently also showcased other modes of failures such as distortional and lateral-torsional buckling characteristic of cold-formed steel. There have been challenges with removing a degree of freedom in displacement, in order to facilitate a two-dimensional experiment; elaborate lateral supports were required [6] [11]. With or without lateral supports, the unseamed outer edges of the specimens could not be expected to behave realistically. Along with normal difficulties in handling full-scale specimens, the coarse nature of complementary FEA makes it virtually impossible to directly compare results with small-scale FEA at significant levels of loading; the primacy of local or global instabilities in K-Span structures is yet to be determined [1].

The loading methods that simulate distributed loading have been largely divided between load-controlled and displacement-controlled techniques. Experiments using sandbags, as seen in Figure 2.31 achieved a better distribution of load, however, an inevitable catastrophic collapse would have allowed little time to observe ultimate failure [6] [36]. Experiments using hydraulic actuators as seen in Figure 2.32 used multiple point loads to represent distributed load in a displacement-controlled manner, allowing accurate measurement of load-deflection and sometimes, strain [1] [12]. Regardless of the loading methods, specimens were loaded symmetrically and asymmetrically to observe the differences in behaviour [1] [6] [12].

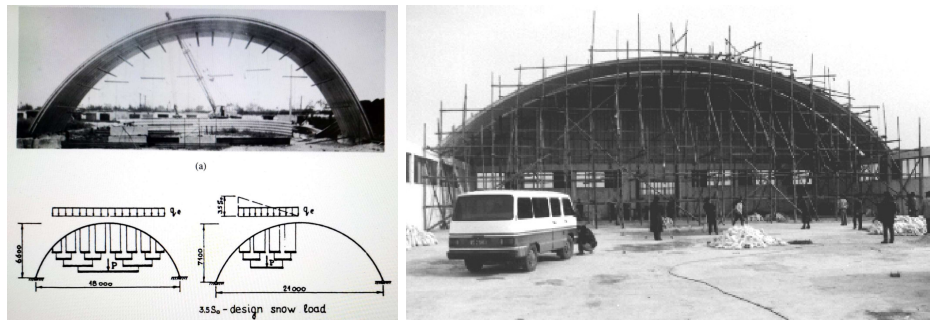


Figure 2.31 - Testing K-Span arches in load-controlled manner [6] [12]

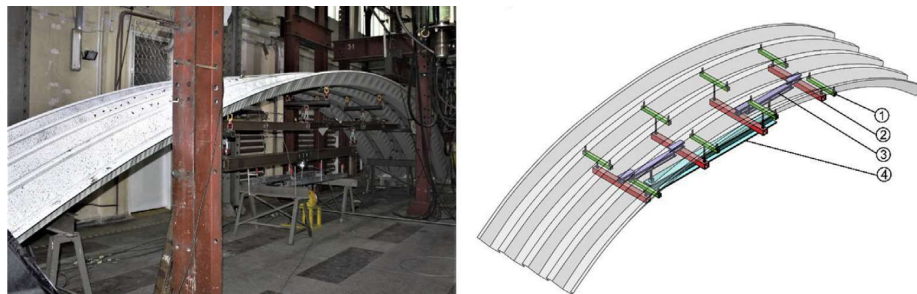


Figure 2.32 - Testing K-Span arches in displacement-controlled manner [1]

2.5.2 Full-Scale Instrumentation

Static testing of K-Span specimens requires basic measurements, namely, load, displacement and perhaps strain data depending on the purpose and scale of the experiments. For small-scale experiments, fine instruments would be installed in order to observe local behaviours. For larger specimens, the precision would be sacrificed as the quantity and magnitude of measurements would compel researchers to use less expensive and coarse instruments [1]. With the exception of Digital Image Correlation (DIC) technology recently used by European researchers to capture strain along with load-deflection data over large areas of interest, most experiments only observed discrete load-deflection in specimens.

The majority of the full-scale experiments have used potentiometers or geodetic methods to observe displacements in two-dimensions, in discrete locations at regular intervals [1] [6] [9] [12] [27] [35]. The locations were predetermined for significance such as mid-span, quarter-span, or, areas with high bending moments or displacements anticipated. Strain was normally not measured, due to the difficulty of pinpointing discrete areas of interest. Although distributed fibre optics sensors have developed and application on K-Span experiments are likely possible, no attempts were found in literature.

Load cells measuring the applied loads were not described in detail. For example, the loading apparatus in Figure 2.32 would have simulated a symmetrically distributed load using 16 point loads [1]. However, it is unclear if all of the 16 loads were equalized to guarantee symmetrical loading, or if load cells were installed at each loading point to measure throughout the test.

2.5.3 Full-Scale Experimental and Numerical Results

Full-scale experiments have been conducted in various locations without formal or standardized methods for instrumentation and loading mechanisms. Geometrical parameters in specimens such as spans, steel thicknesses, profiles and height-to-span ratios have varied widely. Unaltered and strengthened spans ranging between 12 m and 33 m have been tested to record ultimate capacities between 0.27 kPa to 3.3 kPa, while deflecting hundreds of millimeters vertically and horizontally. Divergence in deflection values between FEA and experimental results have ranged between 0% and 237% [1] [6] [11] [12] [27].

General trends could be drawn from past experiments. Larger spans have lower ultimate capacities in terms of snow pressure. Symmetric loading causes initially symmetric deflections, however, specimens always eventually adopt a secondary buckling path and lean to one side. Asymmetric loading schemes usually govern the ultimate capacities. FEA modelling usually overestimates structural capacities.

2.6 Summary

The purpose of this literature review was to introduce to the reader the concepts and the state of the art relevant to the research project. K-Span structures are built using unique cold-formed steel doubly-corrugated arches produced at the construction site. They are built in over 70 countries with diverging construction techniques, conceivably without realizing the significant effects on structural integrity. Currently, no official codes exist to ensure safe designs. Research is generally lacking, uncoordinated and disjointed between efforts studying local and global buckling phenomenon.

The rationale for building most K-Span structures on pinned supports rather than fixed supports is uncertain. It results in excessive displacements and higher positive and negative bending moments along the arches, increasing susceptibility to local and/or global instabilities, and hinge formation leading to collapse. All documented collapses, including the first Canadian collapse in CFB Petawawa, appear to have had deficient support conditions that reduced serviceability and ultimate capacity. Attempted strengthening methods in literature with varying philosophy, complexity, cost and results were explored. This research project hopes to address the deficient support conditions with a cost-effective and practical strengthening method on full-scale specimens.

Chapter 3 MANUSCRIPT: “STRENGTHENING SUPPORT CONDITIONS IN DOUBLE CORRUGATED ARCH STRUCTURES”

3.1 Abstract

This paper proposes an innovative strengthening technique for base support condition-deficient K-Span structures managed by the Department of National Defence (DND). Two K-Span specimens with retrofitted support conditions were loaded with displacement control past ultimate failure, using representative symmetric and asymmetric snow and rain distributed loading patterns as prescribed by the National Building Code of Canada (NBCC). Discrete deflection measurements were used to represent load-deflection behaviours in the in-plane axes and compared to those of similar specimens with completely fixed and pinned support conditions from a parallel project [1]. Under snow and rain load ranges for DND locations, the retrofitted specimens showed increased ultimate capacities of 31.7% and 19.4%, and improved serviceability when compared to pinned specimens.

Three finite element analysis (FEA) approaches evaluated the structural effect of the selected retrofit to be represented by a rotational spring with an average stiffness of approximately 2.4 kN·m/deg. The shell element model used the cross-sectional area reduction equation found in China’s Technical Specification for Arched Corrugated Steel Roof (Trial) CECS 167:2004 (CECS167). It appears likely that the extent of retrofit is scalable, and it could be adapted for support condition-deficient K-Span structures of varying dimensions and environmental conditions.

3.2 Introduction

3.2.1 K-Span Structure

In the 1980s, M.I.C. Industries based in the USA developed trailer-mounted Automatic Building Machines (ABM) that built steel arches on-site, to be seamed into a structure known as the K-Span [2]. K-Span superstructures are logistically simple to build, as they are virtually free of any columns, beams, trusses, or fasteners. They were completely self-supporting, weatherproof and maintenance-free. The ABM was originally meant for sale to the American military engineering community; over time, the economical and adaptable structures became popular in civilian settings [3]. K-Spans are now used in over 70 countries for schools, sports halls, storage buildings and numerous other purposes. DND adopted the MIC-120 version of the ABM in the 1990s and built dozens of K-Span structures across many Canadian Forces Bases (CFB). An example is shown in Figure 3.1 [3] [4].

The ABM is able to produce steel arches of numerous profiles, including the MIC-120 profile used by the DND. MIC-120 is a cold-formed steel profile produced from a 610 mm wide sheet steel coil, with a thickness ranging between 0.5 mm and 1.5 mm [2]. As a thin-walled steel member, it is prone to buckling locally and/or globally, at a stress below yield strength when subject to compression and bending moment. However, the arches are not categorically considered to have failed at the first instance of buckling. Redistribution of

its stresses is possible within its profile, specifically towards bent corners having experienced strain hardening, and the overall arch may sustain further loading in its post-buckled state [3].



Figure 3.1 - Example of MIC-120 K-Span structure at CFB Petawawa [4]

Standard cold-formed steel profiles covered by existing cold-formed steel codes only include corrugations imparted in a single direction. All K-Span profiles, including the MIC-120 profile, are uniquely cold-formed steel members as they encompass a transverse series of corrugations perpendicular to the longitudinal corrugations. The distinctive bi-directional corrugations characterize K-Span profiles as doubly-corrugated, which inhibits the use of existing cold-formed steel codes for design [2] [5] [6]. Recent research comparing singly-corrugated specimens with doubly-corrugated specimens have shown that transverse corrugations cause upwards of 45% losses in bending capacity [2] [5] [7]. Therefore, overestimation of a K-Span structure's capacities is likely to occur while using an existing cold-formed steel code.

Currently, there is no official code in any country for cold-formed steel that covers the unique characteristics of a doubly-corrugated profile [2] [5]. Although not often referenced in literature in the English language, there is a specification that has been under trial in China since 2005, the CECS167 [8]. It provides simple calculations for two-dimensional, in-plane resistance of individual arches against intended loads. It offers equivalent profile and geometrical coefficients for applications covering various steel properties and overall superstructure dimensions, although it is not validated outside of China. Notably, it assumes hinge-like connection method between K-Span arches and bases, diverging from initial K-Span development and construction instruction requiring fixed connections [11] [15].

In 2019, the first recorded K-Span collapse in North America occurred at CFB Petawawa under snow loads [4] [11]. Another structure built in the same manner is shown in Figure 3.1. Deficiency in its support conditions was deemed to have been a key factor in its collapse. Collapses in similarly support condition-deficient structures were reported in Poland, Slovakia, Russia, and China over the recent decades [2] [12]. A particular pair of collapses in Poland drew attention as the K-Span structures were reported to have failed under 30% of allowable snow loads calculated using European standards [13]. Conversely, there are no recorded collapses for K-Span structures built with fixed connections, as per original construction instructions. The recorded collapses suggest that support condition-deficient K-Span structures remain susceptible to collapse under snow loads.

3.2.2 Bending Capacities

MIC-120 profiles were developed in a two-dimensional manner, with each individual arch resisting shear, bending and axial stresses from in-plane environmental loads. The stiffening effect of the end walls was disregarded, as it would provide negligible effect to the majority of the arches in the structure. It is widely accepted that buckling and plastic hinge formation due to bending moments controls the ultimate capacity [1] [11] [14]. It was concluded that failure is governed by positive bending capacity under asymmetrical snow and rain loads, as the seamed flat lips always buckle first, regardless of support conditions [11]. Testing of four-arch specimens involving common K-Span material properties and dimensions established that the positive bending capacity ranges between 6.4 kN·m and 10.4 kN·m, while the negative bending capacity ranges between 9.1 kN·m and 11.6 kN·m [7] [10].

The connection method between the K-Span arches and the base is the most critical aspect that, in practice, has diverged from the original instruction from M.I.C. Industries [9]. Since support conditions influence the magnitude and distribution of bending moments of the arches under load, it is assumed to directly affect the ultimate capacity. The original instruction required K-Span arches to be embedded approximately 180 mm (7 in) in reinforced concrete, as seen in Figure 3.2(a), achieving a fixed connection. Yet, numerous structures in Canada were found to have pinned connections, as seen in Figure 3.2(b).

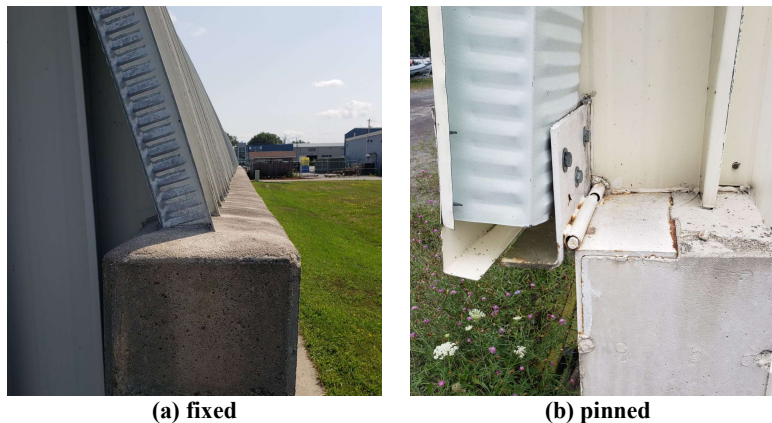


Figure 3.2 - Connection methods defining support conditions

3.2.3 Strengthening Methods

Strengthening of existing K-Span structures through stabilization, load-sharing and bending moment manipulation have been attempted experimentally and numerically in sporadic research, with varying levels of practicality and success. The limited number of attempts and a lack of parametric studies indicate that this field of research is in its early stages.

K-Span structures are very flexible and deflect visibly under loads, which may lead to global buckling and plastic hinge formation. Under symmetrically distributed loads, the arches initially deflect downwards on the primary buckling path, then eventually lean one way on the secondary buckling path. In order to delay the onset of the secondary buckling

behaviour which involves higher bending moments and P-delta effects in the arches, an array of tension cables could be used to stabilize the structure and achieve higher ultimate capacities [12] [15]. However, it is an impractical option as it intrudes into the useable interior space below the arches.

The Quonset Hut, a similar cold-formed steel structure, was strengthened by installing purlins running in the longitudinal direction from the front end wall to rear end wall [16]. Although K-Span arches were designed to individually withstand loads, purlins would enable the loads to be distributed between arches and introduce rigidity in the longitudinal direction. It would incorporate end wall stiffness, although its stiffening effects would diminish as the distance from the end wall increases. This method reduced deflections and increased the buckling load, especially on structures with pinned support conditions [16]. While this method would require lifting equipment and punching holes in an otherwise weatherproof structure, it is considered a practical non-intrusive option.

3.3 Research Objectives and Scope

The main objective of this research was to propose a non-intrusive and effective strengthening technique for existing support condition-deficient K-Span structures in DND. Supposing that an originally-pinned connection could be theoretically modified to perform more like a fixed connection, the project involved:

- Designing a non-intrusive retrofit that could be suitably scaled and adapted to site specific base support dimensions;
- Building pinned supports, implementing retrofits, and loading the specimens symmetrically and asymmetrically to observe modified behaviours and capacities of a specimen; and
- Conducting non-linear numerical analyses with shell, solid and frame element models to quantify the effect of the retrofit.

3.4 Experimental Program

3.4.1 Specimens

As tested in similar research projects in the past, a four-arch specimen width was selected to observe the two inner arches that represent most K-Span arches in a completed structure, away from stiffening effects of end walls [7] [10] [12]. While most DND K-Span arches range between 12 m and 16 m, the experimental program was designed to test 7 m span specimens, given the laboratory dimensions and the construction costs involved. 1.016 mm thick sheet steel coil was used to produce the 7 m span semi-circular specimens. Care was taken to assemble four-arch wide base support conditions according to the as-built drawing details from the structure that collapsed in CFB Petawawa, found in Appendix A. Two sets of four arches were seamed together, and bolted onto pinned supports, as seen in Figure 3.3(a), representing the common four-arch sets that would have been erected during the construction of condition-deficient DND K-Span structures.

3.4.2 Loading Scheme

The specimens were loaded past failure in a displacement-controlled manner using a hydraulic actuator through a system of swivel pulleys and steel cables, as seen in Figure 3.3(a) and Figure 3.3(b). It simulated symmetrical and asymmetrically distributed snow and rain loads as per specified snow load equation from NBCC section 4.1.6.2. Wind loads were excluded from load calculations, as the windward side of the structure would be nearly free of snow according to NBCC, and any wind would counteract the buildup of critical positive bending on the snow-loaded leeward side [11]. Point load locations were determined to best simulate the non-uniform distribution of loads as determined using NBCC, and the process is shown in Appendix B. Figure 3.4 shows the point load locations used to simulate symmetric and asymmetric loading, achieved with 16 and 8 point loads, respectively. The actuator loads that represent some of the 1-in-50-year snow and rain loads in symmetric or asymmetric setups are found in Table 3.1, and sample calculations are shown in Appendix B.

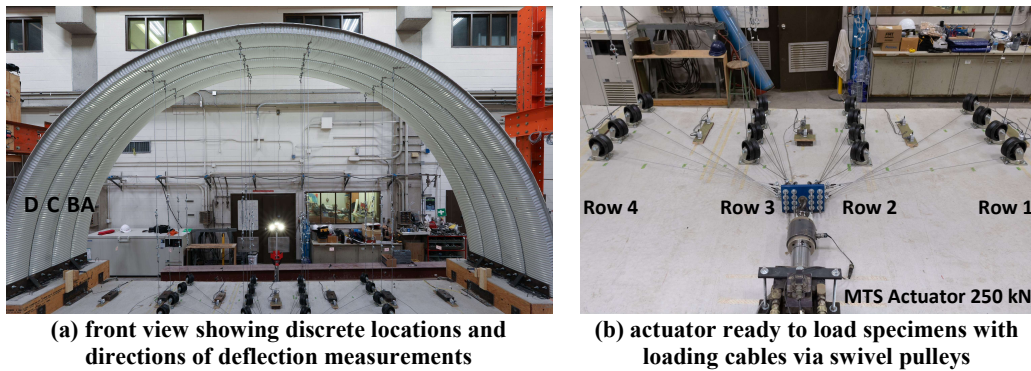


Figure 3.3 - Loading system specifically designed for experiment

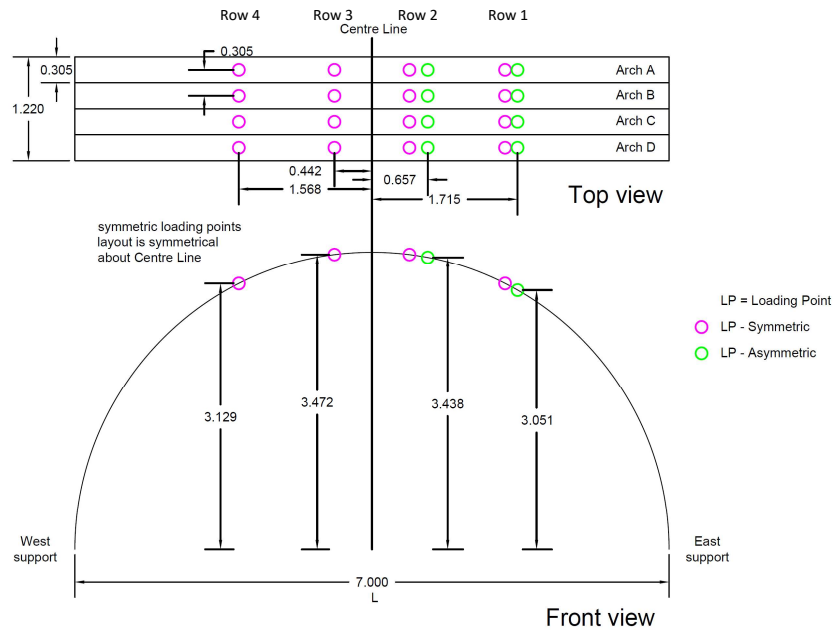


Figure 3.4 - Point load locations for symmetric and asymmetric loading (m)

Table 3.1 - Loads representing 1-in-50-year snow (S_s) and rain (S_r) loads in select Canadian locations

City, Province	S_s (kPa)	S_r (kPa)	Symmetric load (kN)	Asymmetric load (kN)
Toronto, ON	0.9	0.4	5.76	3.57
Petawawa, ON	2.6	0.4	11.29	7.63
Québec, QC	3.6	0.6	16.08	10.81
Goose Bay, NL	5.3	0.4	20.15	14.12

3.4.3 Instrumentation

The experimental data was compiled by a data acquisition system collecting discrete load and deflection measurements at 1 Hz. Two cameras photographed behaviours from the front and side view at regular intervals.

A professionally calibrated load cell for the actuator served as the principal load cell measuring the total load on the specimens. In order to observe the loading points separately, each was equipped with a custom load cell, as seen in Figure 3.5. They allowed for tension in the loading cables to be adjusted uniformly prior to the main loading sequences. All point loads were locally distributed on foam surfaces measuring 140 mm x 140 mm.

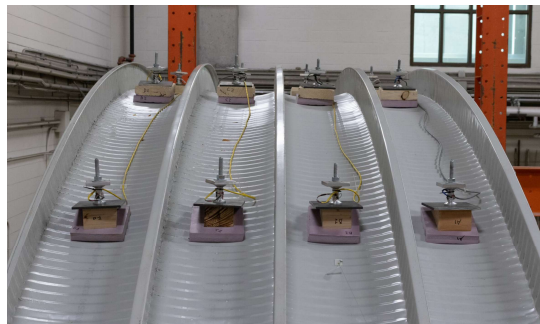


Figure 3.5 - Each loading point equipped with a 20 kN load cell

Deflection measurements were captured using string potentiometers and Linear Variable Displacement Transducers (LVDT). As indicated by orange and red circles in Figure 3.6, two vertical string potentiometers were installed for arches B and C, at every $L/8$ of the span. As indicated by red circles in Figure 3.6, one horizontal string potentiometer was installed on arch B at the $L/8$, $2L/8$, $6L/8$ and $7L/8$ span locations, as they were likely to show the highest deflections. As indicated by blue circles in Figure 3.6, two LVDTs were installed on the centre of the retrofitted hinges to monitor deflections.

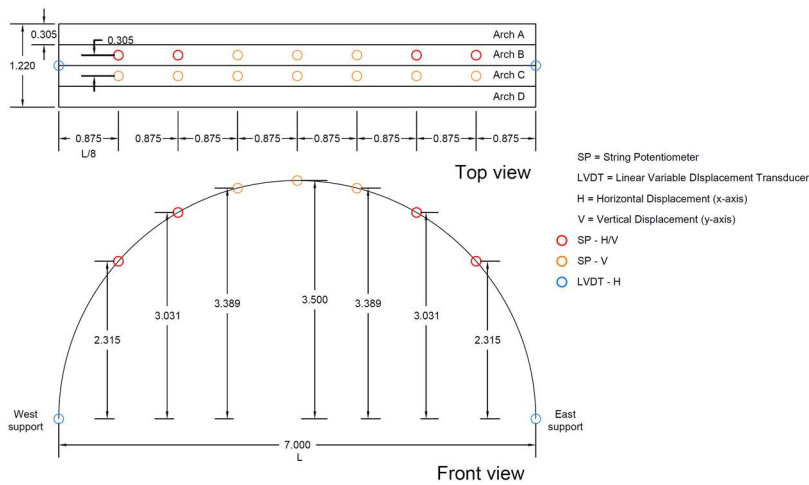


Figure 3.6 - String potentiometer and LVDT locations (m)

3.4.4 Retrofit Design

Working with the hypothesis that deficiency in support conditions is a critical vulnerability of a K-Span structure, two-dimensional, 7 m span, frame element models were created in the commercial software SAP2000 to approximate the bending moment diagrams and visualize the differences to address. Three identical frame element models under non-uniformly distributed symmetric 5.3 kPa snow and 0.4 kPa rain loads are shown in Figure 3.7 with different magnitudes of bending moments depending on the support conditions. Knowing that there are no recorded failures of arches with fixed connections, a simple modification to emulate its bending moment diagram was deemed necessary. Supposing that the bending moment diagram of a fixed arch, seen in Figure 3.7(a), could not be mimicked by an originally-pinned arch, seen in Figure 3.7(b), without the significant effort of adding a jacket of reinforced concrete, employing the effect of a rotational spring was envisioned. A rotational stiffness of 3.4 kN·m/deg was introduced to the originally-pinned connections in Figure 3.7(c) to visualize the modifications sought.

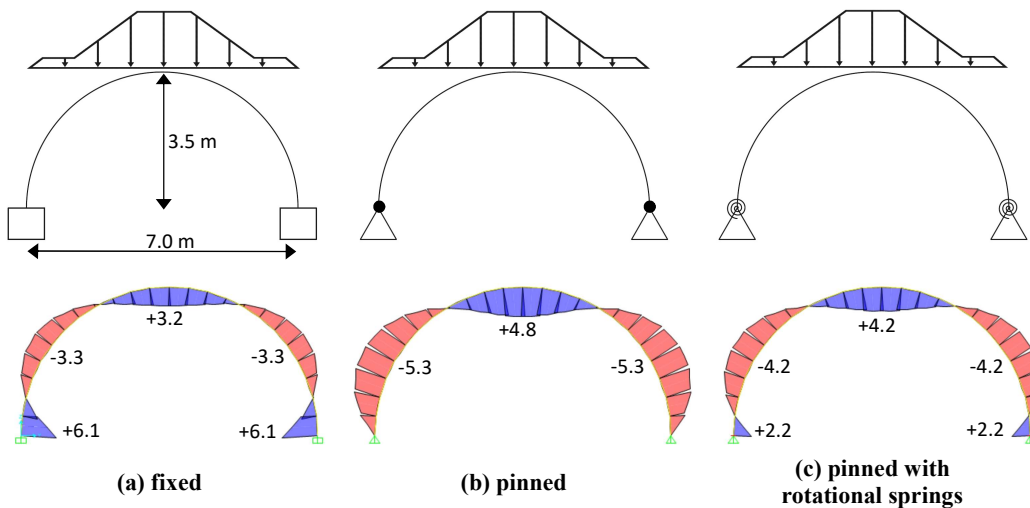


Figure 3.7 - Bending moment diagrams with various support conditions (kN·m)

Two of the main features of K-Span structures are the completely open floor plan and high vaulted ceiling that facilitate various functions, such as sports and warehousing. The retrofit should be minimally intrusive to users, simple and inexpensive to implement. Therefore, the decision was made to stiffen the hinges, that run along the entire longitudinal lengths of the supports. As some of the existing structures with hinges may have rotated to some extent at the supports since construction, a retrofit design adaptable to varying hinge angle was necessary. As well, working from the interior, and avoiding dangerous work at heights, was considered preferable.

Based on bending moments in frame element modeling under extreme loads, the moment resistance to be provided by a retrofit was $20\text{kN}\cdot\text{m}$. Additional structural steel members that, in tension, facilitate the hinge resistance to moment, was considered to be the simplest method of introducing rotational stiffness. Structural steel flat bars measuring 12 mm thick, 49 mm wide and 210 mm long, with a yield strength of 345 MPa, identified by orange components in Figure 3.8 were selected to be welded onto the existing hinges. They would serve to virtually immobilize the hinge, at any hinge angle found on site. The retrofitted support would provide bending moment resistance as the specimen is loaded, theoretically reducing the magnitude of bending moments throughout the arches. Regular on-centre spacing of 305 mm (1 ft) or 610 mm (2 ft) would allow welding to be completed where there is a natural gap between the arches and the hinge assembly, reducing the risk of unintentional damage to the thin arches. It was calculated that bars placed at 610 mm on-centre spacing along the hinges would dramatically reduce deformations in the hinge and provide adequate bending resistance, while the tensile stresses in the bars remain entirely within elastic range. The cross-sectional area of the retrofit would be 588 mm^2 for every 610 mm length along the hinge.

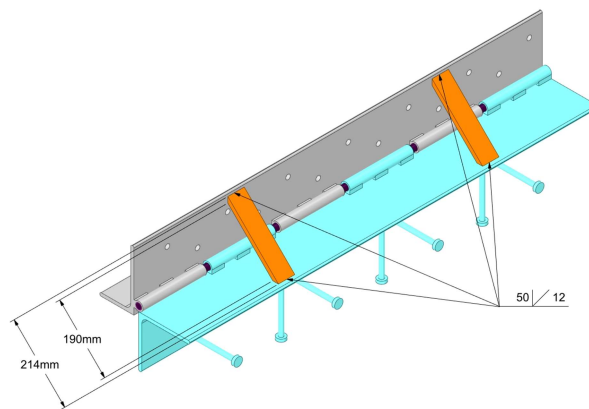


Figure 3.8 - Isometric view of hinge assembly with proposed retrofits

Of the many welding methods that could be used to facilitate the retrofit on existing hinges, as seen in Figure 3.9(a), Shielded Metal Arc Welding (SMAW), also known as stick welding, as seen in Figure 3.9(b), was selected as the welding method based on its simplicity and prevalence in industry. To increase the contact area of flat bar corners with the hinge, they were ground down approximately 4 mm to impart small bevels. The welding locations on the hinges were cleaned with a brush, until the steel was clean and bare. Figure 3.9(c) shows that for the 4 ft wide specimens, two flat bars were SMAW

welded 305 mm (1 ft) from each end, attaining 610 mm (2 ft) on-centre spacing. Appendix C contains details regarding the size, location, material and welding instructions of the retrofit.

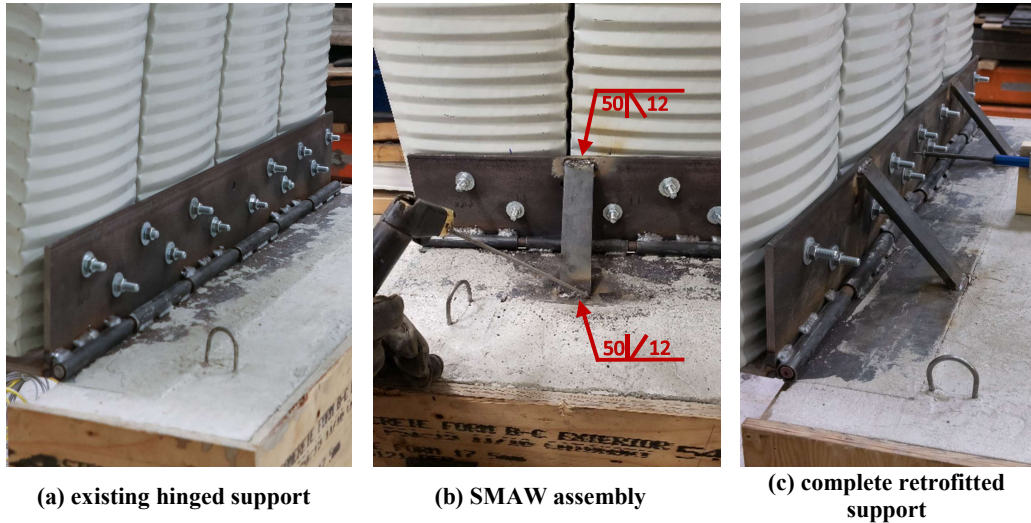


Figure 3.9 - Hinged support stiffened via SMAW welding

3.4.5 Test Procedures

The specimens were lifted, leveled, and bolted onto the pinned supports. The retrofits were welded onto the hinges and allowed to cool to ambient temperature. The string potentiometers and LVDTs were connected to the specimens at the predetermined locations as per Figure 3.6. The symmetric and asymmetric loading schemes were secured onto the specimens as per plan seen in Figure 3.4, and each cable adjusted to a uniform tension. The displacement-controlled tests were run with the actuator stroke rate at 8 mm/min, through the pre-buckling and post-buckling stages. They were run past the observed peak loads and unloaded once they were clearly unable to sustain load.

3.5 Experimental Results

The experimental program gathered two-dimensional load-deflection data to be compared directly with data from Seguin et al. (2022) that used the same specimen specifications, loading systems and instrumentation layout [1]. Comparisons between the performance of retrofitted specimens and pinned specimens confirmed the structural enhancements achieved by the strengthening technique.

As specimens were loaded far into their post-buckling stages, very large deflections were observed, beyond string potentiometer stroke at some discrete locations. The loading points arranged in Rows 1 through 4, as seen in Figure 3.3(b) did not increase in load as uniformly as intended. Rows 2 and 3, closer to the mid-arch, were more heavily loaded than Rows 1 and 4 further from the mid-arch during symmetric loading. Row 2 was more heavily loaded than Row 1 during asymmetric loading. The varying proportions in the loading points were later entered into numerical modelling. At times, the sum of all loads from loading points were upwards of 3% higher than the principal load cell measurements at the actuator.

Therefore, load losses in the loading systems were not determined. The load data from the principal load cell was used for all load-deflection analysis.

The following figures and observations summarize the load-deflection comparisons that highlight the effect of the retrofit, under symmetric and asymmetric loading patterns as prescribed by NBCC. The load-deflection curves for the full experimental range at discrete locations with maximum recorded vertical and horizontal deflections are presented. Green lines represent the intended K-Span design behaviour with fixed connections, red lines represent the currently deficient behaviours with pinned connections, and orange lines represent the behaviour of originally-pinned connections modified through retrofit. Then, load-deflection curves for a smaller load range that pertain to 1-in-50-year snow loads in select Canadian locations are presented. Quantitative and qualitative observations of specimens' behaviour at the interface with fixed, pinned and retrofitted connections are discussed.

3.5.1 Symmetric Loading

Figure 3.10 shows the retrofitted specimen before the loading and unloading stages. As expected, the specimen started on the primary global buckling path by deflecting downward and outwards in a symmetrical manner under load. At the recorded ultimate capacity of 25.4 kN, it underwent bifurcation, adopted the secondary global buckling path, and leaned towards the East support, as seen in Figure 3.10(b). Out of the four symmetrically-loaded tests between Seguin et al. (2022) and this project, this specimen was the only one to eventually lean East instead of West, while adopting the secondary buckling path behaviour [1]. It could be suggested that there were imperfections in the unaltered hinges and/or loading system, causing specimens to lean to the West by default. It appears that the retrofit removed or reduced the imperfection, resulting in a specimen that leaned towards the East.

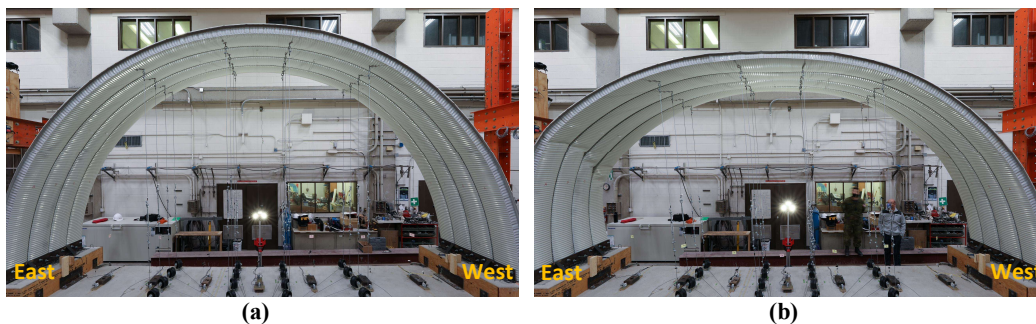


Figure 3.10 - Front view prior to (a) loading and (b) unloading stages

The first instance of buckling occurred at 24.8 kN, prior to the 25.4 kN peak. Notably, buckling under positive moment did not occur first as expected; buckling under positive moment seen in Figure 3.11(a) and negative moment seen in Figure 3.11(b) occurred almost simultaneously. This indicates that the retrofit manipulated the behaviour of the originally-pinned arch such that the internal forces approached the specimen's negative and positive moment capacities almost concurrently, potentially contributing to the 16% increase in ultimate capacity.

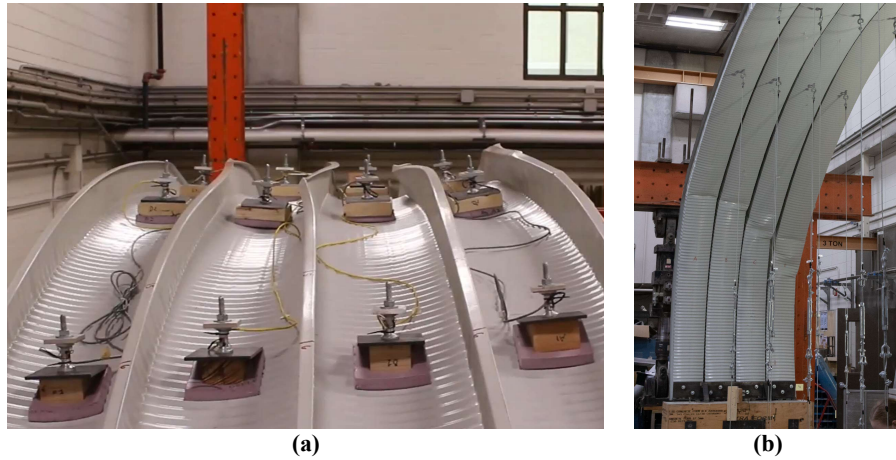


Figure 3.11 - Buckling under (a) positive and (b) negative bending moment

To visualize the effects of the retrofit, load-deflection curves from all string potentiometers were compared with data from symmetrically-loaded specimens from the control experiments [1]. Data from discrete locations with maximum vertical and horizontal deflections during the full range of loading were selected for presentation in Figure 3.12 and Figure 3.13. The load-deflection curves omit data from the initial load balancing and any data that exceeded the string potentiometer stroke. Diagrams inset in Figure 3.12 and Figure 3.13 show the discrete locations on the specimens and the symmetric non-uniformly distributed load pattern as prescribed by the NBCC. The load-deflection curves in Figure 3.12 compare three identical specimens with support conditions as the only variable. Overall, the retrofitted specimen seems to behave roughly midway between fixed and pinned specimens, especially in the pre-peak loading stage. The retrofitted specimen shows improved vertical and horizontal stiffness through its entire loading stage, which appears relatively smooth compared to the pinned specimen that presumably underwent redistribution of loads. It reached an ultimate capacity of 25.4 kN, higher than the pinned specimen's 21.9 kN. This represents a 31.7% improvement in the ultimate capacity gap between pinned and fixed specimens. Figure 3.12(a) shows that post-peak ductility in the vertical direction may have been modified negatively, however, it is difficult to judge due to the string potentiometer stroke limit being reached on the pinned specimen from the control experiments [1]. Figure 3.12(b) shows that the post-peak ductility in the horizontal direction behaves roughly midway between fixed and pinned specimens.

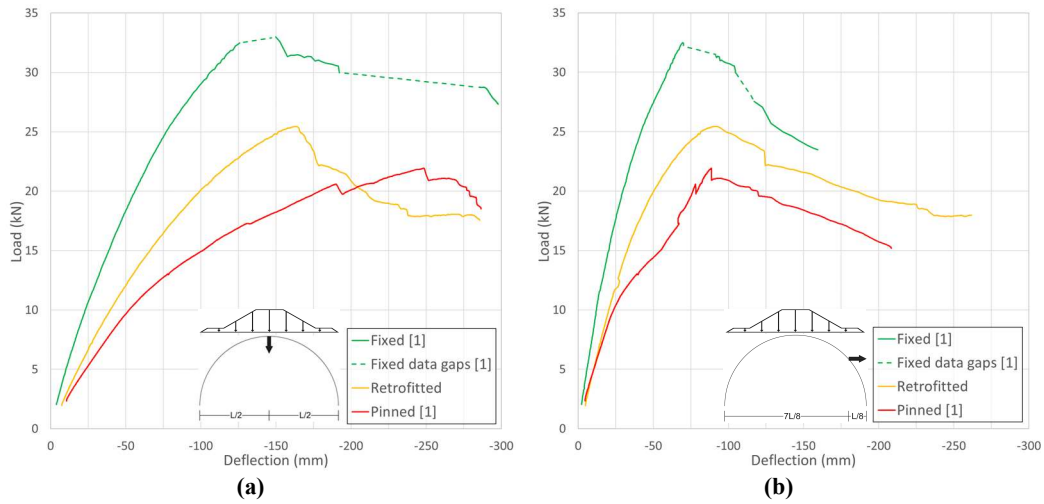


Figure 3.12 - Maximum load-deflection curve comparisons in (a) vertical and (b) horizontal directions

Figure 3.13 focuses on the load range covering 1-in-50-year symmetric snow loading to be expected in select Canadian locations. Petawawa, ON was selected as it is the only location in North America with a recorded collapse. Goose Bay, NL was selected as the DND location with the highest 1-in-50-year snow and rain loads. While serviceability for K-Span arches in terms of deflection as a fraction of its span is not discussed in literature, it was included for vertical deflection in Figure 3.13(a), to emphasize its flexible nature and demonstrate the improvements achieved through retrofit. Supposedly, a retrofitted K-Span structure in Goose Bay, NL would deflect vertically 100 mm instead of 181 mm in a 1-in-50-year snow event, presumably with less permanent deformations in the arches and less risk to the fire sprinkler and utilities attached. Overall, it is demonstrated that the retrofit is able to partially address the performance gap between pinned and fixed support conditions.

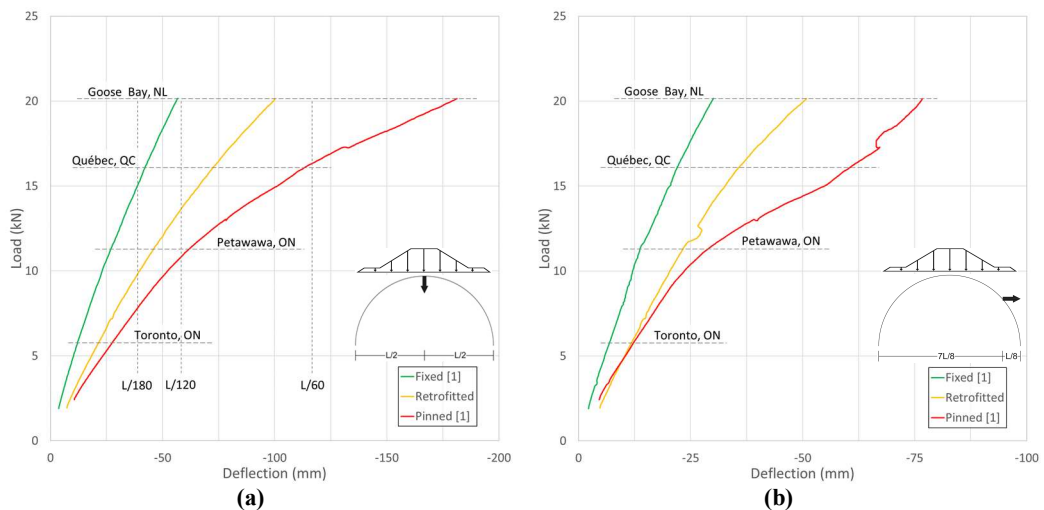


Figure 3.13 - Maximum load-deflection curve comparisons in (a) vertical and (b) horizontal directions with labels corresponding to 1-in-50-year snow loads in select Canadian locations and various serviceability limits

Table 3.2 summarizes the behaviour comparisons between support conditions in terms of ultimate capacities recorded and maximum deflections possible in DND locations during 1-in-50-year snow events.

Table 3.2 - Ultimate capacity and serviceability comparisons under symmetric loading

Support Conditions	Ultimate Capacity		1-in-50-year Max. DND Range Vertical Deflection (mm)	1-in-50-year Max. DND Range Horizontal Deflection (mm)
	(kN)	S_s (kPa)		
Fixed [1]	33.0	9.14	56.4	30.1
Retrofitted	25.4	6.84	100.1	50.8
Pinned [1]	21.9	5.78	181.3	76.7

3.5.2 Asymmetric Loading

Figure 3.14 shows the retrofitted specimen before the loading and unloading stages.

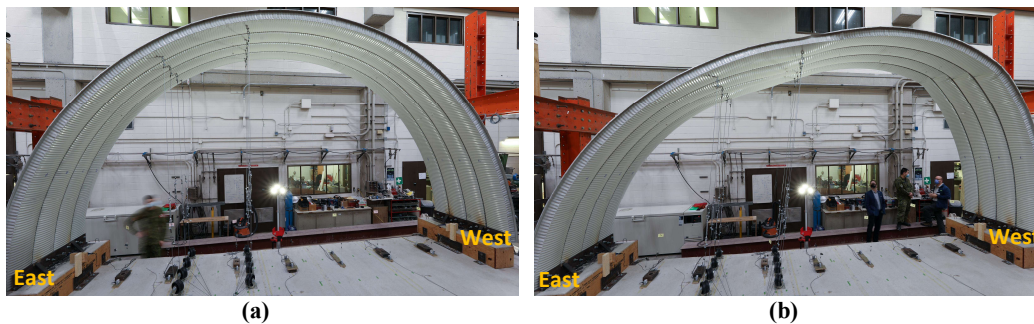


Figure 3.14 - Front view prior to (a) loading and (b) unloading stages

As anticipated from the loading system design, the specimen leaned West and immediately adopted the secondary global buckling path. As expected, the buckling seen in Figure 3.15(a), caused by positive bending moment, governed the overall capacity. The ultimate capacity of 22.3 kN was reached after three small peaks in load-deflection, demonstrating resilience at its near-peak load range when compared to the pinned specimen. Contrary to expectations from MacDonald (2022), the asymmetrically-loaded specimens from the control experiments and this project showed higher ultimate capacities than symmetrically-loaded specimens, in terms of ground snow load pressure, S_s [1] [11]. The retrofitted specimens reached an ultimate capacity corresponding to S_s of 8.64 kPa under asymmetric loading, and S_s of 6.84 kPa under symmetric loading. This anomaly may be attributed to the relatively small specimen spans showing atypical behaviours, compared to specimens in literature ranging from 12 m to 33 m in span [2] [12] [14] [17]. Another source of divergence is the loading scheme, where specimens were subject to a non-uniformly distributed load as per NBCC calculations, while past experiments used uniformly distributed load [2] [12] [14] [17].

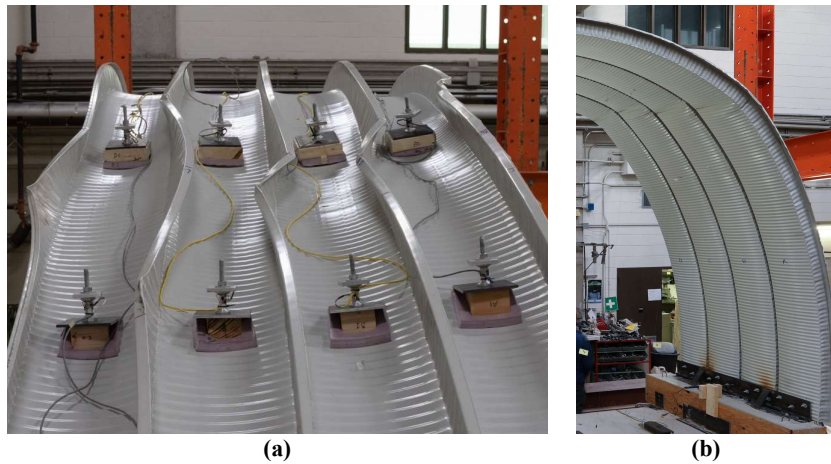


Figure 3.15 - Buckling under (a) positive and (b) negative bending moment

To judge the effects of the retrofit, load-deflection curves from all string potentiometers were compared with data from asymmetrically-loaded specimens [1]. As completed for symmetrically-loaded specimen in Chapter 3.5.1, discrete locations with maximum vertical and horizontal deflections were chosen for presentation in Figure 3.16 and Figure 3.17. The load-deflection curves omit data from the initial load balancing and any data exceeding the string potentiometer stroke. Inset diagrams in Figure 3.16 and Figure 3.17 show the discrete locations and the asymmetric non-uniformly distributed load pattern as prescribed by the NBCC. Figure 3.16 compares the load-deflection curves with support conditions as the only variable. In terms of stiffness, the retrofitted specimen performs between fixed and pinned specimens, especially in the pre-peak loading stage. The increase in stiffness relative to the pinned and fixed specimens is more pronounced in the vertical than the horizontal direction. It reached an ultimate capacity of 22.3 kN, higher than the pinned specimen's 21.2 kN. This represents a 19.4% improvement in the ultimate capacity gap between pinned and fixed specimens. Overall, the specimen showed an increase in ultimate capacity, along with significant improvements in near- and post-peak ductility.

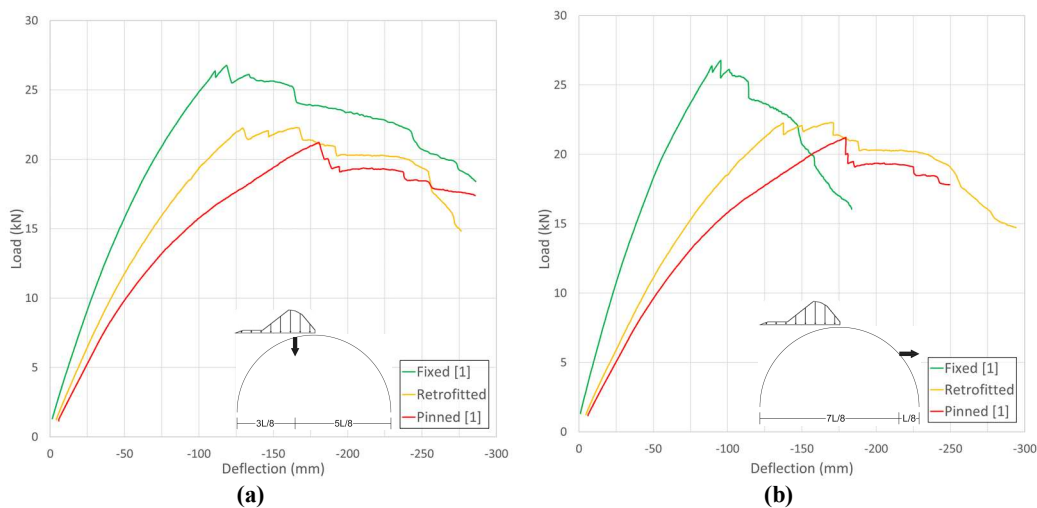


Figure 3.16 - Maximum load-deflection comparisons in (a) vertical and (b) horizontal directions

As detailed for symmetrically-loaded specimens in Chapter 3.5.1, Figure 3.17 below focuses on the load range covering 1-in-50-year asymmetric snow loading to be expected in select Canadian locations. Sample serviceability in terms of deflection as a fraction of its span is also included for vertical deflection in Figure 3.17(a), to demonstrate the improvements achieved. Supposedly, the vertical deflection of a retrofitted K-Span in CFB Petawawa would improve roughly from $L/180$ to $L/240$ under a 1-in-50-year snow event. Notably, unlike with the symmetrically-loaded specimen, the magnitude of deflection in the vertical and horizontal directions are almost identical. It appears in Figure 3.17(b) that the retrofit only modestly restrains the K-Span arches from leaning to one side. Overall, it is demonstrated that the retrofit partially addresses the performance gap between pinned and fixed support conditions.

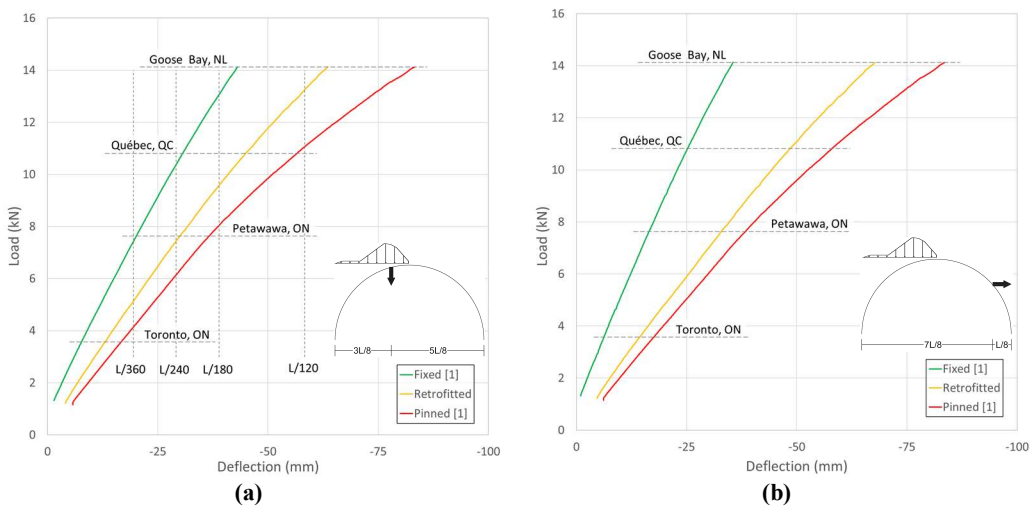


Figure 3.17 - Maximum load-deflection comparisons in (a) vertical and (b) horizontal directions with labels corresponding to 1-in-50-year snow loads in select Canadian locations and various serviceability limits

Table 3.3 summarizes the behaviour comparisons between support conditions in terms of ultimate capacities recorded and maximum deflections possible in DND locations during 1-in-50-year snow events.

Table 3.3 - Ultimate capacity and serviceability comparisons under asymmetric loading

Support Conditions	Ultimate Capacity		1-in-50-year Max. DND Range Vertical Deflection (mm)	1-in-50-year Max. DND Range Horizontal Deflection (mm)
	(kN)	S_s (kPa)		
Fixed [1]	26.8	10.5	43.1	35.5
Retrofitted	22.3	8.64	63.5	67.7
Pinned [1]	21.2	8.18	83.3	83.6

3.5.3 Retrofitted Support Condition

As envisioned during the conceptual stage, and supported by the load-deflection behaviours detailed in Chapters 3.5.1 and 3.5.2, the retrofit is presumed to have been successful in modifying specimens' bending moment diagrams under load. In addition, as

expected, the retrofitted specimens did not reach the capacities of those for originally-fixed supports. Figure 3.18 visually compares three symmetrically-loaded post-peak specimens with their respective support conditions. Hinge angles calculated using LVDT deflection measurements at the centre of the hinge-specimen connection helped characterize the retrofit as a stiff spring. Various qualitative and quantitative observations were drawn by comparing the connection interface between specimens and support conditions.

The specimen fixed in reinforced concrete bases from Seguin et al. (2022), as seen in Figure 3.18(a) experienced no displacement in all directions at the interface. Although the bending moment is theoretically highest in magnitude at the interface, the bending capacity at the interface was also expected to be higher than any other location along the arches [10]. Until the specimen was loaded past its peak and two plastic hinges were formed, there was no visually noticeable activity at the interface. As indicated by red dotted circles in Figure 3.18(a), the seamed lips eventually underwent buckling under positive moment as the post-peak loading progressed, forming the last two plastic hinges that accelerated the loss of load capacity. Since there are no reported collapses for K-Span structures built with fixed support conditions, the final buckling at the interface may only have been observed in laboratory experiments.

The specimen ends bolted onto the hinges as per CFB Petawawa K-Span as-built details, as seen in Figure 3.18(b), showed significant displacement and disfigurement during the experiment [1] [4]. The change in hinge angle and plastic hinge formation, at the location indicated by a red dotted circle in Figure 3.18(b), were clearly visible during the pre-peak loading stage. The excessively bent webs are presumed to have accelerated the displacements that caused the specimen to displace downwards overall, leading to critical mid-arch buckling under positive moment.

The specimen bolted onto retrofitted hinges showed modified behaviour at the hinge-specimen interface. As seen in Figure 3.18(c), the retrofit virtually removed the rotational DOF of the hinge, enabling the specimen to transfer axial load and moment to the reinforced concrete base. At the interface, this was visually confirmed by the reactions along the upper half of the hinge assembly. As discernible from the straight dotted white line for reference in Figure 3.19(b), the upper half of the hinge assembly was temporarily deformed while transferring the moment from the specimen through the retrofit steel bars in tension. However, a limitation of the minimalistic retrofit design became apparent. Unlike the specimen with its entire profile embedded 180 mm (7 in) into reinforced concrete, the transfer of moment occurred through the bolted connections on the web. As such, the lips and portions of the flanges on the compression side of the specimen's neutral axis were unrestrained from buckling, in directions indicated by yellow arrows in Figure 3.19(a). Future retrofit designs could study the effects of incorporating bracing of the lips from buckling under positive moment; it may improve capacities and post-peak ductility.

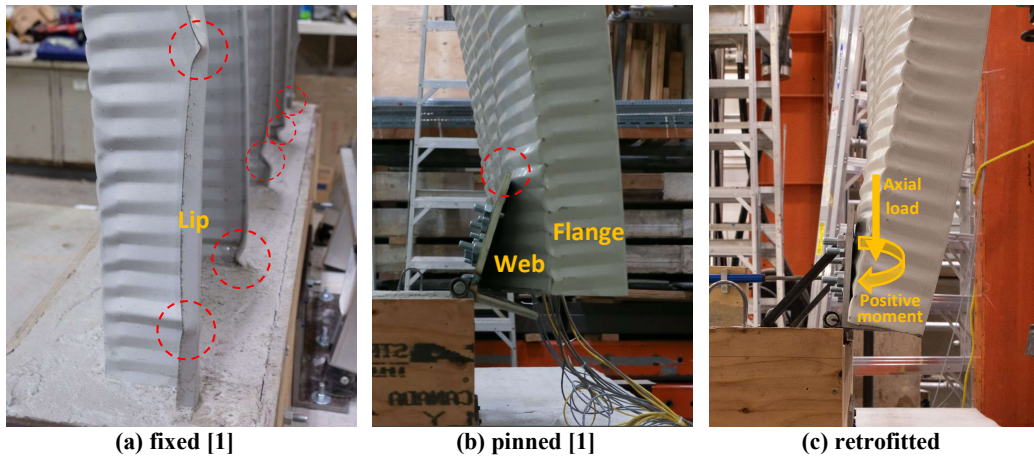


Figure 3.18 - Post-peak specimens on various support conditions

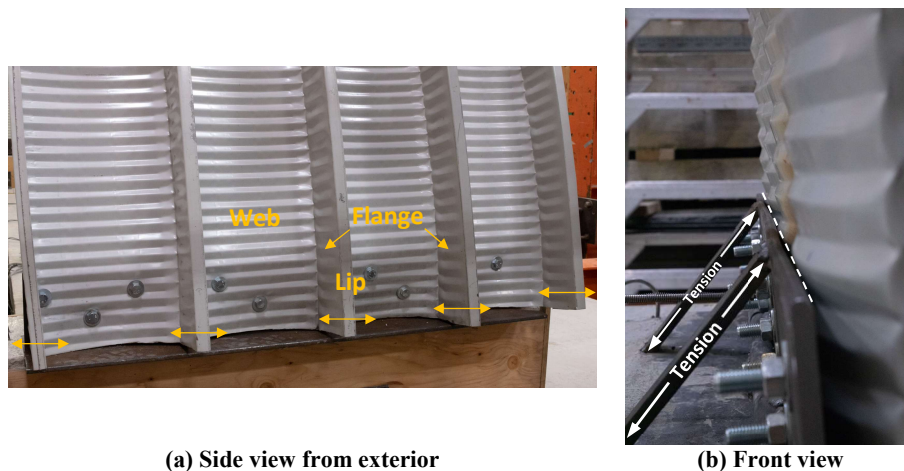


Figure 3.19 - Post-peak retrofitted support condition

LVDT measurements confirmed that the retrofits effectively limited the hinge movement, as seen in Figure 3.20 comparing a retrofitted hinge to its counterpart in a pinned specimen test from [1]. Notably, hinges from the tests on retrofitted support conditions returned to their starting points, demonstrating that it modified the specimen behaviour while tensile stresses in the retrofit bars remained within elastic range. All hinge rotation angles derived from the LVDT deflection measurements revealed a relatively linear relationship with applied loads for both symmetric and asymmetric load patterns, as shown in Figure 3.21. For visualization, secant lines were drawn between the origin and the hinge angles at loads representing 1-in-50-year snow event in Goose Bay, NL. These observations verified that the retrofit successfully introduced the effect of an approximately linear rotational spring, improving ultimate capacity and serviceability.

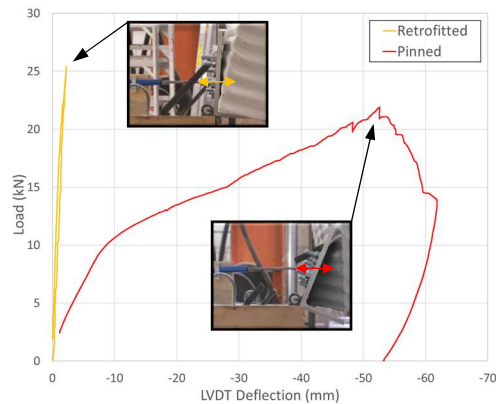


Figure 3.20 - Full range LVDT deflection comparisons under symmetric loading

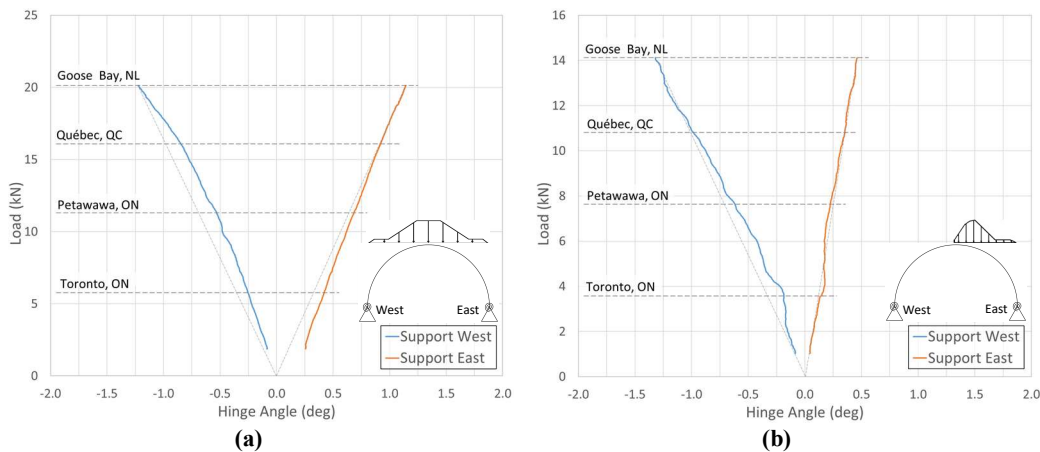


Figure 3.21 - Hinge Load-angle curves under (a) symmetric and (b) asymmetric loading patterns with labels corresponding to 1-in-50-year snow loads in select Canadian locations

3.6 Numerical Work

Non-linear FEA involving shell, solid and frame element models were created and calibrated to largely follow experimental load-deflection data from Seguin et al. (2022). With the purely pinned and fixed models providing the relative boundaries, experimental data from retrofitted specimens quantified the effect achieved by the retrofit.

3.6.1 Shell Model

A planar three-dimensional shell was the most appropriate dimension for modeling the thin-walled steel geometry. Specimens were built without corrugations in commercial software ANSYS, as seen in Figure 3.22. Refined models complete with corrugations for small component buckling modeling from Lepine et al. (2022) was considered computationally unmanageable to scale and model full-scale specimens [3]. To account for the effects of double corrugations, the empirically-determined CECS167 cross-sectional area reduction equation was adopted. The specimen steel thickness of 1.016 mm was replaced with 0.700 mm throughout, except for the seamed lips with quadruple thickness of 2.800 mm. The material yield strength of 360 MPa, ultimate strength of 530 MPa and

Young's Modulus of 200 GPa from the true stress-strain curve from Lepine et al. (2022) were used. Figure 3.22(a) shows the point load locations where loads were assigned in incremental load steps with imperfect distribution, maintaining relative load cell proportions as recorded during the experiments. Figure 3.22(b) shows a quadrilateral-dominant mesh consisting of higher-order SHELL281 elements with 8 nodes and 6 degrees of freedom (DOF). Fixed support conditions as seen in Figure 3.23(a) were attained with blue surfaces constrained in all DOF. Pinned boundary conditions as seen in Figure 3.23(b) were modeled as a revolute joint with blue surfaces having a single rotational DOF around the red hinge pin constrained in all DOF. The retrofitted support condition was evaluated in terms of hinge stiffness, using hinge torsional stiffness inputs on the revolute joint.

As loss of friction in the seamed lips was not observed during the experiments, the lips were represented with bonded contact, which solved linearly. Non-linear material with a bilinear isotropic steel using yield strength of 360 MPa and ultimate strength of 530 MPa was tested, but it produced similar load-deflection curves compared to a linear material. Therefore, the models were run with linear material. The only non-linear aspect employed during the analysis was geometry, because large deflections and rotations were expected. The distributed sparse matrix direct solver used a full Newton-Raphson solution procedure.

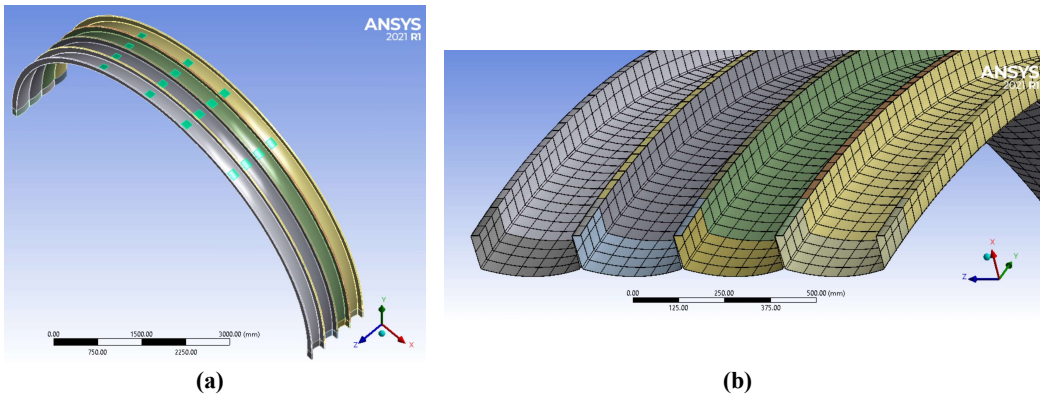


Figure 3.22 - (a) Shell with loading points highlighted green and (b) mesh with mostly 50 mm size elements

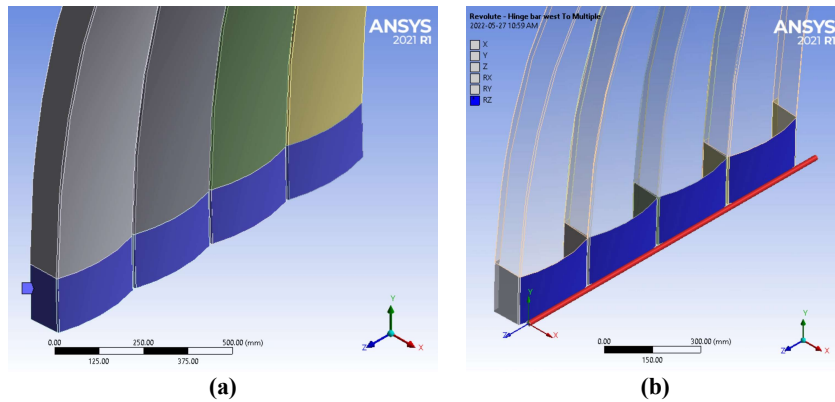


Figure 3.23 - Boundary conditions representing (a) fixed and (b) pinned support conditions

As predicted, the shell models were not able to solve beyond the point at which a local buckling event would occur. Satisfactory amounts of load-deflection curves that generally agreed with experimental data were recorded before encountering solution issues; the majority of the load-deflection curves for fixed and pinned specimens from Seguin et al. (2022) within the DND load ranges were determined and plotted. A similar relative spread between the stiffnesses found experimentally and numerically, based on support conditions, was sought by applying an appropriate stiffness value for the retrofitted model. The dotted lines in Figure 3.25 represent numerical load-deflection curves for maximum vertical and horizontal deflections under symmetric and asymmetric loading. Working within the upper and lower boundaries of fixed and pinned specimens' load-deflection curves, the first approach in quantifying the retrofit consisted of iterative inputs for hinge torsional stiffness and observing its changing load-deflection behaviours. Starting near the lower boundary with K value of 0.5 kN·m/deg, an additional 0.5 kN·m/deg was added for every iteration until the load-deflection curves approached the upper boundary. A stiffness value, K, of 2.0 kN·m/deg was found to characterize the retrofit well, especially within the load ranges indicated for Toronto, ON and Petawawa, ON, which represents the majority of the CAF installations. The fixed, retrofitted and pinned models' curves were mostly stiffer than the experimental load-deflection curves. Figure 3.24 shows a true scale example of a solution achieved with $K = 2.0 \text{ kN}\cdot\text{m}/\text{deg}$, with vertical and horizontal deflections agreeing with experimental data. More advanced numerical work will be required to solve further and calibrate with experimental results, beyond local buckling and load redistribution events. To the author's knowledge, the comparison of experimental K-Span specimen behaviour and numerical work using CECS167 contents in this research paper is the first instance of acknowledging the CECS167 outside of China.

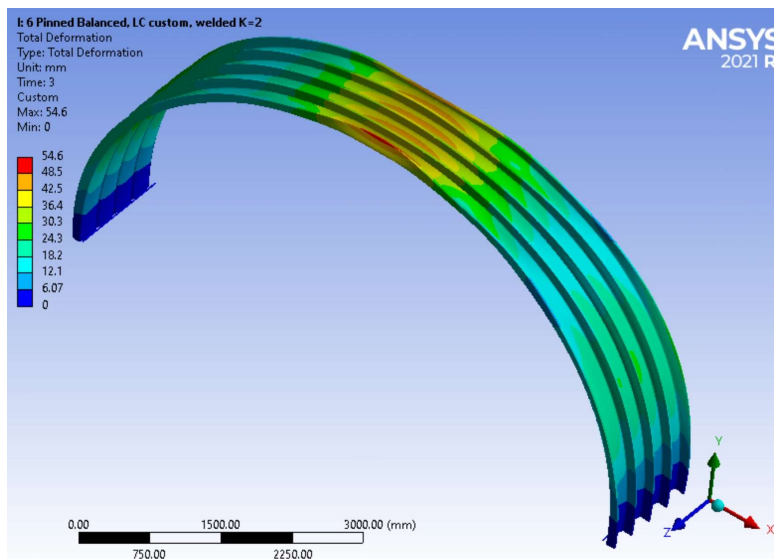


Figure 3.24 - Total deflections of a retrofitted model under 15 kN of symmetric loading (mm)

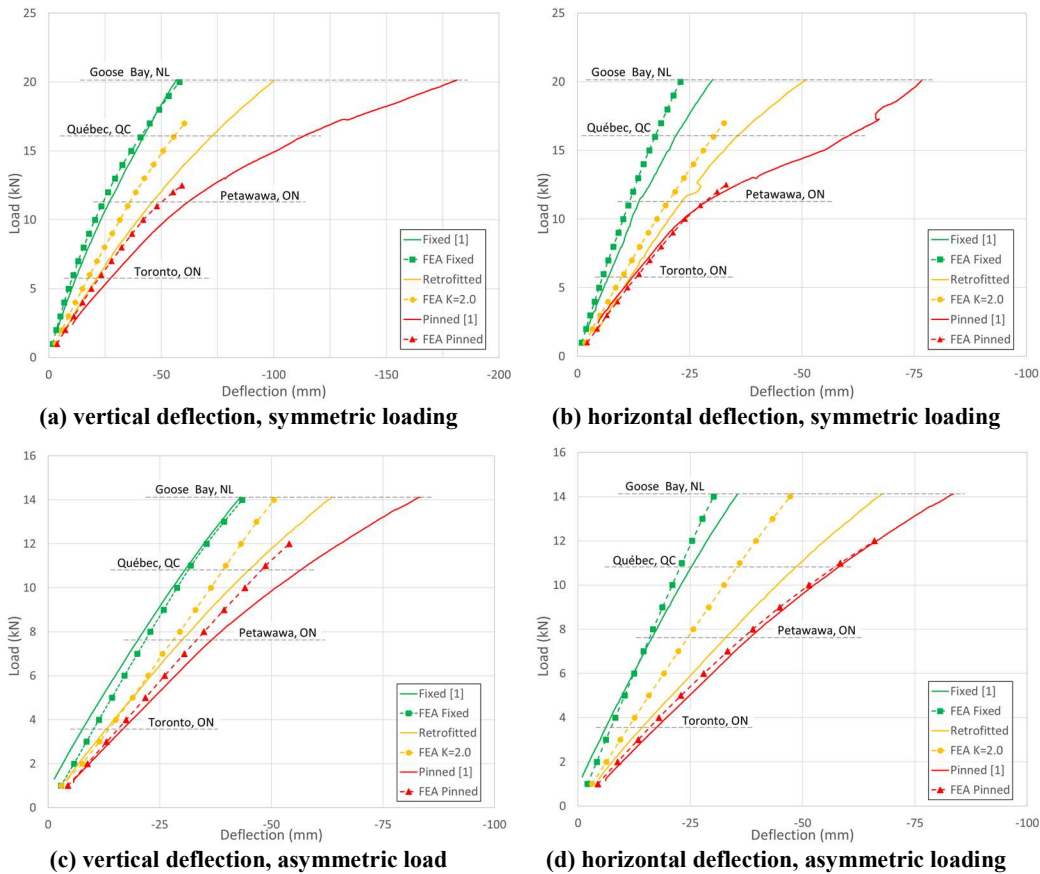


Figure 3.25 - Comparisons of experimental and FEA load-deflection curves with labels corresponding to 1-in-50-year snow loads in select Canadian locations

Theoretically, a model on pinned supports with an infinite rotational stiffness, K , would behave similarly to a model on fixed supports with no rotational or translational DOF. However, it was found that introducing rotational stiffness values of approximately $6.0 \text{ kN}\cdot\text{m}/\text{deg}$ on pinned supports produced load-deflection curves that roughly matched the counterparts from fixed models. This finding indicated that in a situation where a rotational stiffness of $6.0 \text{ kN}\cdot\text{m}/\text{deg}$ could be considered as the effective upper bound of a perfect strengthening technique, the retrofits addressed one third of the performance gap, at approximately $2.0 \text{ kN}\cdot\text{m}/\text{deg}$. It is possible that the proposed strengthening technique providing roughly $2.0 \text{ kN}\cdot\text{m}/\text{deg}$ of stiffness through virtual immobilization of the hinge may already have reached the majority of its full potential. Intuitively, the lack of constraints on the flanges and lips, as seen in Figure 3.19(a) other methods of stabilizing K-Span specimen cross-sections at the support condition interface may be necessary to unlock further improvements.

Table 3.4 shows a mesh convergence study completed on the asymmetrically-loaded pinned model to assess mesh size suitability in modeling global load-deflection behaviours, until iterations changed the result of interest less than 1%.

Table 3.4 - Shell model mesh convergence check using maximum y-axis deflections at 10 kN total load

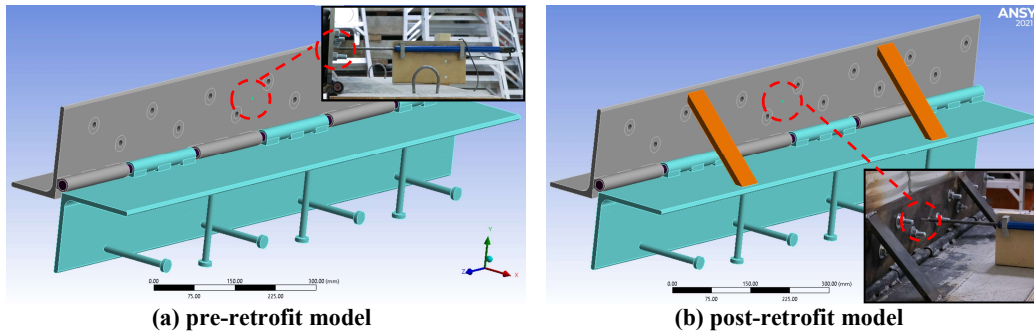
Number of nodes	Max. y-axis deflection (mm)	Increase in deflection (%)
47296	35.4	-
61408	39.2	10.73
77960	42.3	7.91
112,160	44.1	4.26
171,554	44.5	0.91

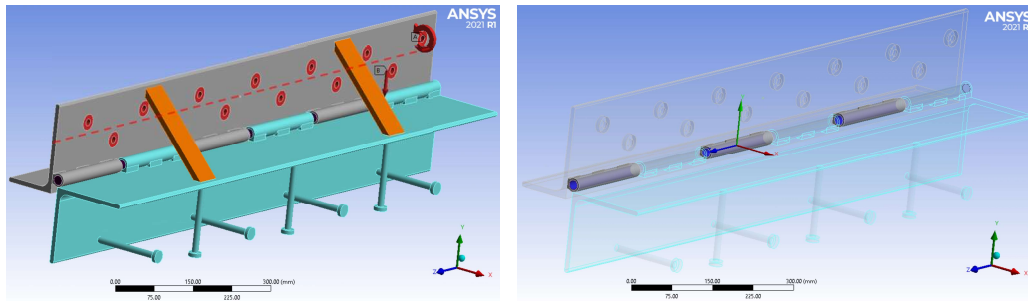
3.6.2 Solid Model

Figure 3.26(a) and (b) show the solid models built to evaluate the hinge assembly pre-retrofit and post-retrofit. The second approach in quantifying the effect of the retrofit consisted of 1) loading the retrofitted hinge assembly with an axial load and moment, 2) observing the deflection at the point the LVDT recorded measurements, and 3) loading the pre-retrofit model with the same axial load and moment and assigning hinge stiffnesses until the same deflection is observed.

The solid models, as well as the physical hinges built for the experiments, were created using as-built drawings from CFB Petawawa Building Records. The steel studs in the lower half of the hinge assembly were embedded in reinforced concrete and provided the fixed boundary condition in FEA. The steel used was ASTM A529, with a yield strength of 345 MPa, ultimate strength of 450 MPa and Young’s Modulus of 200 GPa. SOLID186 brick elements with 20 nodes and 3 DOF, and SOLID187 tetrahedral elements with 10 nodes and 3 DOF were used with mostly 12 mm sizing. Geometric non-linearity was enabled as there was potential for large deflections and rotations. Solutions were attained with the distributed sparse matrix direct solver using the full Newton-Raphson technique.

Figure 3.26(c) shows the bolt hole locations of the hinge where the forces from K-Span arches are passed on to the hinge assembly. The axial loads from the arches were transferred to the hinges through shear resistance in the bolts connecting the arches to the hinge bolt holes. The bending moments from the arches were transferred to the hinges through the application of positive bending moments at the locations of the bolted connections, around the red dotted line at the centroid of the bolt hole locations. The revolute joint with a single rotational DOF around the z-axis, as seen in Figure 3.26(d), served as boundary condition for the upper half of the hinge assembly.



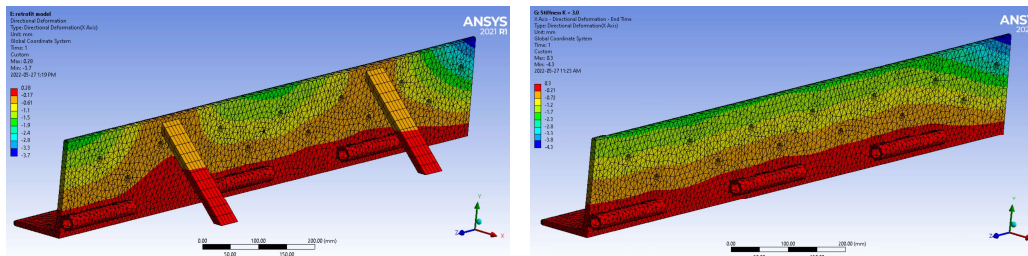


(c) axial load and moment applied via red-highlighted faces

(d) revolute joint - upper half of hinge assembly revolves around the hinge pin

Figure 3.26 - Hinge assembly solid model

Forces at the base of the West, or, the windward side of the K-Span specimen during an asymmetrically-loaded 1-in-50-year snow event in CFB Petawawa was simulated by applying 6.3 kN of axial load and 2.1 kN·m of positive moment incrementally in load steps. The resulting overall x-axis deflection contours agreed with the elastic deformations observed in Figure 3.19(b). The post-retrofit model's x-axis deflection of 0.77 mm at the region of interest indicated in Figure 3.26(b) compared relatively well with the experimental LVDT measurement of 0.62 mm. With the x-axis deflections in Figure 3.27(a) providing benchmark, the pre-retrofit model was loaded and assigned hinge stiffnesses until it attained the same 0.77 mm deflection at the region of interest indicated in Figure 3.26(a). Irrespective of Figure 3.27(b) showing different x-axis deflection contours throughout the upper hinge assembly compared to Figure 3.27(a), it served to calibrate the effect of the retrofit. It was determined that a hinge stiffness value, K , of 3.0 kN·m/deg quantified the effect of the retrofit.



(a) with retrofit

(b) with stiffness value $K=3.0$ kN·m/deg

Figure 3.27 - X-axis deflection in upper half of hinge assembly

Table 3.5 contains a mesh convergence study completed on the post-retrofit solid model, as seen in Figure 3.26(b), to assess mesh size suitability in modeling its load-deflection behaviours, until iterations changed the result of interest less than 1%.

Table 3.5 - Solid model mesh convergence check using x-axis deflections at LVDT location

Number of nodes	X-axis deflection at LVDT location (mm)	Increase in deflection (%)
19190	0.751	-
24075	0.766	2.13
37077	0.774	1.04
45262	0.777	0.39

3.6.3 Frame Element Model

The third and final approach in quantifying the retrofit was observing the relationship between the bending moments found through a frame element analysis and the hinge rotation angle recorded experimentally, as seen in Figure 3.21. The frame models consisted of 24 one-dimensional beam elements connected semi-circularly on fixed, pinned and retrofitted supports. The cross-section of the beam elements consisted of a four-panel profile without accounting for double corrugation, as designed and utilized by MacDonald (2022). The material used was steel with a yield strength of 345 MPa, ultimate strength of 450 MPa and Young's Modulus of 200 GPa. Figure 3.7(c) shows a frame element in SAP2000 representing the retrofitted K-Span specimen, where the bending moment at the retrofitted support depends on the hinge stiffness value. Geometric non-linearity was enabled for large deflections and rotations. Starting with a 2.5 kN·m/deg stiffness, bending moments at retrofitted supports were found for four situations: symmetrically- and asymmetrically-loaded specimens at the 1-in-50-year snow loads for CFB Petawawa and CFB Goose Bay. The four bending moments were divided by the experimentally-found angles of the respective hinges and averaged, resulting in an amended hinge stiffness for the next iteration. Table 3.6 presents the last iteration completed; subsequent iterations changed the stiffness value less than 1%. The simple average of the four hinge stiffness values, K , was determined to be 2.2 kN·m/deg.

Table 3.6 - Iterative process for determining hinge stiffness by observing moment-hinge angle relationship

1-in-50-year Snow Event	Angle West (deg)	Moment West (kN·m)	Angle East (deg)	Moment East (kN·m)	Stiffness (kN·m/deg)
CFB Petawawa – Symmetrical Load	0.529	1.69	0.682	1.69	2.84
CFB Petawawa – Asymmetrical Load	0.617	2.09	0.224	0.221	2.18
CFB Goose Bay – Symmetrical Load	1.214	3.07	1.136	3.07	2.61
CFB Goose Bay – Asymmetrical Load	1.962	3.58	0.680	0.280	1.12
Iteration Average					2.19

3.6.4 Numerical Work Summary

Three separate approaches in non-linear FEA were taken to calibrate or relate the numerical results with experimental data from Seguin et al. (2022) and this project. The shell, solid and frame element analysis in ANSYS and SAP2000 modeled the load-deflection and moment behaviours of the specimens and support conditions sufficiently, concluding with stiffness values of 2.0, 3.0 and 2.2 kN·m/deg, respectively. The rotational stiffness achieved by the retrofit could be described with a non-weighted average value of 2.4 kN·m/deg.

3.7 Conclusions

Support condition-deficient K-Span structures around the world have collapsed under heavy snow events. There is no standardized method for analyzing existing K-Span arch capacities regardless of support conditions, as there is no official code covering the unique doubly-corrugated cold-formed steel profiles. Research into strengthening existing K-Span structures is sporadic and uncoordinated. To strengthen existing support condition-deficient structures in a simple, inexpensive and non-intrusive manner, an innovative technique was developed and tested on full-scale specimens. Key results and observations are as follows:

1. Compared to the pinned specimens, retrofitted specimens demonstrate increased ultimate capacities, +16% under symmetric and +5.2% under asymmetric loading.
2. Retrofitted specimens show improved stiffness, ductility and serviceability over pinned specimens under symmetric and asymmetric loading, behaving approximately midway between fixed and pinned specimens.
3. Introducing rotational springs to the originally-pinned support conditions in FEA modeling is presumed to have reduced the magnitude of the maximum positive and negative bending moments throughout arches under load.
4. A computationally-efficient modeling of load-deflection behaviours in a shell FEA model that accounts for double corrugation is possible using the cross-sectional area reduction equation from CECS167.
5. Shell, solid and frame element model approaches in FEA determines the value of the rotational stiffness to be approximately 2.4 kN·m/deg, achieved by welding steel bars of 588 mm² cross-sectional area every 610 mm along the structural hinge.
6. It is conceivable to suggest that a site-specific installation of a more or less stiff retrofit is feasible through careful selection of retrofit material property and design.

3.8 Acknowledgements

This research project was made possible with funding and technical support from the following DND organizations: Director, Architecture & Engineering Services, A4 CE – 1 Canadian Air Division, Real Property Operations Unit (Ontario) Detachment Petawawa and 14 Construction Engineering Squadron.

3.9 References

- [1] D. Seguin, "Full-Scale Experimental Behaviour of Thin-Walled and Doubly Corrugated Cold-Formed Steel Arched Structure (K-Span) with Varying Base Support Conditions," Royal Military College of Canada MASc Thesis, Kingston, ON, 2022.
- [2] R. Walentynski and P. Piekarczyk, "Experimental and computational approaches to the evaluation of double corrugated arch structures - A review of the latest

- advancements," *Archives of Civil Engineering Polish Academy of Sciences*, vol. 67, no. 2, 2021.
- [3] G. Lepine, "Structural Capacity of Thin-Walled Cold-Formed Steel Doubly-Corrugated Arch Panels," Royal Military College of Canada MASC Thesis, Kingston, ON, 2021.
- [4] *Building Record Archives*, CFB Petawawa: Real Property Detachment Petawawa Engineering Office.
- [5] R. Cybulski, R. Walentynski and M. Cybulska, "Local buckling of cold-formed elements used in arched building with geometrical imperfections," *Journal of Constructional Steel Research*, vol. 96, pp. 1-13, 2014.S.
- [6] Piekarczyk, K. Malowany, P. Wiech, M. Kujawska and P. Sulik, "Stability and bearing capacity of arch-shaped corrugated shell elements: experimental and numerical study," *Bulletin of the Polish Academy of Sciences*, vol. Technical Sciences 63, no. 1, pp. 113-123, 2015.
- [7] R. Walentynski, R. Cybulski and K. Koziel, "Achilles' Heel of the ABM 120 Double Corrugated Profiles," in *International Conference on New Trends in Statics and Dynamics of Buildings*, Bratislava, 2011.
- [8] Technical Specification for Arched Corrugated Steel Roof (Trial) CECS 167:2004, Beijing: Association Standard of the People's Republic of China, China Planning Press, 2005.
- [9] "MIC-120 ABM Training Manual," M.I.C. Industries, Reston, 1993.
- [10] Sweeney, D. Briassoulis and A. Kao, "Evaluation of K-Span as a Rapidly Erectable Lightweight Mobilization Structure (RELMS)," Construction Engineering Research Lab (Army), Champaign, IL, 1991.A.
- [11] A. MacDonald, "Two-dimensional finite element analysis of the automatic building machine (ABM)-120 K-Span structure subjected to asymmetric snow loads," *Defence Research and Development Canada - Centre for Operational Research and Analysis*, 2021.
- [12] X. Liu, Y. Zhang and F. Zhang, "Experimental study on full-sized models of arched corrugated metal roof," in *ICASS'99*, Hong Kong, 1999.
- [13] A. Biegus and A. Kowal, "Collapse of halls made from cold-formed steel sheets," *Engineering Failure Analysis*, vol. 31, pp. 189-194, 2013.
- [14] E. L. Airumyan and O. I. Boyko, "Full-scale testing and design of frameless arch steel roof," in *Structural Assessment: The Role of Large and Full-Scale Testing*, London, UK, E & FN SPON, 1998, pp. 211-217.

- [15] J. Ju and Y. Guo, "In-plane elastic buckling of arch," *Tsinghua Science and Technology*, vol. 7, no. 3, pp. 322-325, 2002.
- [16] G. L. Pierce, W. D. Siddall and G. Abdel-Sayed, "Doubly corrugated barrel cold-formed steel shells," in *International Specialty Conference on Cold-Formed Steel Structures 4*, St. Louis, MO, 1980.
- [17] A. Piekarczyk, "Experimental and numerical studies of double corrugated steel arch panels," *Thin-Walled Structures*, vol. 140, pp. 60-73, 2019.

Chapter 4 CONCLUSIONS AND RECOMMENDATIONS

4.1 General

A literature review for this project confirmed that the recent K-Span structure collapse in CFB Petawawa was not uniquely a Canadian problem; other support condition-deficient structures have collapsed around the world under heavy snow events. As part of a larger ongoing effort studying structural integrity of K-Span structures, this research project aimed to address the deficient support conditions affecting a portion of the K-Span structures in DND inventory.

The experimental program was designed within the confines of the laboratory dimensions and budgets. It involved constructing support conditions as found in CFB Petawawa and implementing an innovative strengthening technique. Two 1.016 mm thick and 7.0 m wide K-Span specimens were loaded symmetrically and asymmetrically, and their load-deflection behaviours were directly compared with the experimental data from [9].

The numerical analyses involved three separate FEA approaches created and calibrated with the experimental data, in order to quantify the effect of the strengthening technique.

4.2 Conclusions

Experimental load-deflection curve comparisons with those from pinned and fixed specimens in [9] clearly demonstrated that a simple retrofit improves serviceability and increases ultimate capacity. Although the exact bending moment distribution could not be measured in the retrofitted specimens, it is presumable that the bending resistance provided by the retrofit was able to reduce the critical magnitude of positive and bending moments along the arches; the retrofitted specimen supported more load before eventually collapsing due to local and/or global buckling. For existing support condition-deficient K-Span structures around the world that could accommodate more bending resistance at the supports, it is plausible to imagine that a simple strengthening technique such as this could be customized and implemented.

Key results and observations are summarized below:

1. The ultimate capacity increased 16.0% for the symmetrically-loaded specimen, representing a 31.7% improvement in the gap between pinned and fixed specimens' ultimate capacities. In terms of unfactored ground snow load pressure, S_s , the specimen capacity was increased from 5.78 kPa to 6.84 kPa.
2. The ultimate capacity increased 5.2% for the asymmetrically-loaded specimen, representing a 19.4% improvement in the gap between pinned and fixed specimens' ultimate capacities. In terms of unfactored ground snow load pressure, S_s , the specimen capacity was increased from 8.18 kPa to 8.64 kPa.
3. Retrofitted specimens showed improved stiffness, ductility and serviceability over the originally-pinned specimens, behaving approximately midway between pinned and fixed counterparts.

4. FEA shell modeling supported the usefulness of the cross-sectional area reduction equation from CECS167 that facilitates simple modeling for load-deflection behaviours.
5. The strengthening technique likely reduces the magnitude of the positive and negative bending moments throughout the arches that lead to collapse.
6. FEA shell, solid and frame element models determined an average rotational spring stiffness of approximately 2.4 kN·m/deg achieved by the retrofit.

4.3 Recommendations

The following recommendations are made for potential future research into K-Span structure strengthening techniques:

1. Improved retrofit designs involving stabilization of the entire K-Span cross-section at the support condition interface should be tested experimentally. As well, the scalability of such designs should be tested experimentally, in order to study the relationships between the retrofit properties and stiffening effects achieved.
2. Non-destructive load tests on existing K-Span structures should be organized pre-retrofit and post-retrofit to validate the effectiveness of a selected strengthening technique.
3. Future experiments should continue to validate the equations and concepts found in CECS167, as its guidance could be adopted worldwide for standardized K-Span arch capacity evaluations and simplified FEA.
4. Incremental loading and unloading sequences should be organized for load-deflection experiments in order to determine the elastic limits, providing guidance to unique K-Span arch serviceability limits.
5. End wall strength should be tested in order to facilitate three-dimensional strengthening techniques. For example, installing purlins that distribute end wall strength and share load bearing between arches would help control excessive local deflections.
6. Novel instrumentation such as DIC and distributed fiber optic sensors should be utilized to augment deflection and strain measurements at the regions of interest.

REFERENCES

- [1] R. Walentynski and P. Piekarczyk, "Experimental and computational approaches to the evaluation of double corrugated arch structures - A review of the latest advancements," *Archives of Civil Engineering Polish Academy of Sciences*, vol. 67, no. 2, 2021.
- [2] *Building Record Archives*, CFB Petawawa: Real Property Detachment Petawawa Engineering Office.
- [3] G. Lepine, "Structural Capacity of Thin-Walled Cold-Formed Steel Doubly-Corrugated Arch Panels," Royal Military College of Canada MASc Thesis, Kingston, ON, 2021.
- [4] M. Arsenault, *Structural integrity of K-Span type structures*, Ottawa: Director, Architecture & Engineering Services, 2019.
- [5] A. Biegus and A. Kowal, "Collapse of halls made from cold-formed steel sheets," *Engineering Failure Analysis*, vol. 31, pp. 189-194, 2013.
- [6] X. Liu, Y. Zhang and F. Zhang, "Experimental study on full-sized models of arched corrugated metal roof," in *ICASS'99*, Hong Kong, 1999.
- [7] A. Piekarczyk, K. Malowany, P. Wiech, M. Kujawinska and P. Sulik, "Stability and bearing capacity of arch-shaped corrugated shell elements: experimental and numerical study," *Bulletin of the Polish Academy of Sciences*, vol. Technical Sciences 63, no. 1, pp. 113-123, 2015.
- [8] R. Cybulski, R. Walentynski and M. Cybulska, "Local buckling of cold-formed elements used in arched building with geometrical imperfections," *Journal of Constructional Steel Research*, vol. 96, pp. 1-13, 2014.
- [9] D. Seguin, "Full-Scale Experimental Behaviour of Thin-Walled and Doubly Corrugated Cold-Formed Steel Arched Structure (K-Span) with Varying Base Support Conditions," Royal Military College of Canada MASc Thesis, Kingston, ON, 2022.
- [10] "Thesis Preparation Guidelines," Royal Military College of Canada, Kingston, 2015.
- [11] S. Sweeney, D. Briassoulis and A. Kao, "Evaluation of K-Span as a Rapidly Erectable Lightweight Mobilization Structure (RELMS)," Construction Engineering Research Lab (Army), Champaign, IL, 1991.

- [12] E. L. Airumyan and O. I. Boyko, "Full-scale testing and design of frameless arch steel roof," in *Structural Assessment: The Role of Large and Full-Scale Testing*, London, UK, E & FN SPON, 1998, pp. 211-217.
- [13] A. Volovitskaya, M. Salakhutdinov and I. Kuznetsov, "Investigation and calculation of a composite arch construction," in *E3S Web of Conferences*, Tashkent, Uzbekistan, 2021.
- [14] J. Zaras and K. R. J. Kowal-Michalska, "A Simplified Computation Model for Arch-Shaped Corrugated Shell Roof," *Thin-Walled Structures-Advances and Develoments*, pp. 109-117, 2001.
- [15] "MIC-120 ABM Training Manual," M.I.C. Industries, Reston, 1993.
- [16] A. MacDonald, "Two-dimensional finite element analysis of the automatic building machine (ABM)-120 K-Span structure subjected to asymmetric snow loads," *Defence Research and Development Canada - Centre for Operational Research and Analysis*, 2021.
- [17] "Install K-Span Cold Storage Bldg Size 16x46.8M," Real Property Operations Unit Ontario -Detachment Kingston, Kingston, ON, 2009.
- [18] Y. Wei-Wen, R. LaBoube and H. Chen, *Cold-Formed Steel Design*, fifth edition, Hoboken, New Jersey: John Wiley & Sons, Inc., 2020.
- [19] W. Yu, *Cold-Formed Steel Structures*, Boca Raton: CRC Press LLC, 1999.
- [20] S136-16 North American specification for the design of cold-formed steel structural members, Toronto, ON: CSA Group, 2016.
- [21] A. Piekarczyk, "Experimental and numerical studies of double corrugated steel arch panels," *Thin-Walled Structures*, vol. 140, pp. 60-73, 2019.
- [22] R. Walentyński, R. Cybulski and R. Sanchez, "Numerical stability analyses and preliminary experimental investigation of doubly corrugated steel arch panels," *Journal of the International Association for Shell and Spatial Structures*, vol. 54, no. 1, pp. 3-14, 2013.
- [23] Technical Specification for Arched Corrugated Steel Roof (Trial) CECS 167:2004, Beijing: Association Standard of the People's Republic of China, China Planning Press, 2005.
- [24] "M.I.C. BuildingWorks Project Report," M.I.C. Industries, Reston, VA, 2019.

- [25] D. Dubina, "Cold-formed Steel Design - Eurocode 3: Design of Steel Structures," Politehnica University Timisoara, Brussels, 2014.
- [26] L. Sun and C. Lin, "Computer Nonlinear Analysis of Ultimate Bearing Capacity of Corrugated-arch Metal Roof," in *International Conference on Intelligent Computation Technology and Automation*, Changsha, Hunan, 2010.
- [27] L. Sun and L. Lin, "Equivalent Analysis of Elastic Constants and Stability Calculation of Corrugated-Arch Metal Roof," *Advanced Materials Research*, vol. 542, pp. 106-110, 2012.
- [28] F. Benussi and A. Mauro, "Half-Barrel Shells Composed of Cold-Formed Profiles," *Thin-Walled Metal Structures in Buildings*, vol. 49, pp. 263-268, 1986.
- [29] J. Ju and Y. Guo, "In-plane elastic buckling of arch," *Tsinghua Science and Technology*, vol. 7, no. 3, pp. 322-325, 2002.
- [30] C. A. Dimopoulos and C. J. Gantes, "Nonlinear in-plane behavior of circular steel arches with hollow circular cross-section," *Journal of Constructional Steel Research*, vol. 64, pp. 1436-1445, 2008.
- [31] National Building Code of Canada Part 4 Structural Design, Ottawa, ON: National Research Council, 2015.
- [32] R. Walentynski, R. Cybulski and K. Koziel, "Achilles' Heel of the ABM 120 Double Corrugated Profiles," in *International Conference on New Trends in Statics and Dynamics of Buildings*, Bratislava, 2011.
- [33] G. L. Pierce, W. D. Siddall and G. Abdel-Sayed, "Doubly corrugated barrel cold-formed steel shells," in *International Specialty Conference on Cold-Formed Steel Structures 4*, St. Louis, MO, 1980.
- [34] X. Wang, M. Liu, G. Yang and Z. Li, "Enhancement Measures of 35.6m Span Arched Corrugated Steel Roof," *Applied Mechanics and Materials*, vol. 105, pp. 2279-2283, 2012.
- [35] G. Abdel-Sayed, F. Monasa and W. Siddall, "Cold-Formed Steel Farm Structures, Part II: Barrel Shells," *Journal of Structural Engineering*, vol. 111, no. 10, pp. 2090-2104, 1985.
- [36] S. M. Zahurul Islam, A. A. Abang-Abdullah and M. S. Jafor, "An Investigation on structural performance of profiled steel sheet to develop self-supporting roofing system," *Journal of Advance Steel Construction*, vol. 2, pp. 87-108, 2006.

APPENDICES

Appendix A SELECT AS BUILT DRAWINGS FROM THE COLLAPSED K-SPAN STRUCTURE

This appendix presents select excerpt from the as-built drawings and plans from the collapsed K-Span structure in CFB Petawawa relevant to the development of the strengthening technique.

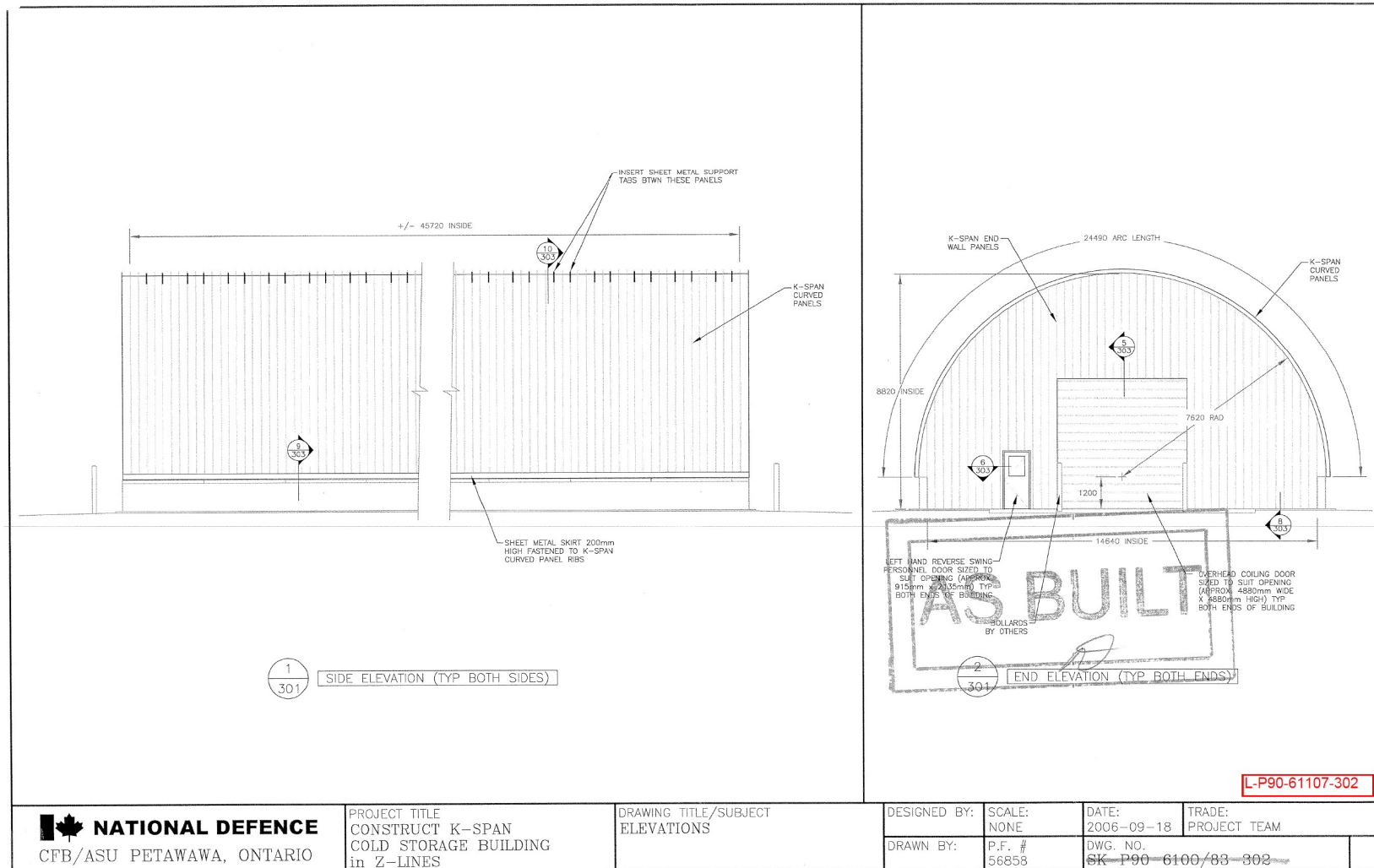


Figure A.1 - Side and front elevation views (mm) [2]

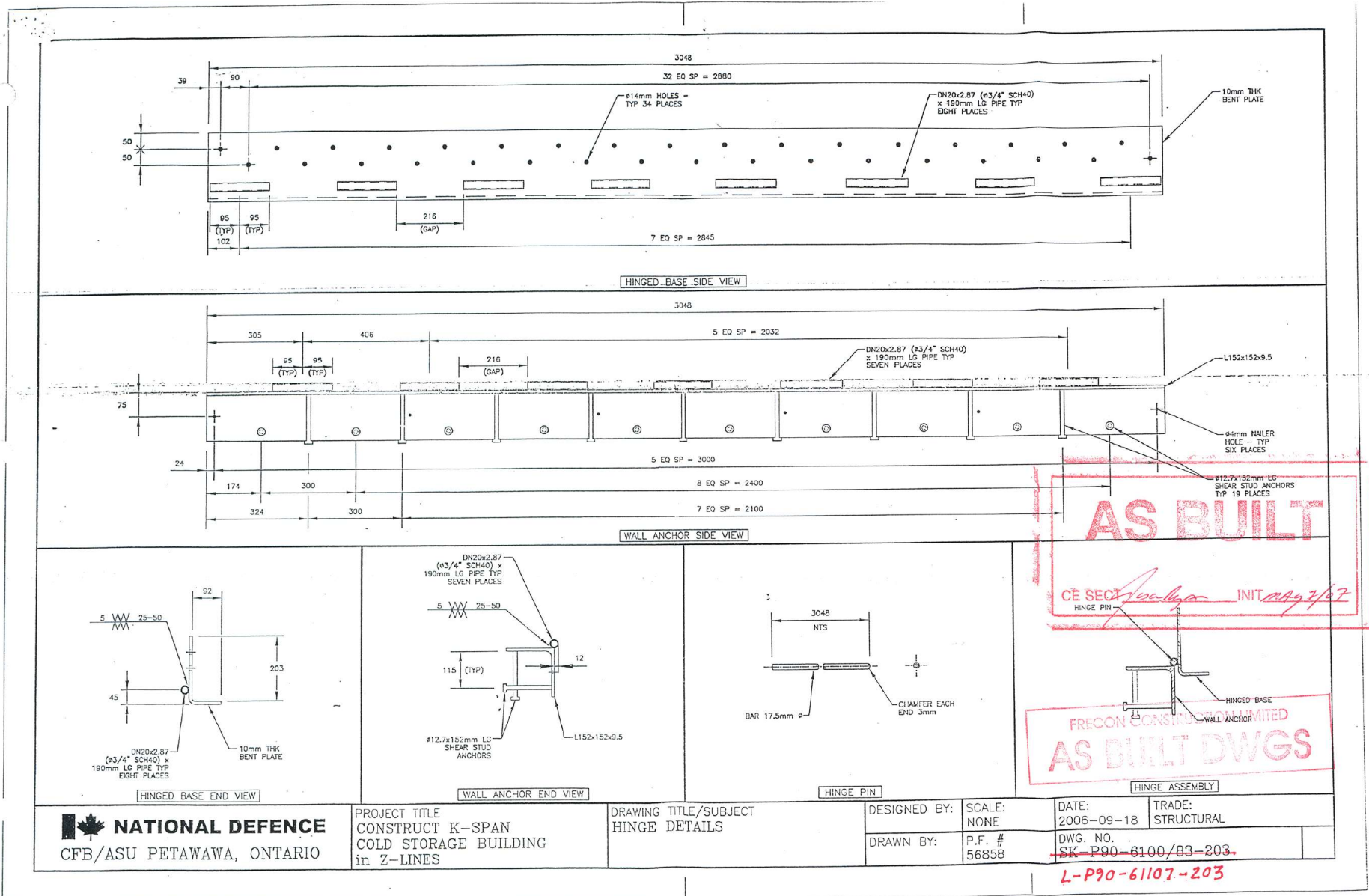


Figure A.2 - Hinge support condition details (mm) [2]

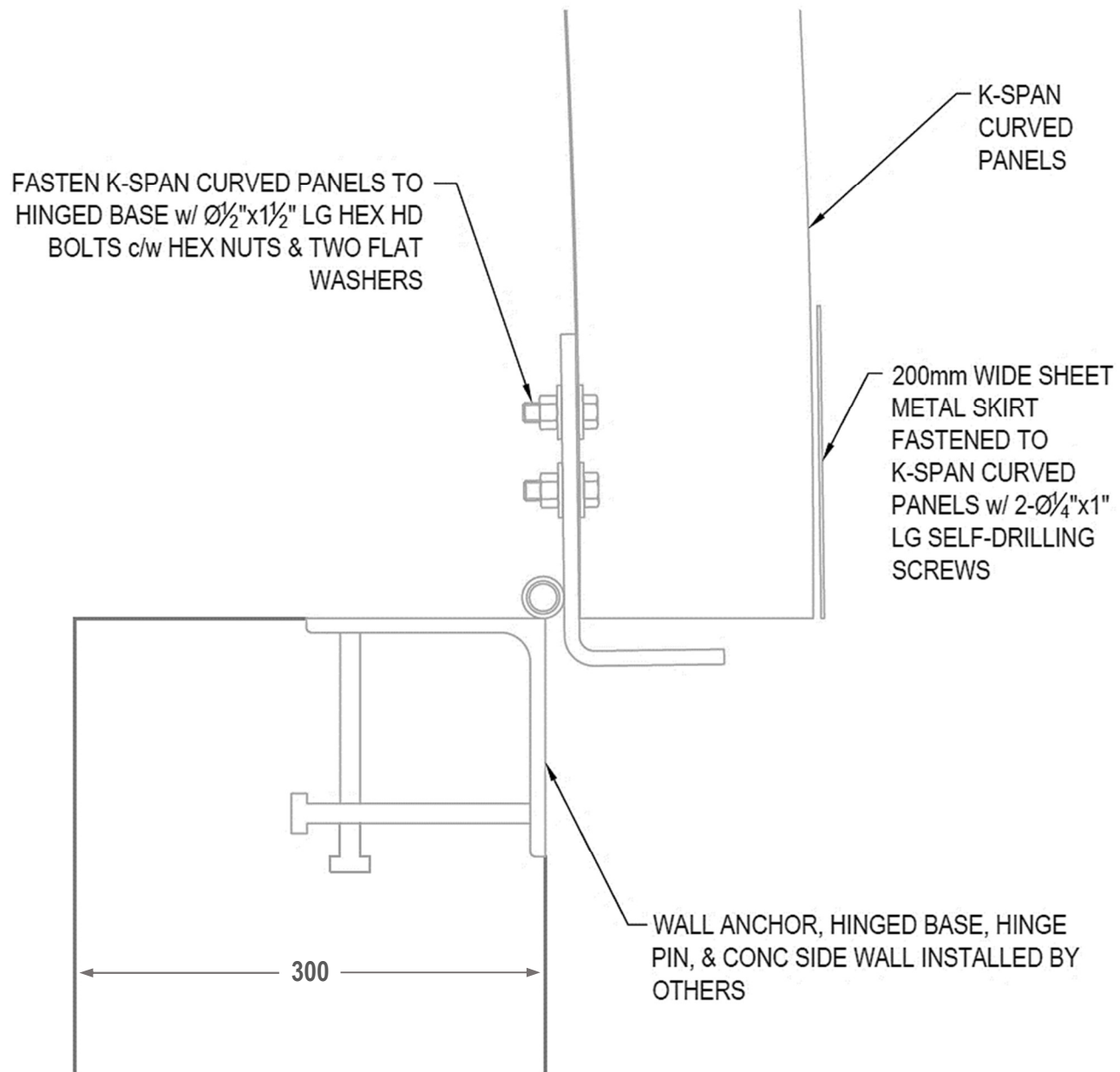


Figure A.3 - Excerpt from K-Span arch installation detail (mm) [2]

Appendix B NBCC SNOW AND RAIN LOAD CONVERSION TO POINT LOADS AND ACTUATOR LOADS

This appendix describes the steps taken to determine the experimental loading scheme that facilitates roof loading patterns prescribed by the NBCC.

In order to load specimens with symmetric and asymmetric non-uniformly distributed loads as per NBCC section 4.1.6.2., the patterns were converted to a practical number of point loads to be applied in a displacement-controlled manner. Two-dimensionally, the rows of point loads, each containing four point loads across the four arches, were to be determined as a horizontal distance from the arch peak. One half-arch was split into 12 equal slices, each with an internal angle of 7.5 deg, with 13 points indicating the start and end of each slice. The specified snow loads, in terms of pressure (kPa), was found for each of the 13 points using the equation found in Figure B.1, with the average 1-in-50-year snow and rain loads of 2.4 kPa and 0.4 kPa, respectively, for CAF installations [16]. Then, they were turned into distributed loads applicable at each point, as a load per distance (kN/m), as seen in Figure B.2. The visualization of the distributed loads over the half arch for the symmetric and asymmetric loading pattern could be seen in Figure B.3 and Figure B.4, respectively. By determining the centroid and half-centroids of the distributed load over a half-arch, the locations of the point load rows were determined. For the symmetrical pattern, the locations of the point load rows were mirrored onto the other side.

The hydraulic actuator loads that represent various 1-in-50-year snow and rain events for CAF installations were found by calculating the sum of the loads on each of the 12 slices; the sum was doubled for the symmetric pattern. An example completed for CFB Goose Bay could be found in Figure B.5.

$S=I_s[S_s(C_bC_wC_sC_a)+S_r]$	
where	S is the specified snow load (kPa);
	I_s is the importance factor for snow load;
	S_s 1-in-50-year ground snow load (kPa);
	C_b basic roof snow load factor;
	C_w wind exposure factor;
	C_s slope factor;
	C_a accumulation factor; and
	S_r 1-in-50-year associated rain load (kPa).
	I_s 0.8 based on building importance;
	S_s ranging between 1.6 kPa and 5.3 kPa;
	C_b 0.8 based on structural geometry;
	C_w 1.0 based on structural criteria;
	C_s ranging between 0 and 1;
	C_a ranging between 0 and 2.5; and
	S_r 0.4 kPa based on DND locations.

Figure B.1 - Specified snow and rain load equation from NBCC section 4.1.6.2.

Pattern	Point	Slope (deg)	x (m)	I _s	S _s (kPa)	C _b	C _w	C _s	C _a	S _r (kPa)	S (kPa)	DL (kN/m)
Symmetric	1	90.0	3.472	0	0	0	0	0.000	1.000	0	0.000	0.000
	2	82.5	3.442	0.8	5.3	0.8	1.0	0.000	1.000	0.4	0.320	0.399
	3	75.0	3.354	0.8	5.3	0.8	1.0	0.000	1.000	0.4	0.320	0.399
	4	67.5	3.208	0.8	5.3	0.8	1.0	0.000	1.000	0.4	0.320	0.399
	5	60.0	3.007	0.8	5.3	0.8	1.0	0.000	1.000	0.4	0.320	0.399
	6	52.5	2.755	0.8	5.3	0.8	1.0	0.167	1.000	0.4	0.885	1.103
	7	45.0	2.455	0.8	5.3	0.8	1.0	0.333	1.000	0.4	1.451	1.808
	8	37.5	2.114	0.8	5.3	0.8	1.0	0.500	1.000	0.4	2.016	2.512
	9	30.0	1.736	0.8	5.3	0.8	1.0	0.667	1.000	0.4	2.581	3.217
	10	22.5	1.329	0.8	5.3	0.8	1.0	0.833	1.000	0.4	3.147	3.921
	11	15.0	0.899	0.8	5.3	0.8	1.0	1.000	1.000	0.4	3.712	4.626
	12	7.5	0.453	0.8	5.3	0.8	1.0	1.000	1.000	0.4	3.712	4.626
	13	0.0	0.000	0.8	5.3	0.8	1.0	1.000	1.000	0.4	3.712	4.626
Pattern	Point	Slope (deg)	x (m)	I _s	S _s (kPa)	C _b	C _w	C _s	C _a	S _r (kPa)	S (kPa)	DL (kN/m)
Asymmetric	1	90.0	3.472	0	0	0	0	0.000	2.500	0	0.000	0.000
	2	82.5	3.442	0.8	5.3	0.8	1.0	0.000	2.500	0.4	0.320	0.399
	3	75.0	3.354	0.8	5.3	0.8	1.0	0.000	2.500	0.4	0.320	0.399
	4	67.5	3.208	0.8	5.3	0.8	1.0	0.000	2.500	0.4	0.320	0.399
	5	60.0	3.007	0.8	5.3	0.8	1.0	0.000	2.500	0.4	0.320	0.399
	6	52.5	2.755	0.8	5.3	0.8	1.0	0.167	2.500	0.4	1.733	2.160
	7	45.0	2.455	0.8	5.3	0.8	1.0	0.333	2.500	0.4	3.147	3.921
	8	37.5	2.114	0.8	5.3	0.8	1.0	0.500	2.500	0.4	4.560	5.683
	9	30.0	1.736	0.8	5.3	0.8	1.0	0.667	2.500	0.4	5.973	7.444
	10	22.5	1.329	0.8	5.3	0.8	1.0	0.833	1.913	0.4	5.729	7.139
	11	15.0	0.899	0.8	5.3	0.8	1.0	1.000	1.294	0.4	4.710	5.869
	12	7.5	0.453	0.8	5.3	0.8	1.0	1.000	0.653	0.4	2.534	3.158
	13	0.0	0.000	0.8	5.3	0.8	1.0	1.000	0.000	0.4	0.320	0.399

Figure B.2 - Distributed load calculations with average S_s and S_r that applies for CAF installations across Canada

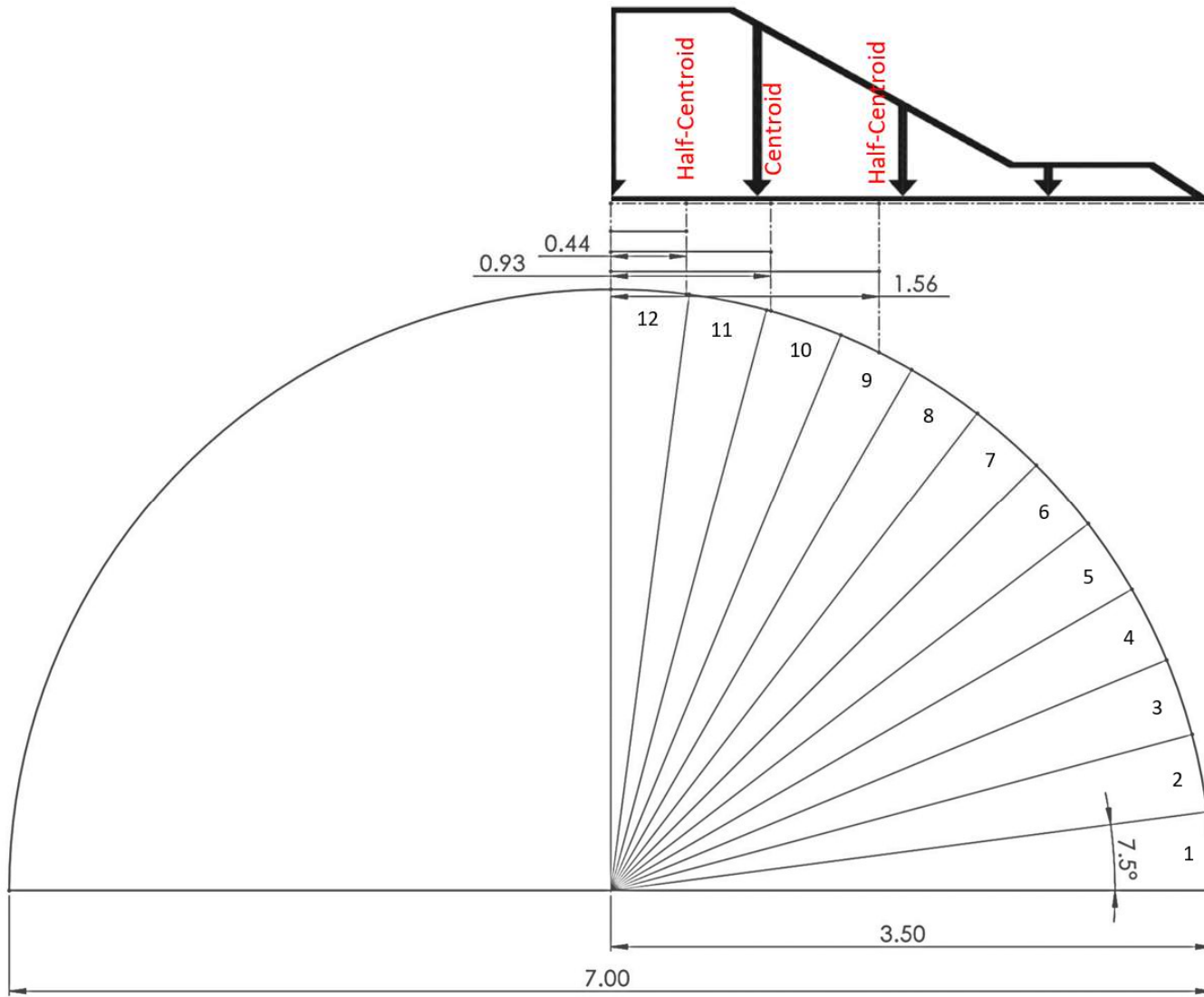


Figure B.3 - Half-arch for symmetric loading points (m)

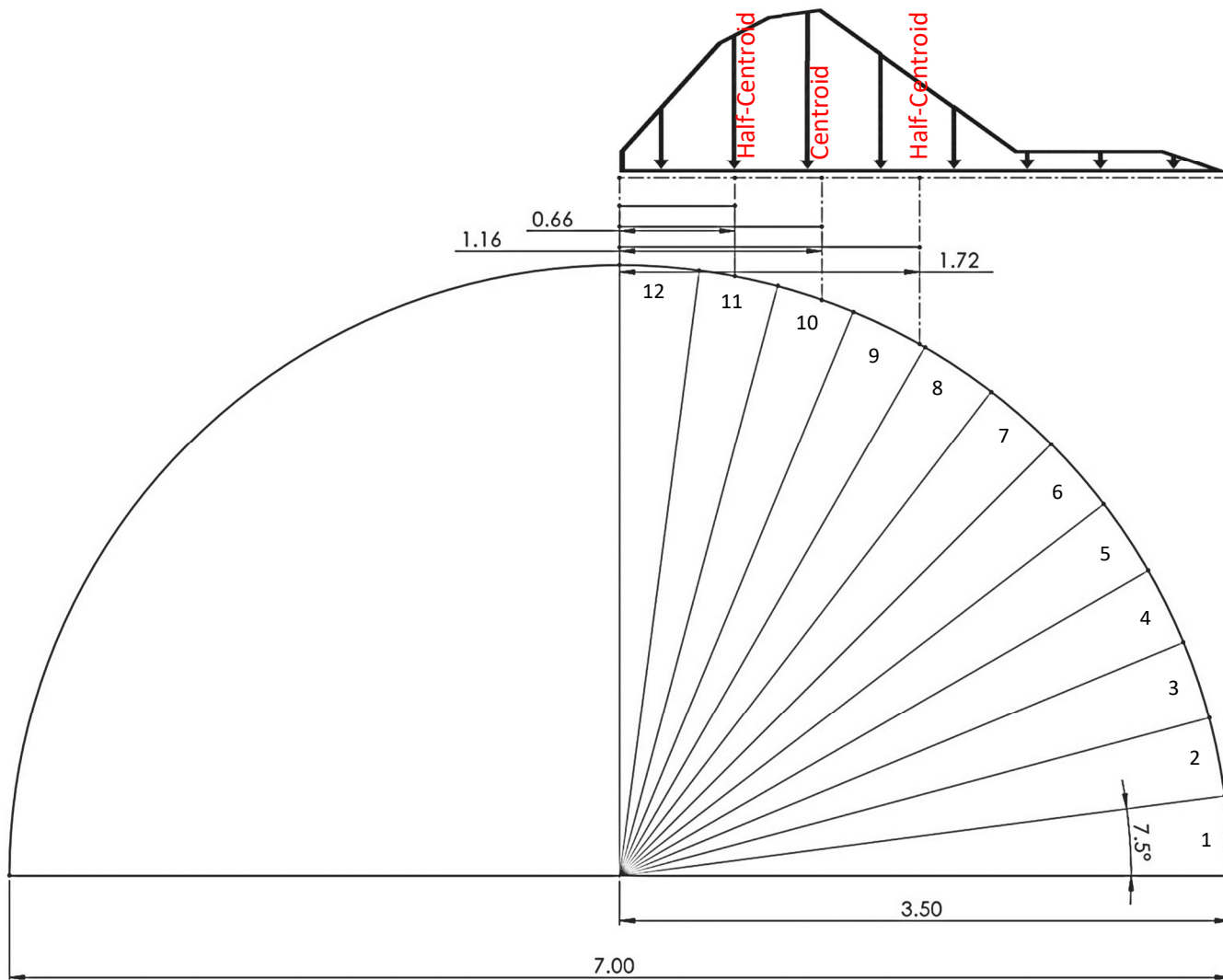


Figure B.4 - Half-arch for asymmetric loading points (m)

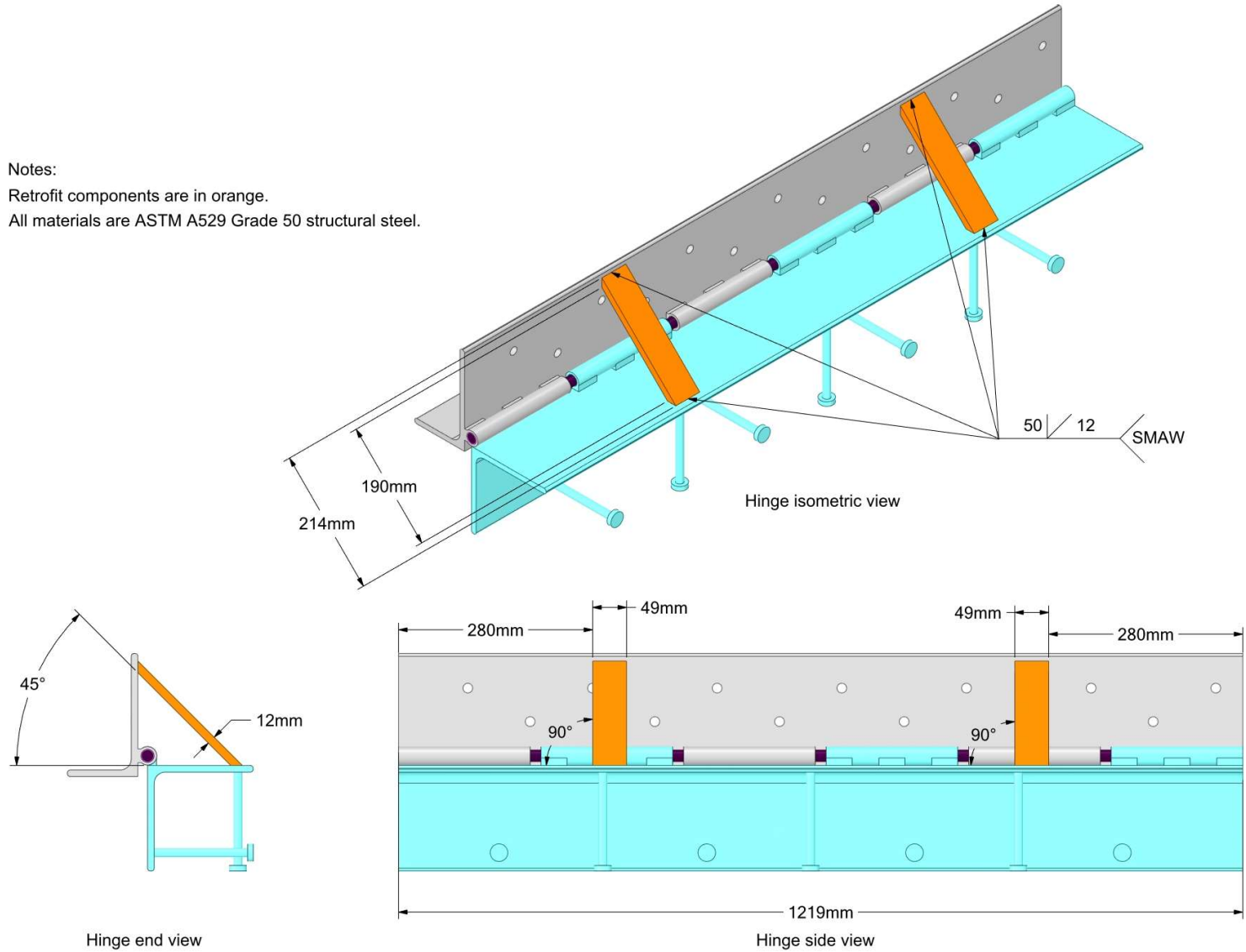
Pattern	Point	DL (kN/m)		Slice	x (m)	Force (kN)
Symmetric	1	0.000		1	0.030	0.006
	2	0.399		2	0.089	0.035
	3	0.399		3	0.146	0.058
	4	0.399		4	0.201	0.080
	5	0.399		5	0.252	0.190
	6	1.103		6	0.299	0.436
	7	1.808		7	0.341	0.738
	8	2.512		8	0.378	1.082
	9	3.217		9	0.407	1.454
	10	3.921		10	0.430	1.838
	11	4.626		11	0.445	2.061
	12	4.626		12	0.453	2.096
	13	4.626		Symmetric Total (mirrored)		20.15
Pattern	Point	DL (kN/m)		Slice	x (m)	Force (kN)
Asymmetric	1	0.000		1	0.030	0.006
	2	0.399		2	0.089	0.035
	3	0.399		3	0.146	0.058
	4	0.399		4	0.201	0.080
	5	0.399		5	0.252	0.323
	6	2.160		6	0.299	0.911
	7	3.921		7	0.341	1.640
	8	5.683		8	0.378	2.480
	9	7.444		9	0.407	2.970
	10	7.139		10	0.430	2.797
	11	5.869		11	0.445	2.010
	12	3.158		12	0.453	0.806
	13	0.399		Asymmetric Total		14.12

Figure B.5 - Calculations for forces representing 1-in-50-year snow and rain events in CFB Goose Bay, under symmetric asymmetric loading patterns

Appendix C PROPOSED STRENGTHENING TECHNIQUE

This appendix presents the dimensions, location, material property and welding details of only the retrofit proposed as a strengthening technique.

Notes:
Retrofit components are in orange.
All materials are ASTM A529 Grade 50 structural steel.



CURRICULUM VITAE

Name: Yung Ku Kang

Place and date of birth: Busan, Busan Metropolitan City, Republic of Korea
17 December 1990

Education: Royal Military College of Canada
BEng in Civil Engineering, 2013

Experience: Requirements Officer / Deputy Officer Commanding
Real Property Operations Unit (Ontario) Detachment Borden
CFB Borden
July 2019 - July 2020

Adjutant / Deputy Commandant
Canadian Forces Fire and CBRN Academy
CFB Borden
October 2017 - June 2019

Building Services Officer
Real Property Operations Unit (Ontario) Detachment Borden
CFB Borden
May 2016 - September 2017

Contracts Officer
Real Property Operations Unit (Ontario) Detachment Borden
CFB Borden
November 2014 - April 2016

Plans Officer
Real Property Operations Unit (Ontario) Detachment Borden
CFB Borden
April 2014 - April 2015